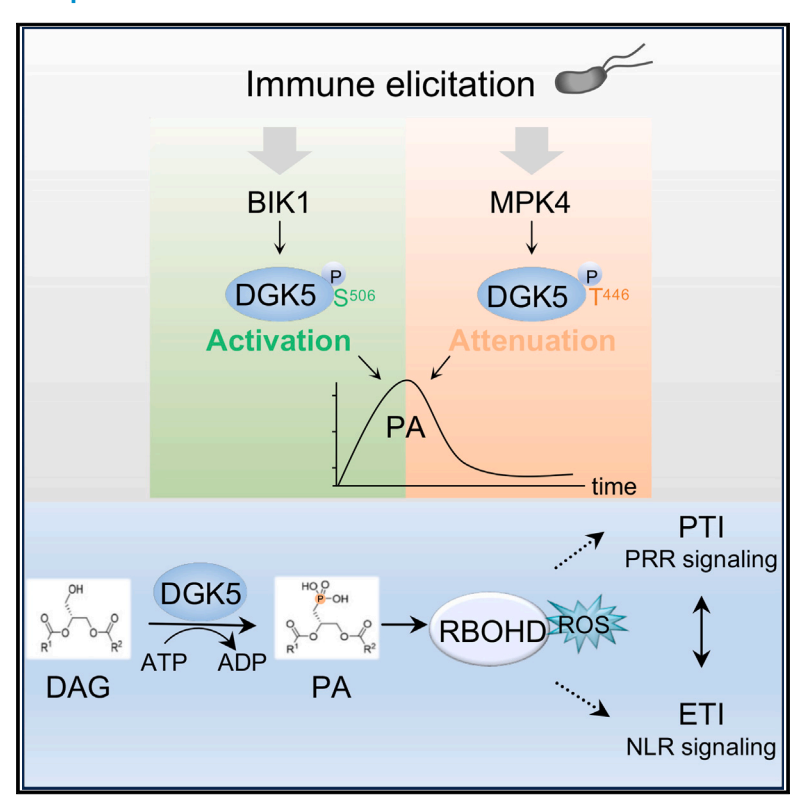


Dual phosphorylation of DGK5-mediated PA burst regulates ROS in plant immunity

Graphical abstract



Authors

Liang Kong, Xiyu Ma, Chao Zhang, ..., Teun Munnik, Ping He, Libo Shan

Correspondence

xiyu.ma@childrens.harvard.edu (X.M.), pinghemi@umich.edu (P.H.), liboshan@umich.edu (L.S.)

In brief

The differential phosphorylation of the lipid kinase DGK5 by PRR-activated protein kinases BIK1 and MPK4 opposingly regulates PA burst in modulating ROS production in plant immunity.

Highlights

- Immune elicitation triggers two distinct phosphorylation patterns of DGK5
- BIK1- and MPK4-mediated DGK5 phosphorylation opposingly regulates PA burst
- PA binds and stabilizes the NADPH oxidase RBOHD in regulating ROS production
- DGK5 is involved in plant PRR- and NLR-mediated immunity





Cell



Article

Dual phosphorylation of DGK5-mediated PA burst regulates ROS in plant immunity

Liang Kong,^{1,2,5} Xiyu Ma,^{2,5,*} Chao Zhang,^{1,2} Sung-II Kim,^{1,2} Bo Li,² Yingpeng Xie,^{1,2} In-Cheol Yeo,^{1,2} Hem Thapa,² Sixue Chen,³ Timothy P. Devarenne,² Teun Munnik,⁴ Ping He,^{1,2,*} and Libo Shan^{1,2,6,*}

Department of Molecular, Cellular, and Developmental Biology, University of Michigan, Ann Arbor, MI 48109, USA

SUMMARY

Phosphatidic acid (PA) and reactive oxygen species (ROS) are crucial cellular messengers mediating diverse signaling processes in metazoans and plants. How PA homeostasis is tightly regulated and intertwined with ROS signaling upon immune elicitation remains elusive. We report here that *Arabidopsis* diacylglycerol kinase 5 (DGK5) regulates plant pattern-triggered immunity (PTI) and effector-triggered immunity (ETI). The pattern recognition receptor (PRR)-associated kinase BIK1 phosphorylates DGK5 at Ser-506, leading to a rapid PA burst and activation of plant immunity, whereas PRR-activated intracellular MPK4 phosphorylates DGK5 at Thr-446, which subsequently suppresses DGK5 activity and PA production, resulting in attenuated plant immunity. PA binds and stabilizes the NADPH oxidase RESPIRATORY BURST OXIDASE HOMOLOG D (RBOHD), regulating ROS production in plant PTI and ETI, and their potentiation. Our data indicate that distinct phosphorylation of DGK5 by PRR-activated BIK1 and MPK4 balances the homeostasis of cellular PA burst that regulates ROS generation in coordinating two branches of plant immunity.

INTRODUCTION

Metazoans and plants have evolved complex innate immune systems to fend off microbial infections. 1-5 The plasma membrane (PM)-resident pattern recognition receptors (PRRs) perceive microbe- or pathogen-associated molecular patterns (MAMPs/PAMPs) to initiate pattern-triggered immunity (PTI). 6-9 The plant intracellular immune receptors are predominantly nucleotide-binding leucine-rich repeat proteins (NLRs), which sense effectors secreted by pathogens to activate effector-triggered immunity (ETI). 10,111 PRR and NLR activation triggers a plethora of overlapping signaling responses yet with different strengths and temporal dynamics, including the production of reactive oxygen species (ROS), activation of mitogen-activated protein kinases (MAPKs), and transcriptional reprogramming of defense-associated genes. 12,13 PRR and NLR signaling converges at multiple modules and mutually potentiates each other for an integrated and robust plant immunity. 14-17

Lipid signaling plays a crucial role in diverse cellular and physiological processes, including immune responses, across all kingdoms of life. Phosphatidic acid (PA), mainly present in cell membranes, functions as a universal second messenger relaying multiple cellular signaling events. PA can be gener-

ated by different enzymatic reactions, including diacylglycerol kinase (DGK)-mediated phosphorylation of diacylglycerol (DAG), and phospholipase D (PLD)-mediated hydrolysis of membrane phospholipids, such as phosphatidylcholine (PC) or phosphatidylethanolamine (PE). DAG is generated by phospholipase C (PLC) family proteins that hydrolyze phosphatidylinositol 4-mono phosphate (PIP) and phosphatidylinositol 4, 5-bisphosphate (PIP₂). *Arabidopsis* contains 12 PLDs, 7 DGKs, and 9 PLCs.^{20,21} Plant non-specific phospholipase C (NPC) could also generate DAG from structural phospholipids.²² Unlike animals, plants have a high abundance of DAG and lack protein kinase C, which underpins the importance of PA generated from DAG in signal transduction.²³

In plants, PA production is rapidly induced by multiple abiotic stresses, including submergence, hypoxia, osmotic stress, and temperature changes, involving both PLD and DGK pathways. ^{21,24–26} MAMPs and pathogen effectors could also induce a transient spike of PA. ^{27–32} In addition, PLDs and PLCs have been shown to regulate PTI signaling, ^{28,33–35} supporting the importance of PA in plant immunity. However, how PA burst is generated and dynamically regulated upon immune activation, and how it mediates the immune signaling network remains elusive.



²Department of Biochemistry & Biophysics, Texas A&M University, College Station, TX 77843, USA

³Department of Biology, University of Mississippi, Oxford, MS 38677, USA

⁴Department of Plant Cell Biology, Green Life Sciences Cluster, Swammerdam Institute for Life Sciences, University of Amsterdam, Amsterdam 1098XH, the Netherlands

⁵These authors contributed equally

⁶Lead contact

^{*}Correspondence: xiyu.ma@childrens.harvard.edu (X.M.), pinghemi@umich.edu (P.H.), liboshan@umich.edu (L.S.) https://doi.org/10.1016/j.cell.2023.12.030





RESULTS

BIK1 interacts with DGK5

BOTRYTIS-INDUCED KINASE 1 (BIK1), a PM-resident receptorlike cytoplasmic kinase (RLCK), associates with multiple PRRs and relays diverse signaling events, including ROS burst and cytosolic calcium rise via phosphorylation of nicotinamide adenine dinucleotide phosphate (NADPH) oxidase RESPIRATORY BURST OXIDASE HOMOLOG D (RBOHD) and calcium-permeable channels, respectively. 36-39 To gain insight into the PRR complex activation and signaling relay, we carried out a yeast two-hybrid screen for BIK1-interacting proteins using BIK1^{G2A}, carrying a mutation in the myristoylation motif for its PM association, as the bait toward the Arabidopsis cDNA library, 40 and identified DGK5 as a BIK1 interactor (Figures S1A-S1C). DGK5 contains an amino (N)-terminal catalytic domain (DGK_C), an accessory domain (DGKA), and a calmodulin-binding domain (DGK_{CBD}) (Figure S1A).²⁵ Co-immunoprecipitation (coIP) assays showed that BIK1 immunoprecipitated with DGK5 in Arabidopsis protoplasts (Figure S1D) and in transgenic plants expressing DGK5-HA under its native promoter and BIK1-GFP under the cauliflower mosaic virus (CaMV) 35S promoter (Figure 1A). The association between BIK1 and DGK5 was reduced upon treatment with flg22, a 22-amino acid synthetic peptide of bacterial flagellin (Figures 1A and S1D). An in vitro pull-down assay showed that recombinant glutathione S-transferase (GST)tagged DGK5 pulled down maltose-binding protein (MBP)tagged BIK1 (Figure 1B). Further, bimolecular fluorescence complementation (BiFC) assays showed that BIK1 was associated with DGK5 on the PM (Figure S1E). Moreover, Förster resonance energy transfer (FRET)-fluorescence lifetime imaging (FLIM) experiments revealed that BIK1-GFP was in the close vicinity of DGK5-mCherry but not the receptor kinase (RK) BAK1-INTERACTING RECEPTOR-LIKE KINASE 2 (BIR2)-mCherry (Figures 1C and 1D). Notably, we did not observe an interaction of DGK5 with the fla22 receptor FLAGELLIN SENSING 2 (FLS2) or its coreceptor BRASSINOSTEROID INSENSITIVE 1 (BRI1)-ASSOCIATED KINASE 1 (BAK1) (Figure S1F).

DGK5 regulates PTI

The flg22-induced ROS burst was reduced in dgk5-1 (sail_1212_e10) and dgk5-2 (sail_127_b03) mutants (Figures 1E, S1G, and S1H). Transgenic plants expressing DGK5-HA under its native promoter (line 1 [L1] and L2) in dgk5-1 complemented flg22-induced ROS burst to the wild-type (WT) level (Figures 1F and S1I). The expression of early PTI-responsive genes (WRKY29 and FRK1) and late defense genes (PR1 and PR5) was reduced in dgk5-1 upon flg22 treatment or Pseudomonas syringae pv. tomato (Pst) DC3000 infection (Figures 1G and 1H). Consistently, the accumulation and secretion of PR1 proteins induced by Pst DC3000 were reduced in dgk5-1 (Figure 1I). Moreover, flg22-induced stomatal closure was compromised in dgk5-1 compared with WT plants (Figure 1J). Yet, flg22-induced MAPK activation did not show a detectable difference between WT and dgk5-1 (Figures S1J and S1K). Furthermore, dgk5 mutants exhibited enhanced susceptibility to the virulent bacterium P. syringae pv. maculicola (Psm) ES4326, Pst DC3000, and necrotrophic bacterium Erwinia carotovora subsp. carotovora SCC1 (Figures 1K and S1L-S1N). Notably, DGK5 complementation lines restored the disease susceptibility to the WT level (Figures 1K, S1M, and S1N). In addition, flg22-primed plant resistance against Pst DC3000 was reduced in dgk5-1 compared with WT plants (Figure 1L). Together, our data demonstrate that DGK5 is an essential component in PTI signaling and plant immunity.

Multiple MAMPs induce dynamic phosphorylation of DGK5

DGK5 displayed a mobility shift in regular immunoblotting upon flg22 treatment (Figures 1A and S1D). We also detected an additional migration band of DGK5 upon flg22 treatment in the upper part of Phos-tag gels (Figures 2A, top panel, and S2A), implying that DGK5 probably possesses multiple phosphorylation patterns upon immune elicitation. We named the lower and upper migration bands of phosphorylated DGK5 as pDGK5-L and pDGK5-U, respectively. The phosphorylation of DGK5 was confirmed with a kinase inhibitor K252a and lambda phosphatase (λ-PP), which blocked or removed flg22-induced DGK5 mobility shifts, respectively (Figures 2B and 2C). The flg22induced phosphorylation of pDGK5-U occurred as early as 1 min, reaching its peak at 2-3 min, whereas pDGK5-L phosphorylation became evident at 2 min and reached its peak at 5 min (Figure 2A). Both pDGK5-U and pDGK5-L gradually returned to the basal level by 90 min. Apparently, pDGK5-U phosphorylation occurred slightly earlier than pDGK5-L phosphorylation. The flg22-induced phosphorylation of DGK5 no longer occurred in fls2 but could be restored by expressing FLS2 (Figure S2B). Consistently, a similar phosphorylation pattern of DGK5 upon flg22 treatment was observed in DGK5-HA transgenic plants in dgk5-1 (Figure S2C). In addition to flg22, other MAMPs and phytocytokines, including elf18 (an 18-aa synthetic peptide from bacterial elongation factor-Tu), chitin, Pep1 (a plant-derived phytocytokine), pg23 (a 23-aa synthetic peptide from fungal endopolygalacturonase), and nlp20 (a 20-aa synthetic peptide from necrosis and ethylene-inducing peptide 1-like proteins), also induced DGK5 phosphorylation (Figure 2D). Together, the data support that multiple MAMPs induce two distinct phosphorylation patterns of DGK5.

BIK1 phosphorylates DGK5 at Ser⁵⁰⁶

Overexpression of BIK1, but not BIK1KM (BIK1 kinase-dead mutant),41 markedly enhanced pDGK5-U, but not pDGK5-L, upon flg22 treatment (Figure 2E). Consistently, pDGK5-U, but not pDGK5-L, induced by flg22 was reduced in bik1 (Figure 2F), supporting that BIK1 is required for the phosphorylation of pDGK5-U but not pDGK5-L. An in vitro kinase assay indicates that recombinant GST-BIK1, but not GST-BIK1KM, phosphorylated DGK5 (Figure 2G). Phosphorylation of DGK5 appeared to be specific as MBP-BAK1^{CD} (BAK1 cytosolic domain), phosphorylated BIK1 but not DGK5 (Figure 2G). Furthermore, RLCKs AVRPPHB SUSCEPTIBLE 1-LIKE 30 (PBL30) and PBL31, which are involved in pg23- and nlp20-activated PRR signaling, ¹⁷ also phosphorylated DGK5 in vitro (Figure S2D). pg23 and nlp23 are perceived by RECEPTOR-LIKE PROTEIN 42 (RLP42) and RLP23, respectively. 42,43 Collectively, the data



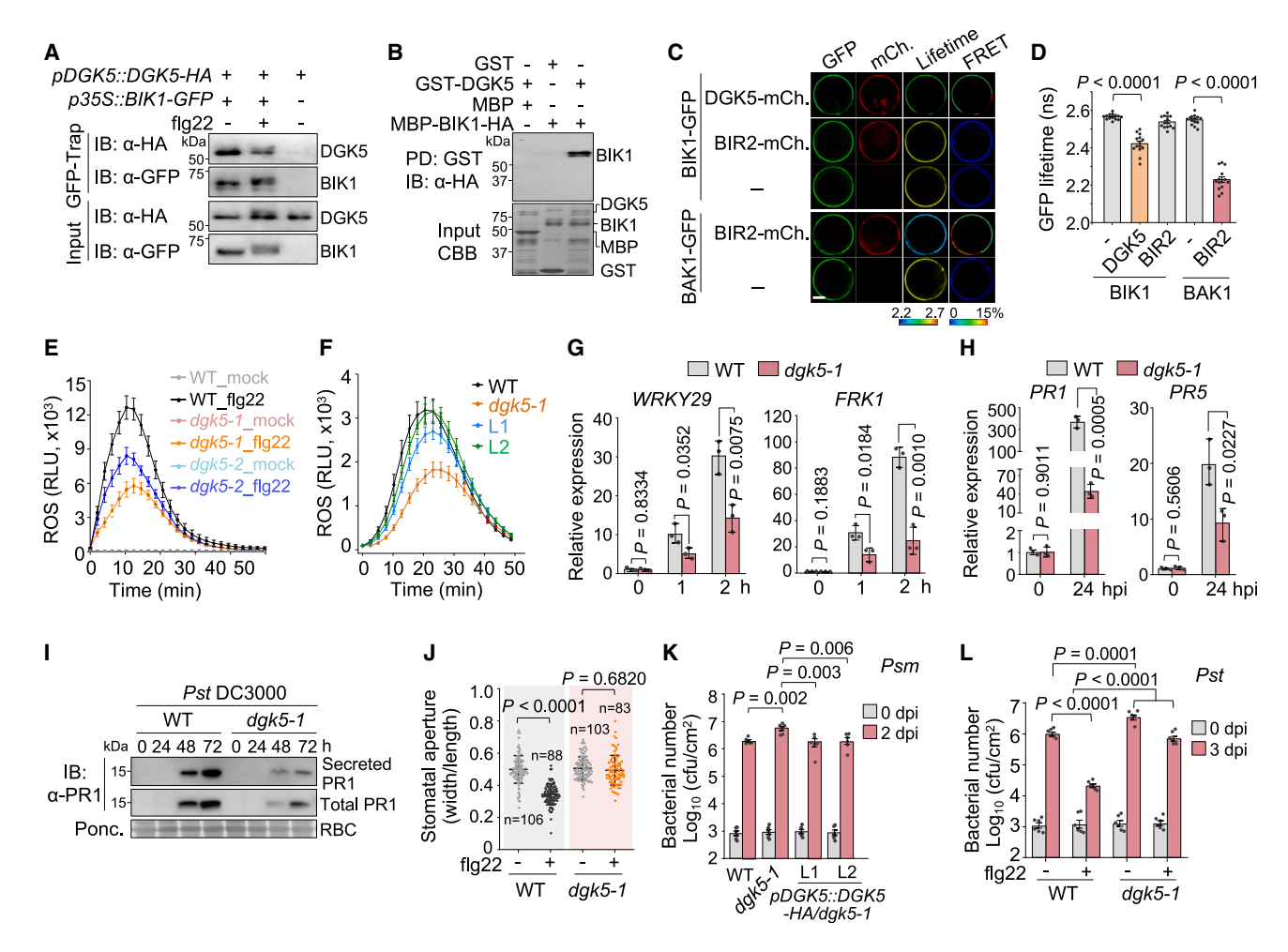


Figure 1. DGK5 interacts with BIK1 and regulates PTI signaling

(A) BIK1 associates with DGK5 in Arabidopsis transgenic plants. 2-week-old transgenic seedlings carrying pDGK5::DGK5-HA/p35S::BIK1-GFP or pDGK5::DGK5-HA were treated with 0.2 μM flg22 for 10 min. Proteins were immunoprecipitated with GFP-trap agarose and analyzed by immunoblotting (IB) with α-HA or α-GFP antibodies (top two) with input proteins shown (bottom two). The molecular weight (kDa) is labeled on the left of regular SDS-PAGE in this study. (B) BIK1 interacts with DGK5 in a pull-down assay. Eluted proteins were subjected to immunoblotting with α -HA antibodies (top). Input proteins are shown by Coomassie brilliant blue (CBB) staining.

(C and D) BIK1 interacts with DGK5 in a FRET-FLIM assay. Localization of GFP-fused proteins and mCherry-fused proteins in protoplasts is shown (C). The lifetime (τ) distribution and apparent FRET efficiency are presented as pseudocolor images according to the scale (C). Scale bars, 10 μm. Quantification of GFP fluorescence lifetime (τ) is shown as mean \pm SEM (n = 14) (D).

- (E) DGK5 is required for flg22-induced ROS burst. Leaf discs from 4-week-old soil-grown plants were treated with or without 0.1 μM flg22, and ROS production was measured as relative light units (RLUs) by a luminometer. Data represent mean \pm SEM (n = 12).
- $(F) DGK5-HA \ restores \ flg 22-induced \ ROS \ burst \ in \ dgk5-1. \ L1 \ and \ L2 \ are \ complementation \ lines \ of \ pDGK5-HA \ in \ dgk5-1. \ Data \ represent \ mean \ \pm \ SEM \ (n=1) \ dgk5-1. \$ 24 for WT; n = 32 for dgk5-1 and L1; n = 28 for L2).
- (G) Reduced expression of WRKY29 and FRK1 in dgk5-1. 10-day-old seedlings were treated without (0 h) or with 0.1 μM flg22. Gene expression was normalized to UBQ10 and presented as fold change relative to WT 0 h treatment. Data represent mean \pm SD (n = 3).
- (H) Reduced expression of PR1 and PR5 in dgk5-1.4-week-old soil-grown plants were inoculated with Pst DC3000 at 5 × 10⁵ colony-forming unit (CFU)/mL, and samples were collected at 24 h post-inoculation (hpi).
- (I) Reduced total and secreted PR1 proteins in dgk5-1. 4-week-old soil-grown plants were hand-inoculated with Pst DC3000 at 5 × 10⁵ CFU/mL. PR1 proteins were detected with α-PR1 antibodies with protein loading shown by Ponceau S staining for Rubisco (RBC).
- (J) Compromised flg22-induced stomatal closure in dgk5-1. Stomatal apertures were measured after 0.1 µM flg22 treatment for 2 h under light. Data represent mean ± SD.
- (K) Increased susceptibility to Psm ES4326 in dgk5-1. 4-week-old soil-grown plants were hand-inoculated with Psm at 5×10^5 CFU/mL. Data represent mean \pm
- (L) Compromised flg22-induced resistance to Pst DC3000 in dgk5-1. 4-week-old soil-grown plants were pre-infiltrated with 0.1 µM flg22 or ddH₂O for 24 h before Pst DC3000 hand-inoculation at 5×10^5 CFU/mL. Data represent mean \pm SEM (n = 6).
- Experiments were repeated three (A-I) or four (J-L) times with similar results. Data were analyzed by unpaired two-tailed Student's t test (G, H, and K) or one-way ANOVA followed by the Tukey's test (D, J, and L).

See also Figure S1.



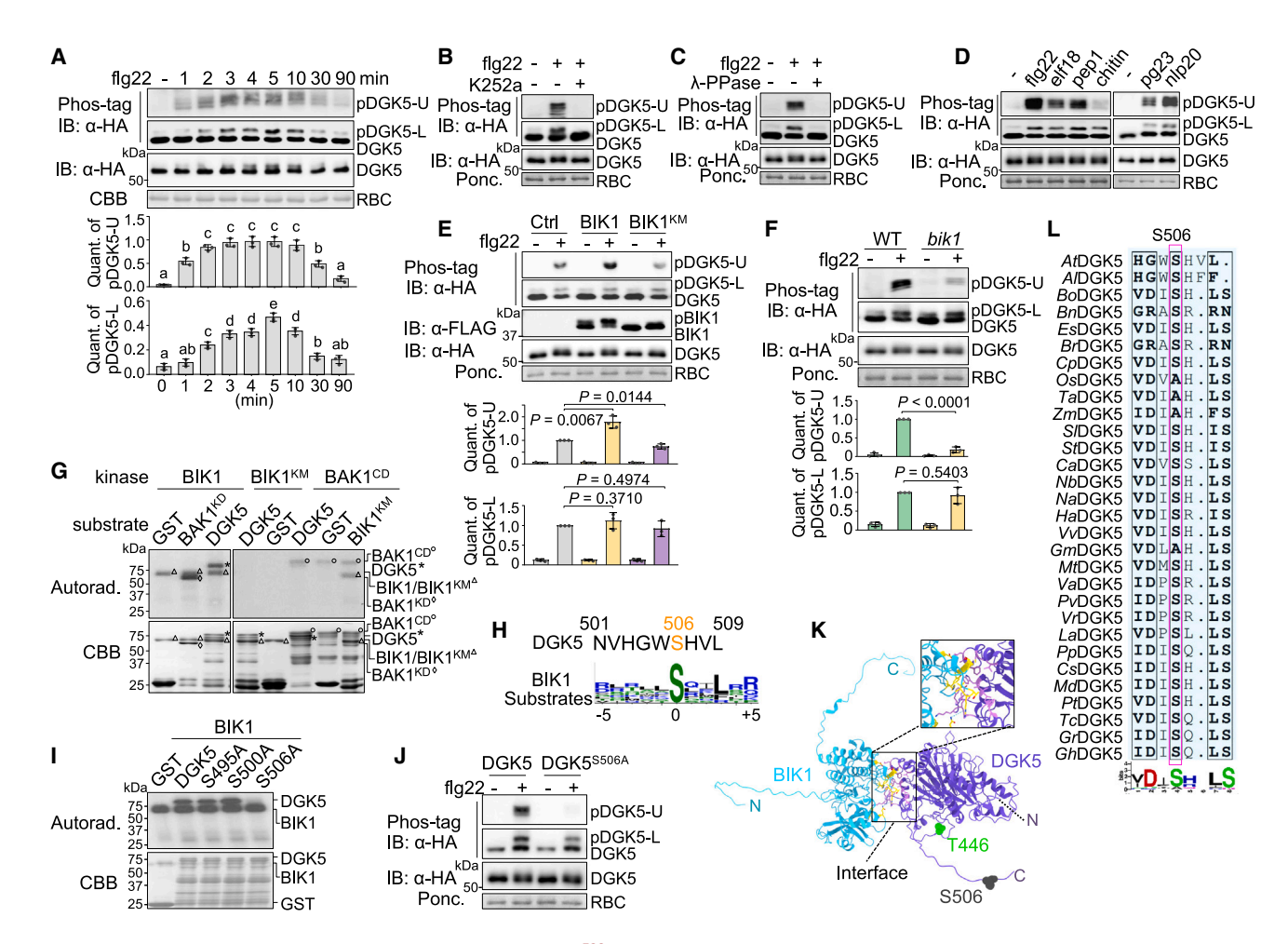


Figure 2. MAMP-activated BIK1 phosphorylates DGK5 at Ser⁵⁰⁶

(A) Fig22 induces two DGK5 phosphorylation patterns. Proteins from protoplasts expressing DGK5-HA upon 0.1 μM fig22 treatment were separated with Mn²⁺-Phos-tag (top two) or regular SDS-PAGE (middle two), followed by immunoblotting with α-HA antibodies. pDGK5-U and pDGK5-L indicate the upper and lower shifted bands of phosphorylated DGK5, respectively. Protein loading is shown by CBB staining for RBC. Quantification of pDGK5-U and pDGK5-L represents the ratio of phosphorylated to unphosphorylated DGK5 analyzed by ImageJ (bottom two). Data represent mean ± SD (n = 3). Different letters denote statistically significant differences according to one-way ANOVA followed by the Tukey's test (p < 0.05).

(B and C) K252a blocks (B) and λ-phosphatase removes (C) flg22-induced DGK5 phosphorylation. Protoplasts expressing DGK5-HA were pre-treated with 1 μM K252a for 30 min before 0.1 μM flg22 treatment for 10 min. For λ-phosphatase treatment, cell extracts from protoplasts expressing DGK5-HA were treated with 1.0 μL (400 U) λ-phosphatase (λ-PPase) for 1 h at 30°C.

- (D) Multiple MAMPs induce DGK5 phosphorylation. Protoplasts expressing DGK5-HA were treated with 0.1 μM flg22, 1 μM elf18, 0.1 μM pep1, or 100 μg/mL chitin for 10 min, 1 μ M pg23 or nlp20 for 30 min.
- (E) BIK1, not BIK1^{KM}, enhances flg22-induced pDGK5-U phosphorylation. Protoplasts co-expressing DGK5-HA with BIK1-FLAG or BIK1^{KM}-FLAG were treated with or without 0.1 µM flg22 for 10 min. Quantification was performed as in (A). The value of Ctrl (empty vector) with flg22 treatment was set as 1.0. Data represent mean \pm SD (n = 3) analyzed by unpaired two-tailed Student's t test.
- (F) The flg22-induced pDGK5-U phosphorylation is reduced in bik1. The experiment and quantification were performed as in (E) (n = 3).
- (G) BIK1 phosphorylates DGK5 in vitro. The kinase assay was performed using GST-tagged proteins. Phosphorylation was analyzed by autoradiography (top) with protein loading shown by CBB staining.
- (H) DGK5^{SS06} is a conserved phosphorylation site by BIK1. Phosphorylation motif pS-xx-L was generated by WebLogo 3 using BIK1-phosphorylated sites of RBOHD, CNGC2, and CNGC4.
- (I) DGK5^{S506} is required for BIK1 phosphorylation with the *in vitro* kinase assay.
- (J) DGK5^{S506} is required for flg22-induced phosphorylation of pDGK5-U, but not pDGK5-L.
- (K) Ser⁵⁰⁶ is not in the interface of BIK1-DGK5 complex predicted by AlphaFold2. Ser⁵⁰⁶ and Thr⁴⁴⁶ are marked in gray and green, respectively. Residues in the interface of BIK1 and DGK5 are marked in yellow and pink, respectively. N and C represent N and C termini of BIK1 (cyan) and DGK5 (purple).
- (L) DGK5^{S506} is a conserved site across plant species. Multiple sequence alignment and WebLogo analyses of DGK5 residues surrounding AtDGK5^{S506} from different plant species listed in the figure legend of Figure S2J are shown. The conserved serine residue is boxed in pink.

Experiments were repeated three times (A-F and I) or twice (G and J) with similar results.

See also Figure S2.



suggest that DGK5 is involved in both RK and RLP signaling through RLCK-mediated phosphorylation.

To identify BIK1-mediated DGK5 phosphorylation sites, we aligned phosphorylation sites of BIK1's known substrates, including RBOHD, CYCLIC NUCLEOTIDE-GATED CHANNEL 2 (CNGC2), and CNGC4,³⁷⁻³⁹ and identified a consensus sequence of pS-x-x-L, of which the third amino acid following the phosphorylated serine (Ser) is leucine (Leu), and x represents any amino acid (Figure 2H). DGK5 harbors this motif (S⁵⁰⁶-H-V-L) at its C terminus (Figures 2H and S2E). We mutated Ser⁵⁰⁶ of DGK5 to alanine (A) (DGK5^{S506A}), as well as serine residues (Ser $^{\rm 495}$ and Ser $^{\rm 500}$) close to Ser $^{\rm 506}$ (Figure S2E). BIK1 phosphorylated DGK5, DGK5^{S495A}, and DGK5^{S500A}, but not DGK5^{S506A} (Figure 2I). Additionally, flg22-induced phosphorylation of pDGK5-U, but not pDGK5-L, was abolished in DGK5^{S506A} (Figure 2J). Thus, BIK1 phosphorylates DGK5 at Ser⁵⁰⁶, which accounts for flg22-induced phosphorylation of pDGK5-U, but not pDGK5-L.

AlphaFold structural analysis showed that Ser⁵⁰⁶ locates in a disordered region of DGK5 (Figure S2F). The AlphaFold-predicted BIK1 structure overlaid with the crystal structure of BIK1 truncation (52–360 aa),⁴⁴ which does not include the disordered regions at N and C termini (Figure S2G). We further predicted the BIK1-DGK5 complex structure using the ColabFold platform based on the AlphaFold2 source code.⁴⁵ BIK1 interfaces with DGK5 in a region without Ser⁵⁰⁶ (Figure 2K), hinting that BIK1 docks and phosphorylates different sites of DGK5. Consistently, coIP and pull-down assays showed that DGK5^{S506A} did not affect its interaction with BIK1 (Figures S2H and S2I).

Interestingly, Ser⁵⁰⁶ is uniquely present in DGK5 but not in other *Arabidopsis* DGK members (Figure S2E). In addition, phylogenetic analysis showed that DGK5 is broadly conserved across plant species (Figure S2J), and Ser⁵⁰⁶ is conserved among DGK5 orthologs (Figure 2L), suggesting that DGK5^{S506} phosphorylation might represent a conserved mechanism in mediating immune signaling.

MPK4 phosphorylates DGK5 at Thr⁴⁴⁶

To gain insight into flg22-induced phosphorylation of pDGK5-L, we expressed DGK5-FLAG in *Arabidopsis* protoplasts treated with flg22 and isolated bands corresponding to DGK5 for liquid chromatography-tandem mass spectrometry (LC-MS/MS) analysis (Figure S3A). Seven phosphorylated sites were identified, with four (Thr⁴⁴⁶, Ser⁴⁶³, Thr⁴⁷⁸, and Ser⁴⁸⁸) bearing high confidence (Figures 3A and S3B). Alanine substitution showed that DGK5^{T446A}, but not others, blocked flg22-induced phosphorylation of pDGK5-L (Figures 3B and S3C), but not the phosphorylation of pDGK5-U (Figure 3C). The data support that flg22 treatment induces two uncoupled phosphorylation events of DGK5 with Ser⁵⁰⁶ by BIK1 and Thr⁴⁴⁶ by another kinase.

DGK5^{T446} resides in the sequence of ⁴⁴³DPSTPR⁴⁴⁸ (Figure S3D), which bears the MAPK consensus phosphorylation site (PxpS/pTP).⁴⁶ This prompted us to test whether flg22-induced pDGK5-L is mediated by MAPKs. Treatment with MAPK inhibitor PD184161 or co-expression of MAPK phosphatase MKP reduced flg22-triggered pDGK5-L phosphorylation (Figure 3D, 2nd panel) but did not affect pDGK5-U phosphoryla-

tion (Figure 3D, top panel), highlighting the involvement of MAPKs in pDGK5-L phosphorylation. Perception of flg22 induces two parallel MAPK cascades, leading to the activation of MPK3/MPK6 and MPK4, respectively. 47-49 Remarkably, flg22induced pDGK5-L (DGK5^{T446}) phosphorylation was reduced in mpk4 compared with Ler-0 control plants (Figure 3E) and remained unchanged in mpk6/amiR-MPK3 plants (Figure S3E), in which MPK3 was silenced by an inducible artificial microRNA in mpk6,50 suggesting the requirement of MPK4 in flg22-induced DGK5^{T446} phosphorylation. Consistently, overexpression of MPK4 enhanced flg22-induced pDGK5-L phosphorylation (Figure S3F). MPK4-FLAG immunoprecipitated from flg22 treated-protoplasts phosphorylated GST-DGK5, but not GST-DGK5^{T446A} proteins (Figure 3F), corroborating that MPK4 phosphorylates DGK5 at Thr⁴⁴⁶. DGK5^{T446} is not conserved among different DGK members in Arabidopsis (Figure S3D), but the MAPK phosphorylation site containing Thr⁴⁴⁶ is highly conserved among DGK5 orthologs across different plant species (Figure S3G), implying a conserved MAPK-mediated phosphorylation of DGK5.

MPK4 interaction with DGK5 was confirmed by coIP assays in protoplasts (Figure S3H) and *pDGK5::DGK5-HA/dgk5-1* transgenic plants (Figure 3G). The association of DGK5 with endogenous MPK4 was reduced upon flg22 treatment when *DGK5* was expressed under the native promoter (Figure 3G). GST-DGK5, but not GST, could pull down HIS-MPK4 (Figure S3I). Furthermore, DGK5-GFP was in the close vicinity of MPK4-mCherry, but not BIR2-mCherry, with a FRET-FLIM assay (Figures 3H and 3I). Notably, DGK5^{T446A} did not affect its interaction with MPK4 (Figures S3I and S3J), consistent with the predicted MPK4-DGK5 complex structure showing that DGK5^{T446} is not at the interface of MPK4 and DGK5 (Figure 3J). Taken together, the data suggest that MPK4 interacts with and phosphorylates DGK5 at Thr⁴⁴⁶, attributing to flg22-induced phosphorylation of pDGK5-L.

Distinct phosphorylation by BIK1 and MPK4 opposingly regulates DGK5 activity in producing PA

We next tested whether DGK5 exhibits a DGK activity *in vitro*. Using [γ^{-32} P]-ATP labeling, we observed PA production when HIS-DGK5 or GST-DGK5 was incubated with DAG analogs (1, 2-dioleoyl-sn-glycerol [DOG] or 1-stearoyl-2-arachidonoyl-sn-glycerol [SAG]) (Figures 4A and S4A). DGK inhibitor R59022 abrogated the activity (Figure 4A). Further, the plant cell lysate also produced PA with DOG as a substrate (Figure S4A), likely mediated by endogenous DGKs.

We further examined whether BIK1- and MPK4-mediated phosphorylation of DGK5 affects its activity in PA production. Compared with HIS-MBP, pre-incubation with HIS-BIK1 enhanced DGK5 enzymatic activity, resulting in an elevated PA production (Figure 4B). By contrast, GST-MPK4^{ac}, the active MPK4 carrying D198G/E202A mutations,⁵¹ suppressed DGK5 activity (Figure 4C). Subsequently, we tested if phosphorylation at Ser⁵⁰⁶ or Thr⁴⁴⁶ affects DGK5 activity. The phosphomimetic DGK5^{S506D} variant (mimicking BIK1 phosphorylation) exhibited an enhanced activity, whereas DGK5^{T446D} (mimicking MPK4 phosphorylation) showed a reduced activity in PA production (Figures 4D and 4E). Notably, the phospho-deficient mutants





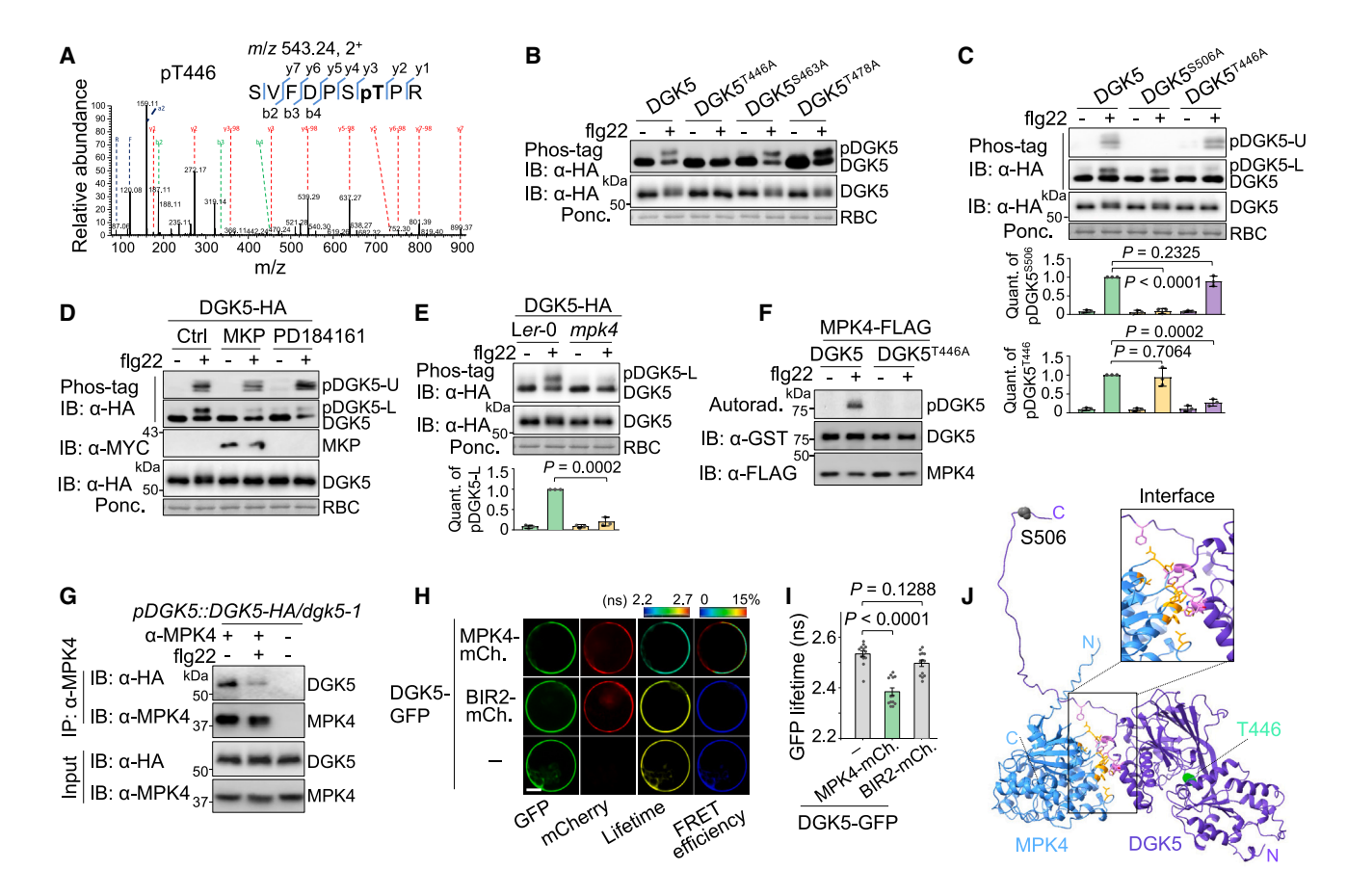


Figure 3. MAMP-activated MPK4 phosphorylates DGK5 at Thr⁴⁴⁶

(A) Flg22 induces DGK5 phosphorylation at Thri⁴⁴⁶ by LC-MS/MS analysis. MS/MS spectrum of the peptide containing phosphorylated DGK5^{T446} is shown. (B) DGK5^{T446A} blocks flg22-induced DGK5 phosphorylation. Proteins from protoplasts were separated with Mn²⁺-Phos-tag or regular SDS-PAGE, followed by immunoblotting with α -HA antibodies.

- (C) DGK5^{S506} and DGK5^{T446} mediate two distinct flg22-induced DGK5 phosphorylation events. Experiment and quantification were performed as in Figure 2E. Data represent mean \pm SD (n = 3) analyzed by unpaired two-tailed Student's t test.
- (D) Flg22-induced pDGK5-L, but not pDGK5-U, is blocked by MAPK phosphatase (MKP) or PD184161. MKP-MYC was co-expressed with DGK5-HA in protoplasts. PD18416 (5 μM) was added 30 min before flg22 treatment.
- (E) Flg22-induced DGK5^{T446} phosphorylation (pDGK5-L) is abolished in mpk4. Ler-0 is the parental line of mpk4.
- (F) Fig22-activated MPK4 phosphorylates DGK5, but not DGK5^{T446A}. Activated MPK4-FLAG was immunoprecipitated with α-FLAG agarose from protoplasts expressing MPK4-FLAG treated with 0.1 µM flg22 for 10 min for the kinase assay.
- (G) DGK5 associates with MPK4 in transgenic plants. CoIP was carried out with α-MPK4 antibodies using 2-week-old transgenic plants treated with or without 0.2 uM fla22 for 10 min.
- (H and I) MPK4 associates with DGK5 in a FRET-FLIM assay. Experiment and quantification were performed as in Figures 1C and 1D (n = 13).
- (J) Thr⁴⁴⁶ is not in the interface of MPK4-DGK5 complex predicted by AlphaFold. Thr⁴⁴⁶ and Ser⁵⁰⁶ are marked with green and gray, respectively. Residues in the interface of MPK4 and DGK5 are marked with orange and pink, respectively. N and C represent N and C termini of MPK4 (steel blue) or DGK5 (purple). Experiments were repeated three times (B-E and G-I) or twice (F) with similar results.

See also Figure S3.

DGK5^{S506A} and DGK5^{T446A} did not affect DGK5 activity in vitro (Figures 4D and 4E). Together, these data suggest that BIK1-mediated phosphorylation at Ser⁵⁰⁶ enhances, whereas MPK4-mediated DGK5 phosphorylation at Thr⁴⁴⁶ inhibits DGK5 activity in producing PA. Interestingly, DGK5^{S506D/T446D} exhibited a similar activity with DGK5^{T446D} showing a reduced activity compared with DGK5 (Figures S4B and S4C), implying that Thr⁴⁴⁶ phosphorylation is epistatic to Ser⁵⁰⁶ phosphorylation. Notably, MPK4 still phosphorylated DGK5^{S506D} and BIK1 still phosphorylated DGK5^{T446D} (Figures S4D and S4E), reinforc-

ing the independent phosphorylation of DGK5 by BIK1 and MPK4.

The differential phosphorylation of DGK5 plays opposite roles in plant immunity

To understand how the differential phosphorylation of DGK5 by BIK1 at Ser506 and by MPK4 at Thr446 contributes to PTI responses, we generated transgenic plants expressing DGK5-HA or phosphorylation variants of DGK5^{S506A}, DGK5^{T446A}, $DGK5^{S506D}$, and $DGK5^{T446D}$ under its native promoter in



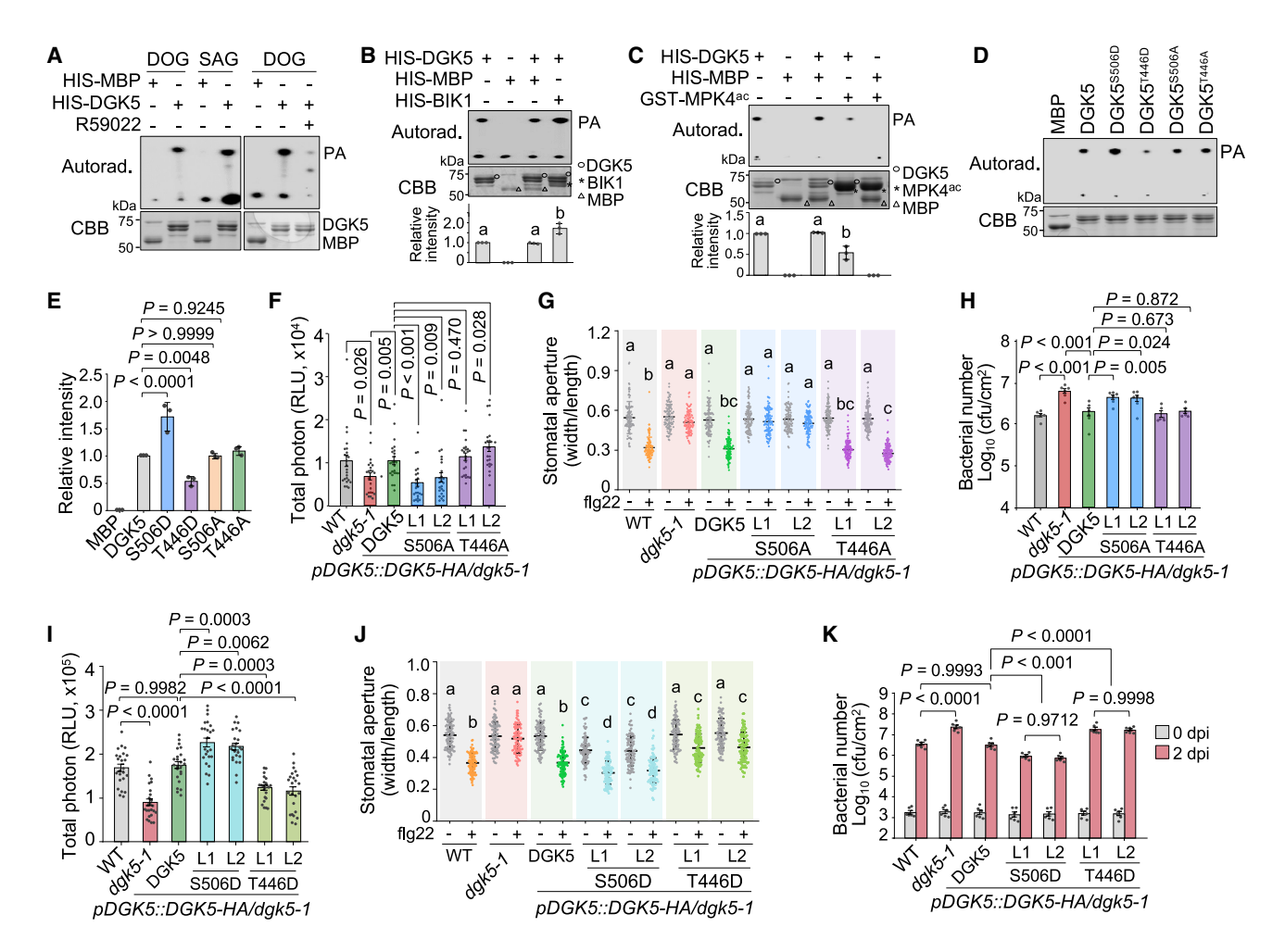


Figure 4. DGK5^{S506} positively regulates, while DGK5^{T446} negatively regulates DGK5 activity and plant immunity

(A) DGK5 phosphorylates DOG and SAG for PA production. HIS-MBP or HIS-DGK5 was incubated with DOG or SAG in a reaction buffer containing [\gamma-3^2P]-ATP for 30 min. PA was detected by autoradiography in the TLC plate (top) with input proteins shown by CBB staining. R59022 (20 μM), a DGK inhibitor.

(B) BIK1 enhances DGK5-mediated PA production. The experiment was performed as in (A) with or without HIS-BIK1 using DOG as a substrate. Quantification of PA was calculated as relative band intensities, and the value of HIS-DGK5 alone was set as 1. Data represent mean ± SD (n = 3).

(C) MPK4ac reduces DGK5-mediated PA production. The experiment and quantification were performed as in (B) (n = 3).

(D and E) DGK5^{S506D} enhances PA production, while DGK5^{T446D} reduces PA production compared with DGK5. The experiment and quantification were per-

(F) DGKS^{5506A}, but not DGK5^{T446A}, fails to restore flg22-induced ROS production in dgk5-1. Leaf discs from 4-week-old soil-grown transgenic plants were treated with or without 0.1 µM flg22, and ROS production was measured as RLU over 50 min with total ROS photons shown as mean ± SEM (n = 24). L1 and L2 are two

(G) DGK5 S506A , but not DGK5 T446A , fails to restore flg22-induced stomatal closure. Stomatal apertures were measured after 0.1 μ M flg22 treatment for 2 h under light. Data represent mean \pm SD (n = 99).

(H) DGK5^{5506A}, but not DGK5^{T446A}, fails to restore disease resistance to Pst DC3000. 4-week-old soil-grown plants were hand-inoculated with Pst DC3000 at 5 × 10^5 CFU/mL. Bacterial growth at 2 dpi is shown as mean \pm SEM (n = 6).

(I) DGK5^{S506D}, but not DGK5^{T446D}, enhances flg22-induced ROS production. The experiment was performed as in (F) (n = 24).

(J) DGK5^{S506D}, but not DGK5^{T446D}, enhances flg22-induced stomatal closure. The experiment was performed as in (G) (n = 99).

(K) DGK5^{S506D}, but not DGK5^{T446D}, mediates elevated disease resistance to Psm. The experiment was performed as in (H) (n = 6).

Experiments were repeated three (A-E, G, and J) or four (F, H, I, and K) times with similar results. Data were analyzed by unpaired two-tailed Student's t test (F and H) or one-way ANOVA followed by the Tukey's test (B, C, E, G, and I-K). Different letters in (B, C, G, and J) denote statistically significant differences (p < 0.05). See also Figure S4.

dgk5-1. Notably, DGK5^{S506A} failed to restore flg22-induced ROS burst and stomatal closure, and disease resistance to Psm and Pst DC3000 in dgk5-1 (Figures 4F-4H and S4F), indicating that BIK1-phosphorylated DGK5^{S506} is indispensable to activate flg22-induced immune signaling and disease resistance. By contrast, DGK5^{T446A} restored flg22-induced ROS burst and stomatal closure, and disease resistance to Psm and Pst DC3000 (Figures 4F-4H and S4F). In line with the above observations, phosphomimetic DGK5^{S506D} transgenic plants showed enhanced flg22-induced ROS burst, stomatal closure, and





disease resistance to *Psm* (Figures 4I–4K). Conversely, phosphomimetic DGK5^{T446D} transgenic plants exhibited compromised flg22-triggered ROS burst, stomatal closure, and disease resistance to *Psm* (Figures 4I–4K). Together, the data support that BIK1-mediated DGK5 phosphorylation at Ser⁵⁰⁶ positively regulates PTI signaling, whereas MPK4-mediated DGK5 phosphorylation at Thr⁴⁴⁶ plays a negative role in plant immunity.

BIK1-DGK5-mediated PA production is important in PTI signaling

Next, we determined if the BIK1-DGK5 axis regulates PA production in PTI signaling. Using the radiolabeled thin-layer chromatography (TLC) assay, we detected a rapid and transient PA spike upon flg22 treatment in protoplasts (Figure 5A). Importantly, flg22-triggered PA production was reduced in *bik1* and *dgk5-1* compared with WT plants (Figure 5B), suggesting that DGK5 and BIK1 are essential for flg22-induced PA production. Consistently, cell lysates from *bik1* and *dgk5-1* exhibited a reduced PA production upon flg22 treatment compared with WT (Figure S5A), corroborating the importance of flg22-induced BIK1 phosphorylation on DGK5 in PA production.

Plant hormone abscisic acid (ABA) and salt treatments induced PA production, which could be monitored by a FRET-based PA biosensor PAleon (1–250 aa of RBOHD) in transgenic plants. We tested whether PAleon could monitor MAMP-induced PA production. Similar to salt treatment, flg22 or Pep1 treatment induced a rapid increase of PA in roots (Figures 5C, 5D, S5B, and S5C). Importantly, flg22-triggered PA production was compromised in *dgk5-1* or upon DGK inhibitor R59022 treatment (Figures 5C and 5D), further supporting the importance of DGK5 in flg22-induced PA production.

We next determined whether the reduced PA production in *dgk5* mutants attributed to their defects in PTI signaling. Exogenous PA treatment substantially complemented the compromised flg22-induced ROS production in *dgk5-1* (Figures 5E and 5F). Notably, PA alone did not elicit a detectable ROS production (Figure 5F). Consistently, flg22-induced ROS production, detected by H₂DCFDA, a cell-permeable ROS dye, was reduced in *dgk5-1* but was restored by PA treatment (Figures 5G and 5H). Pre-treatment of PA also rescued the defects of *dgk5-1* in flg22-induced stomatal closure and disease resistance to *Psm* or *Pst* DC3000 (Figures 5I, 5J, and S5D). Additionally, we observed an increased resistance in WT plants treated with PA (Figures 5J and S5D). Together, these data support that DGK5-derived PA is crucial in PTI signaling and plant immunity.

DGK5-derived PA stabilizes NADPH oxidase RBOHD in regulating ROS production

The *dgk5* mutants exhibited defects in flg22-induced ROS production (Figures 1E and 1F). flg22 treatment increased protein levels of RBOHD, ^{14,15} a key enzyme in PTI-triggered ROS burst.⁵³ Interestingly, flg22-induced RBOHD protein abundance was blocked in *dgk5-1* (Figure 6A), whereas PA treatment restored RBOHD abundance in *dgk5-1* (Figure 6B). In addition, PA treatment slightly increased RBOHD protein levels in WT and *dgk5-1* without flg22 treatment (Figure S5E). The data suggest that DGK5-derived PA regulates RBOHD protein levels.

Notably, the *RBOHD* transcript level did not change in *dgk5* (Figure S5F).

PLD-derived PA binds to RBOHD and regulates ABA-induced ROS production.⁵⁴ Four arginine (R) residues (R149, 150, 156, and 157) at the N terminus of RBOHD (RBOHD^N) mediate its PA-binding (Figure 6C).⁵⁴ We determined whether PA-binding is important for the RBOHD protein abundance by mutating four arginine residues to alanine in the full-length RBOHD (RBOHD^{4A}) or RBOHD^N (RBOHD^{N-4A}), respectively. When expressed under either the constitutive 35S promoter or native promoter in Nicotiana benthamiana, RBOHD4A or RBOHDN-4A showed reduced protein abundance compared with WT RBOHD or RBOHD^N, respectively (Figures S5G and S5H), suggesting that PA-binding could stabilize RBOHD. Similarly, RBOHD^{4A} or RBOHD^{N-4A} showed considerably reduced protein abundance compared with WT RBOHD or RBOHD^N under either 35S or its native promoter in multiple independent transgenic Arabidopsis lines in rbohd (Figures 6D and S5I). Proteasome inhibitor MG132 increased the protein abundance of RBOHD^{4A} and RBOHD^{N-4A} (Figures 6E and S5J), implying the involvement of 26S proteasome-mediated degradation in regulating RBOHD protein abundance.

Protein ubiquitination is implicated in regulating RBOHD stability. Stability. An *in vivo* ubiquitination assay indicated that RBOHD proteins underwent ubiquitination in the *p35S:: RBOHD-HA/rbohd* transgenic plants (Figure S5K). Notably, flg22 treatment led to a reduction of RBOHD ubiquitination (Figure S5K), which is in line with the increased RBOHD protein levels following flg22 treatment (Figure 6A). Importantly, the flg22-triggered reduction of RBOHD ubiquitination was partially impaired in *dgk5-1* but could be restored upon PA treatment (Figure 6F). Additionally, RBOHD and RBOHD^{N-4A} exhibited elevated ubiquitination levels compared with WT RBOHD or RBOHD^N, respectively (Figures 6G and S5L). Taken together, our data support that flg22-induced PA suppresses RBOHD ubiquitination, consequently enhancing its protein stability upon immune elicitation.

DGK5-derived PA regulates ETI

Considering the role of DGK5-derived PA in regulating RBOHD stability and ROS production, we examined whether DGK5 is involved in ETI-triggered ROS (ROSETI) burst. Infection with Pst DC3000 or Pst DC3000 strain D36E (deletion of 36 effector genes)56,57 carrying avrRpt2 (Pst avrRpt2 or D36E avrRpt2) induced a strong ROS production detected by H2DCFDA staining (Figures 7A and 7B) at 5 h post-infection. Similar to a previous report. 15 Pst D36E did not induce ROS production at this time point (Figures S6A and S6B). The fluorescent signals in the apoplasts of dgk5-1 were reduced compared with WT plants upon Pst avrRpt2 or D36E avrRpt2 infection (Figures 7A and 7B), implying a role of DGK5 in ETI-induced ROS production. Furthermore, PA treatment partially restored avrRpt2-induced ROS production in dgk5-1 (Figures 7A and 7B), suggesting that DGK5-mediated PA production is important for the ETI-triggered ROS burst. Additionally, dexamethasone (Dex)-induced AvrRpt2 expression led to a reduced ROS production in the dgk5-1 background compared with WT plants (Figures S6C and S6D). Similarly, PA treatment partially restored the fluorescence signals



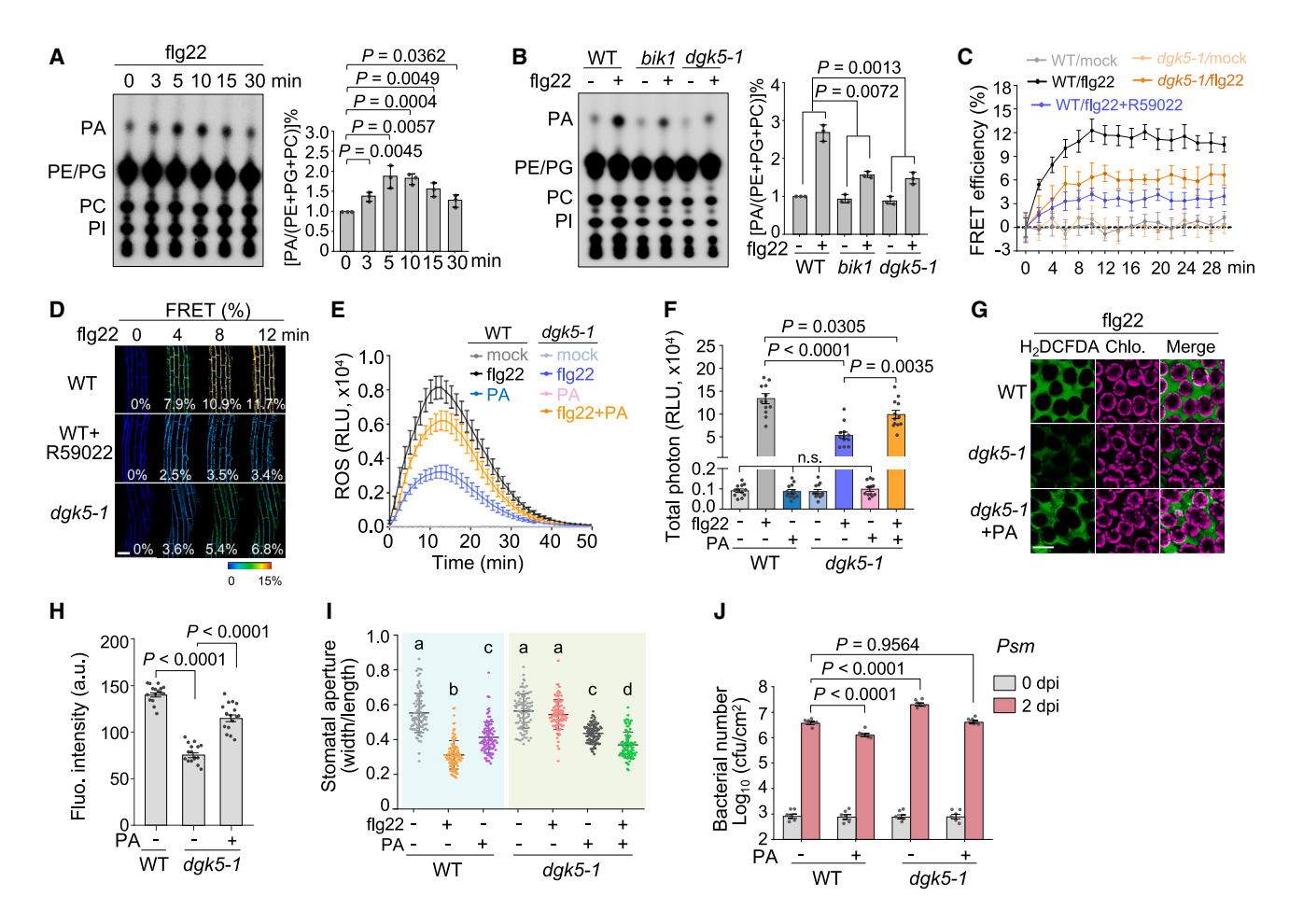


Figure 5. DGK5-mediated PA production regulates ROS burst and plant immunity

(A) Flg22 induces transient PA production. Protoplasts from WT plants were pre-incubated with 32 P-orthophosphate followed by 0.1 μ M flg22 treatment. Total lipids were separated by TLC plate, and phospholipids were detected by autoradiography. Relative band intensities of PA production were normalized to the sum of phosphatidylethanolamine (PE), phosphatidylgycerol (PG), and phosphatidylcholine (PC). The value of the sample without treatment is set as 1.0. Data represent mean \pm SD (n = 3) analyzed by unpaired two-tailed Student's t test.

(B) Flg22-induced PA production is reduced in *dgk5-1* and *bik1* mutants. The experiment (0.1 μM flg22, 5 min) and quantification (n = 3) were performed as in (A). (C and D) Flg22-induced PA production is reduced in *dgk5-1* with a PA biosensor assay. PA production was monitored in root maturation zones of 5-day-old WT or *dgk5-1* seedlings expressing PAleon. R59022 (20 μM) were pre-treated for 1 h, and 0.5 μM flg22 was treated for the indicated time. FRET efficiency (%) was recorded by a confocal microscope. Data represent mean ± SEM (n = 6) (C). Representative confocal images from (C) are shown (D). Scale bars, 50 μm.

(E and F) PA treatment partially restores flg22-induced ROS burst in dgk5-1. Leaf discs from 4-week-old plants were treated with or without 0.1 μ M flg22 and/or 25 μ M PA liposomes for ROS measurement (E). Total ROS is shown as mean \pm SEM (n = 12) (F).

(G and H) PA treatment restores flg22-induced ROS production in dgk5-1 detected by fluorescent dye H₂DCFDA. Leaves of 4-week-old plants were infiltrated with 0.1 μ M flg22 with or without 12.5 μ M PA liposomes for 25 min and then stained with H₂DCFDA for 5 min for confocal imaging (G). Scale bars, 50 μ m. Fluorescence intensities were quantified by ImageJ software, shown as mean \pm SEM (n = 16) (H).

(I) PA treatment partially restores flg22-induced stomatal closure in *dgk5-1*. Stomatal apertures were measured after treatment with 0.1 μM flg22, 25 μM PA liposomes, or in combination. Data represent mean ± SD (n = 93).

(J) PA treatment reduces the susceptibility of dgk5-1 to Psm. Leaves of 4-week-old plants were pre-infiltrated with 10 μ M PA liposomes for 24 h, followed by hand-inoculation with bacteria at 5×10^5 CFU/mL. Data represent mean \pm SEM (n = 6).

Experiments were repeated three (A–I) or four (J) times with similar results. Data in (F and H–J) were analyzed by one-way ANOVA followed by the Tukey's test. n.s., not significant (F). Different letters in (I) denote statistically significant differences (p < 0.05). See also Figure S5.

detected by H₂DCFDA staining in *dgk5-1* (Figures S6C and S6D), further corroborating the role of DGK5 and PA in ETI-induced ROS production.

The dgk5-1 mutant exhibited enhanced susceptibility to Pst avrRpt2 or Pst avrRpm1, and two complementation lines restored the disease susceptibility of dgk5-1 to the WT level

(Figures 7C and S6E). Moreover, *Pst avrRpt2*- or D36E *avrRpt2*-induced total and secreted PR1 proteins were reduced in *dgk5-1* compared with WT (Figure 7D). We did not observe a difference for *Pst avrRpt2*- or D36E *avrRpt2*-induced hypersensitive response (HR) in *dgk5-1* and WT plants (Figure S6F). This aligns with previous reports that disease resistance and HR





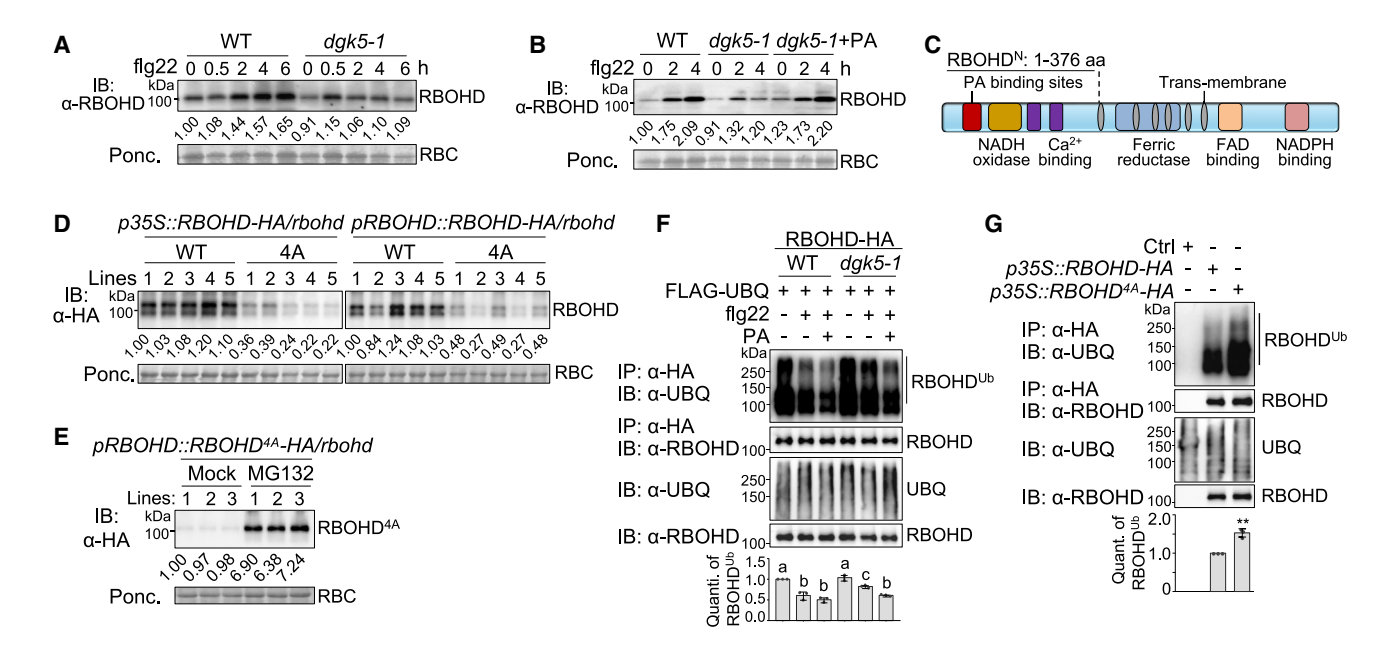


Figure 6. DGK5-mediated PA production regulates RBOHD stability and ubiquitination

(A) Flg22-induced RBOHD protein accumulation is reduced in dgk5-1. RBOHD proteins from 10-day-old seedlings treated with or without 0.1 μ M flg22 were detected by immunoblotting using α -RBOHD antibodies.

- (B) PA treatment restores RBOHD protein accumulation in dgk5-1. The experiment was performed as in (A) with 25 µM PA liposome treatment.
- (C) Diagram of RBOHD domains. Four arginine (R) residues (149, 150, 156, and 157) are important for PA-binding. RBOHD^N: 1–376 aa.
- (D) Mutation of RBOHD PA-binding sites (RBOHD^{4A}) reduces RBOHD protein accumulation. RBOHD or RBOHD^{4A} tagged with $3 \times HA$ under the 35S or native promoter was transformed into rbohd, and multiple transgenic lines were subjected for immunoblotting using α -HA antibodies.
- (E) MG132 stabilizes RBOHD^{4A} proteins in transgenic plants. 10-day-old seedlings of three transgenic lines were treated with 100 μM MG132 or Mock (DMSO) for 4 h.

(F) DGK5-derived PA is involved in flg22-regulated RBOHD ubiquitination. Proteins from protoplasts expressing RBOHD-HA and FLAG-UBQ treated with or without 0.1 μ M flg22, and 10 μ M PA liposomes were immunoprecipitated with α -HA beads and followed by immunoblotting using α -UBQ or α -RBOHD antibodies (top two panels) with input proteins shown (3rd and 4th panels). Quantification of ubiquitinated RBOHD^{Ub} (top panel) was normalized to immunoprecipitated RBOHD (2nd panel) by ImageJ, with the value of WT or no treatment set as 1.0. Data represent mean \pm SD (n = 3). Different letters denote statistically significant differences according to one-way ANOVA followed by the Tukey's test (p < 0.05).

(G) Increased ubiquitination in the RBOHD PA-binding mutant. Proteins were extracted from 10-day-old seedlings and subjected to immunoprecipitation, immunoblotting, and quantification as in (F). Asterisks denote statistically significant differences according to unpaired two-tailed Student's t test. (p < 0.01.) Relative band intensities of RBOHD normalized to protein loading (RBC) were labeled underneath the immunoblotting images (A, B, D, and E), and the value of WT samples and/or mock treatment was set as 1.0. Experiments were repeated three times with similar results.

See also Figure S5.

could be uncoupled. 58,59 Together, our data support that DGK5-derived PA regulates ROS burst and disease resistance in ETI.

The involvement of DGK5 in ETI-mediated ROS production and disease resistance prompted us to investigate whether ETI also induces DGK5 phosphorylation and PA production. Expression of AvrRpt2 or AvrRpm1 induced two phosphorylation patterns of DGK5 in protoplasts (Figures 7E and S6G). In addition, AvrRpt2 also induced PA production at 2, 3, and 4 h after Dex treatment (Figure S6H). Notably, flg22 treatment induced DGK5 phosphorylation and PA production at early time points (5 min) but not at late time points (Figures S6I and S6J). Importantly. AvrRpt2-induced PA production was reduced in dgk5-1 compared with WT plants detected by TLC or PAleon-based FRET assays (Figures 7F and S6K), indicating that DGK5 is required for PA production upon the activation of NLR signaling. Furthermore, DGK5^{S506A} failed to restore, whereas DGK5^{S506D} enhanced D36E avrRpt2-induced ROS production and Pst avrRpt2-mediated disease resistance in dgk5-1 (Figures S7A-

S7C). DGK5^{T446A}, but not DGK5^{T446D}, restored D36E *avrRpt2*-induced ROS production and *Pst avrRpt2*-mediated disease resistance (Figures S7A–S7C). Taken together, the data support that DGK5 phosphorylation-mediated PA production is also involved in plant NLR signaling.

PTI triggers a short-lived ROS burst, which is potentiated by ETI for a sustained ROS production via the activity of RBOHD. 14,15 To investigate whether DGK5 is involved in the PTI-ETI-potentiated ROS production, we monitored flg22-potentiated AvrRpt2-induced ROS production in *Dex::avrRpt2/WT* and *Dex::avrRpt2/dgk5-1* transgenic plants (Figure 7G). As previously reported, 14,15 flg22 treatment triggered a rapid and transient first ROS burst with a peak at 10–20 min and potentiated the second long-lasting ROS burst induced by AvrRpt2 in *Dex::avrRpt2/WT* transgenic plants, denoted as ROSPTI-ETI with a peak at 2–3 h (Figures 7G and 7H). Importantly, flg22-potentiated AvrRpt2-induced second-phase ROS burst (ROSPTI-ETI) is reduced in *Dex::avrRpt2/dgk5-1* plants (Figures 7G and 7H),



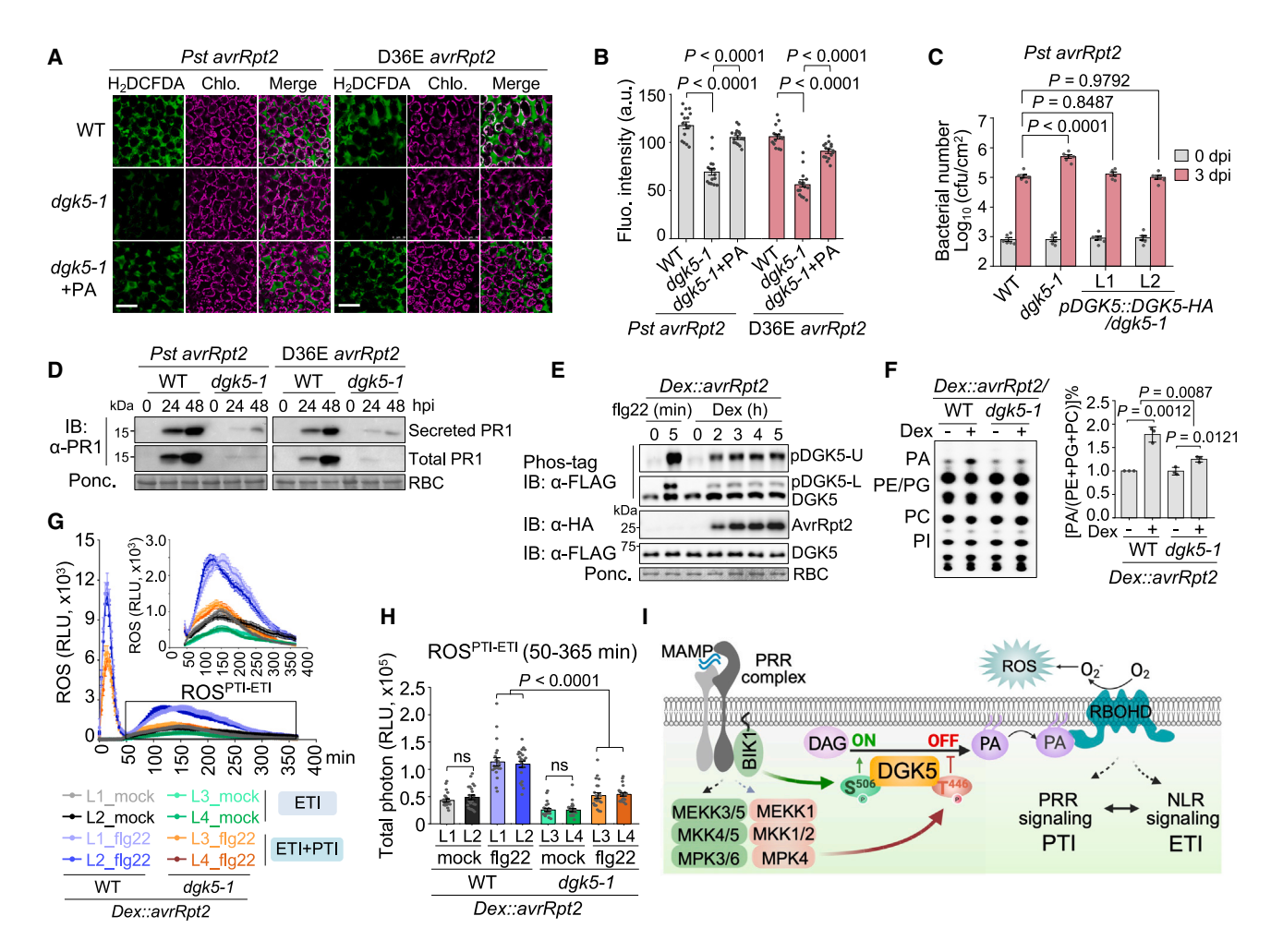


Figure 7. DGK5-mediated PA production is required in ETI signaling

(A and B) PA treatment restores avrRpt2-induced ROS production in dgk5-1. ROS production was detected with H2DCFDA in WT and dgk5-1 leaves 5 h after infiltration of Pst DC3000 avrRpt2 or D36E avrRpt2 at 2 × 107 CFU/mL or in combination with 12.5 µM PA liposomes. Chlo., chlorophyll. Scale bars, 100 µm. Fluorescence intensities were quantified by ImageJ software, shown as mean \pm SEM (n = 16) (B).

(C) Increased susceptibility to Pst DC3000 avrRpt2 in dgk5-1. Leaves of 4-week-old plants were hand-inoculated with bacteria at 5 × 10⁵ CFU/mL. Data represent mean \pm SEM (n = 6).

(D) Reduced PR1 accumulation triggered by Pst DC3000 avrRpt2 and D36E avrRpt2 in dgk5-1. 4-week-old plants were hand-inoculated with bacteria at 5 × 10⁵ CFU/mL. Secreted or total PR1 proteins were detected by immunoblotting using α-PR1 antibodies.

(E) AvrRpt2 induces two DGK5 phosphorylation patterns. Proteins from protoplasts co-expressing Dex::avrRpt2-HA and DGK5-FLAG treated with 2 µM Dex or 0.1 µM flg22 were separated with Mn²⁺-Phos-tag (top two) or regular SDS-PAGE (bottom three), followed by immunoblotting.

(F) AvrRpt2 induces DGK5-dependent PA production. Protoplasts from WT and dgk5-1 expressing Dex::avrRpt2-HA were pre-incubated with 32P-orthophosphate for 2 h, followed by 2 μ M Dex treatment for 3 h. Data represent mean \pm SD (n = 3) analyzed by unpaired two-tailed Student's t test.

(G and H) flg22-potentiated AvrRpt2-induced ROS burst (ROSPTI-ETI) is reduced in dqk5-1. Leaf discs from two lines of Dex::avrRpt2/WT and Dex::avrRpt2/dgk5-1 were treated with 25 μ M Dex and without (mock) or with 0.1 μ M flg22. ROS production was measured as RLU over 365 min (E). ROS burst during 50–365 min (ROS^{PTI-ETI}) was highlighted on top right (G), and total ROS^{PTI-ETI} is shown in (H) as mean \pm SEM (n = 22).

(I) A model of DGK5 phosphorylation by BIK1 and MPK4 in regulating PA homeostasis and plant immunity. MAMP perception by the PRR complex triggers BIK1 phosphorylation and activation of two MAPK cascades. BlK1 phosphorylates DGK5 at Ser⁵⁰⁶ and enhances its activity for PA production. By contrast, PRRactivated MPK4 phosphorylates DGK5 at Thr⁴⁴⁶, leading to a reduced DGK5 activity and PA production. Furthermore, PA binds and stabilizes RBOHD in mediating MAMP-induced ROS production. DGK5-mediated PA production is also required for intracellular NLR receptor RPS2-triggered ROS production and resistance. The figure was created with BioRender.

Experiments were repeated three times with similar results. Data in (B), (C), and (H) were analyzed by one-way ANOVA followed by the Tukey's test. n.s., not significant (H).

See also Figures S6 and S7.

suggesting the involvement of DGK5 in PTI-ETI-potentiated ROS production. In addition, we silenced DGK5 in WT and Dex:: avrRpt2/WT transgenic plants by virus-induced gene silencing (VIGS) targeting two fragments of DGK5 (DGK5-F1 and DGK5-F2) (Figure S7D). Consistently, DGK5-silenced plants (RNAi-DGK5-F1 and -F2) exhibited a reduced flg22-potentiated





AvrRpt2-triggered second-phase ROS burst (ROS^{PTI-ETI}) compared with VIGS-GFP controls in *Dex::avrRpt2* plants (Figures S7E and S7F). The data highlight a role of DGK5-derived PA in mediating ETI and the PTI-ETI potentiation, likely by regulating the ROS production via an action on RBOHD.

DISCUSSION

MAMP-triggered rapid and transient PA production in plants was initially observed two decades ago. 28-32,60 However, the underlying mechanisms remained largely unknown. Our data reveal that RLCK BIK1, a key kinase associated with PRR complexes, interacts with and phosphorylates DGK5 for regulating PA production, providing a molecular link between PRR activation and lipid signaling. Our findings are substantiated by a recent report showing that DGK5 is involved in flg22 signaling and flg22-induced PA burst in Arabidopsis suspension cells.2 We further demonstrate that MAMP perception induces BIK1mediated phosphorylation of DGK5 at Ser506 in activating DGK5 enzymatic activity for a rapid PA burst. Meanwhile, MAMP-activated MPK4 phosphorylates DGK5 at Thr⁴⁴⁶, leading to attenuated PA production. The phospho-regulation of DGK5 is also involved in ETI. As an important second messenger, the spatial and temporal regulation of PA production is essential to maintain normal growth and signaling. PA homeostasis is usually regulated by the coordinated action of PA kinases and phosphatases.⁶¹ Here, our data uncover a mechanism for maintaining PA homeostasis via two uncoupled phosphorylation events of DGK5 at different phosphorylation sites by two distinct kinases that opposingly regulate PA production and plant immunity (Figure 7I).

ROS production is considered a first layer of defense against pathogens because of its toxicity to pathogens and signaling roles.⁵³ PA generation likely functions upstream of the ROS burst since PA inhibitors suppress PTI- and ETI-induced ROS production.³¹ We show here that DGK5-derived PA stabilizes RBOHD and promotes ROS production in plant PTI and ETI, connecting these two crucial second messengers. RBOHD stability is coordinately regulated by protein phosphorylation and ubiquitination.55 We further show that flg22-induced PA counteracts RBOHD ubiquitination, leading to the stabilization of RBOHD. It is conceivable that PA-binding may play a role in regulating RBOHD interactions with kinases or E3 ubiquitin ligases, thereby influencing the phosphorylation and/or ubiquitination status of RBOHD in modulating its stability. DGK5 also plays a role in the regulation of flg22-induced stomatal closure and the production of pathogen-induced PR1. Whether this regulation is dependent or independent of the DGK5-mediated ROS burst remains uncertain. Notably, ROS are recognized as significant regulators of stomatal movement. 62,63 There is a possibility that DGK5derived PA governs ROS production, subsequently modulating stomatal movement during PTI. This aligns with the function of PLD-generated PA in promoting ROS production and inducing stomatal closure in ABA signaling.⁵⁴

Upon phosphorylation, specific regions of proteins could undergo conformational changes, leading to activation or deactivation of protein functions.⁶⁴ In addition, phosphorylation sites are often found in disordered and loop regions, which undergo

conformational changes in a phosphorylation-dependent stimulation (PDS) manner. For instance, phosphorylation in the flexible PDS loop of SUPPRESSOR OF ZEST 12, a subunit of polycomb repressive complex 2, induces a structural conformational change that stabilizes the enzyme's active site, resulting in enhanced enzymatic activity.⁶⁵ In the case of DGK5, our predicted structural analysis shows that Ser506 is located within an intrinsically disordered region at the C terminus, whereas Thr446 is situated within a loop region. Phosphorylation of DGK5 at Ser506 and Thr446 has opposite effects on its enzymatic activity. One plausible explanation is that distinct phosphorylation events may induce different conformational changes in DGK5 within the loop or C-terminal disordered region, leading to either reduced or enhanced activity. Alternatively, phosphorylation of DGK5 at different sites could differentially impact its subcellular localization, interaction with partners, membrane binding, affinity for or accessibility to its substrate DAG, as well as its coactivators such as Mg2+ and ATP, and the release of PA. Future structural analysis of DGK5 in its native state and under phosphorylation mediated by BIK1 or MPK4 will provide insights into how DGK5 exhibits opposing enzymatic activity following distinct phosphorylation

DGK5 is involved in both PTI and ETI, aligning with its role in PTI- and ETI-induced ROS production. It remains unknown how DGK5 is activated during ETI. Recent studies suggest the convergence and reciprocal enhancement between PTI and ETI. BIK1 is a convergent point connecting PTI- and ETI-mediated ROS production and immunity. Nonetheless, it remains unclear whether BIK1 or other RLCKs also contribute to the regulation of DGK5 phosphorylation for PA and ROS production in ETI. ROS burst generated by RBOHD represents a critical early signaling event connecting PTI and ETI. PA regulates the RBOHD stability for ROS production, thereby facilitating the convergence and potentiation of two branches of plant immunity.

Limitations of the study

Our findings underscore the pivotal role of DGK5 in orchestrating the PA burst, which, in turn, regulates ROS production in PTI and ETI. Other enzymes, such as PLDs, also generate PA and contribute to plant defense response.^{28,35} Presently, distinguishing PA produced by DGK5 and that generated by other enzymes poses a significant technical challenge. It is plausible that the regulation of enzymes, such as DGK5 by BIK1 and MPK4 in PTI, serves as a primary determinant in shaping the specific PA production in response to distinct stimuli. Our study highlights that PA produced by DGK5 plays a role in regulating ETImediated disease resistance rather than HR. Notably, exogenous application of high concentrations of PA could induce cell death.³² It remains formidable to ascertain whether endogenous PA induced in ETI could reach such high levels in triggering cell death. In addition, the methods we used to monitor in vivo PA alterations, including ³²P-orthophosphate labeling and FRETbased PA biosensor PAleon, detect the newly synthesized or PM-based PA changes. Nevertheless, the effect of DGK5 on cellular PA levels and homeostasis remains unexplored, particularly related to the plant response to pathogen defense.





STAR*METHODS

Detailed methods are provided in the online version of this paper and include the following:

- KEY RESOURCES TABLE
- RESOURCE AVAILABILITY
 - Lead contact
 - Materials availability
 - Data and code availability
- EXPERIMENTAL MODEL AND STUDY PARTICIPANT **DETAILS**
 - O Arabidopsis thaliana and growth conditions
 - O Nicotiana benthamiana and growth conditions
 - O Bacterial and yeast strains
- METHOD DETAILS
 - O Plasmid construction and transgenic plant generation
 - O Yeast two-hybrid (Y2H) assay
 - O Protoplast isolation and co-immunoprecipitation (Co-IP) assays
 - O Recombinant protein isolation and in vitro kinase assays
 - Immunocomplex kinase assay
 - Pull-down assay
 - O Bimolecular fluorescence complementation (BiFC) and FRET-FLIM assays
 - O Pathogen infection and hypersensitive response assays
 - O Detection of ROS burst
 - O Detection of PR1 proteins
 - O MAPK activation and in vivo DGK5 mobility shift assays
 - O Total RNA isolation and RT-qPCR analysis
 - O Measurement of stomatal aperture
 - Mass spectrometry analysis of phosphorylation sites
 - In vitro diacylglycerol kinase activity assay
 - In vivo and in vitro PA detection
 - Protein accession number
- QUANTIFICATION AND STATISTICAL ANALYSIS

SUPPLEMENTAL INFORMATION

Supplemental information can be found online at https://doi.org/10.1016/j.cell. 2023.12.030.

ACKNOWLEDGMENTS

We thank Arabidopsis Biological Resource Center (ABRC) for providing T-DNA insertion lines, Drs. Wenhua Zhang (Nanjing Agricultural University, China) and Chris Staiger (Purdue University, USA) for providing PAleon transgenic plants and construct, Dr. Fumiaki Katagiri (University of Minnesota, USA) for providing D36E and D36E avrRpt2 strains, and members of the laboratories of L.S. and P.H. for discussions and comments. The study was supported by the National Science Foundation (NSF) (IOS-1951094, MCB-1906060) and the National Institutes of Health (NIH) (R35GM149197) to P.H., NIH (R35GM144275) and NSF (IOS-2049642) to L.S.

AUTHOR CONTRIBUTIONS

X.M., L.K., P.H., and L.S. conceived the project, designed experiments, and analyzed data. X.M. identified DGK5; generated transgenic plants; and performed phenotypical, phosphorylation, and interaction assays. L.K. performed microscopic, lipid, phenotypical, phosphorylation, and interaction assays. C.Z. performed in vivo PA assays. S.-I.K. contributed to DGK5 in ETI. B.L. performed the initial transgenic and biochemical assays. Y.X. contributed to DGK5 in RLP signaling. I.-C.Y. contributed to lipid assays. H.T. in T.P.D.'s laboratory established DGK activity assays. S.C. identified DGK5 phosphorylation sites. T.M. contributed to disease and lipid assays. L.K., X.M., P.H., and L.S. wrote the manuscript with input from all authors.

DECLARATION OF INTERESTS

The authors declare no competing interests.

Received: April 17, 2023 Revised: October 5, 2023 Accepted: December 21, 2023 Published: January 19, 2024

REFERENCES

- 1. Jones, J.D., and Dangl, J.L. (2006). The plant immune system. Nature 444,
- 2. Zhou, J.M., and Zhang, Y. (2020). Plant immunity: danger perception and signaling. Cell 181, 978-989.
- 3. Ngou, B.P.M., Jones, J.D.G., and Ding, P. (2022). Plant immune networks. Trends Plant Sci. 27, 255-273.
- 4. Lopes Fischer, N., Naseer, N., Shin, S., and Brodsky, I.E. (2020). Effectortriggered immunity and pathogen sensing in metazoans. Nat. Microbiol. 5, 14-26
- 5. Ausubel, F.M. (2005). Are innate immune signaling pathways in plants and animals conserved? Nat. Immunol. 6, 973-979.
- 6. DeFalco, T.A., and Zipfel, C. (2021). Molecular mechanisms of early plant pattern-triggered immune signaling. Mol. Cell 81, 4346.
- 7. Saijo, Y., Loo, E.P., and Yasuda, S. (2018). Pattern recognition receptors and signaling in plant-microbe interactions. Plant J. 93, 592-613.
- 8. Yu, X., Feng, B., He, P., and Shan, L. (2017). From chaos to harmony: responses and signaling upon microbial pattern recognition. Annu. Rev. Phytopathol. 55, 109-137.
- 9. Böhm, H., Albert, I., Fan, L., Reinhard, A., and Nürnberger, T. (2014). Immune receptor complexes at the plant cell surface. Curr. Opin. Plant Biol. 20, 47-54.
- 10. Lolle, S., Stevens, D., and Coaker, G. (2020). Plant NLR-triggered immunity: from receptor activation to downstream signaling. Curr. Opin. Immunol. 62, 99-105.
- 11. Cui, H., Tsuda, K., and Parker, J.E. (2015). Effector-triggered immunity: from pathogen perception to robust defense. Annu. Rev. Plant Biol. 66, 487-511.
- 12. Tsuda, K., and Katagiri, F. (2010). Comparing signaling mechanisms engaged in pattern-triggered and effector-triggered immunity. Curr. Opin. Plant Biol. 13, 459-465.
- 13. Thomma, B.P., Nürnberger, T., and Joosten, M.H. (2011). Of PAMPs and effectors: the blurred PTI-ETI dichotomy. Plant Cell 23, 4-15.
- 14. Ngou, B.P.M., Ahn, H.-K., Ding, P., and Jones, J.D.G. (2021). Mutual potentiation of plant immunity by cell-surface and intracellular receptors. Nature 592, 110-115.
- 15. Yuan, M., Jiang, Z., Bi, G., Nomura, K., Liu, M., Wang, Y., Cai, B., Zhou, J.-M., He, S.Y., and Xin, X.-F. (2021). Pattern-recognition receptors are required for NLR-mediated plant immunity. Nature 592, 105–109.
- 16. Tian, H., Wu, Z., Chen, S., Ao, K., Huang, W., Yaghmaiean, H., Sun, T., Xu, F., Zhang, Y., Wang, S., et al. (2021). Activation of TIR signalling boosts pattern-triggered immunity. Nature 598, 500-503.
- 17. Pruitt, R.N., Locci, F., Wanke, F., Zhang, L., Saile, S.C., Joe, A., Karelina, D., Hua, C., Fröhlich, K., Wan, W.-L., et al. (2021). The EDS1-PAD4-ADR1





- node mediates Arabidopsis pattern-triggered immunity. Nature 598, 495–499.
- Yoon, H., Shaw, J.L., Haigis, M.C., and Greka, A. (2021). Lipid metabolism in sickness and in health: emerging regulators of lipotoxicity. Mol. Cell 81, 3708–3730.
- Cannon, A.E., and Chapman, K.D. (2021). Lipid signaling through G proteins. Trends Plant Sci. 26, 720–728.
- Xing, J., Zhang, L., Duan, Z., and Lin, J. (2021). Coordination of phospholipid-based signaling and membrane trafficking in plant immunity. Trends Plant Sci. 26, 407–420.
- Kim, S.C., and Wang, X. (2020). Phosphatidic acid: an emerging versatile class of cellular mediators. Essays Biochem. 64, 533–546.
- 22. Fan, R., Zhao, F., Gong, Z., Chen, Y., Yang, B., Zhou, C., Zhang, J., Du, Z., Wang, X., Yin, P., et al. (2023). Insights into the mechanism of phospholipid hydrolysis by plant non-specific phospholipase C. Nat. Commun. 14, 194.
- Munnik, T., and Testerink, C. (2009). Plant phospholipid signaling: "in a nutshell". J. Lipid Res. 50 (Suppl), S260–S265.
- Testerink, C., and Munnik, T. (2011). Molecular, cellular, and physiological responses to phosphatidic acid formation in plants. J. Exp. Bot. 62, 2349–2361
- Arisz, S.A., Testerink, C., and Munnik, T. (2009). Plant PA signaling via diacylglycerol kinase. Biochim. Biophys. Acta 1791, 869–875.
- Arisz, S.A., van Wijk, R., Roels, W., Zhu, J.K., Haring, M.A., and Munnik, T. (2013). Rapid phosphatidic acid accumulation in response to low temperature stress in Arabidopsis is generated through diacylglycerol kinase. Front. Plant Sci. 4. 1.
- Cacas, J.L., Gerbeau-Pissot, P., Fromentin, J., Cantrel, C., Thomas, D., Jeannette, E., Kalachova, T., Mongrand, S., Simon-Plas, F., and Ruelland, E. (2017). Diacylglycerol kinases activate tobacco NADPH oxidasedependent oxidative burst in response to cryptogein. Plant Cell Environ. 40, 585-598
- Xing, J., Li, X., Wang, X., Lv, X., Wang, L., Zhang, L., Zhu, Y., Shen, Q., Baluška, F., Šamaj, J., and Lin, J. (2019). Secretion of phospholipase Dô functions as a regulatory mechanism in plant innate immunity. Plant Cell 31, 3015–3032.
- 29. Kalachova, T., Škrabálková, E., Pateyron, S., Soubigou-Taconnat, L., Djafi, N., Collin, S., Sekereš, J., Burketová, L., Potocký, M., Pejchar, P., and Ruelland, E. (2022). DIACYLGLYCEROL KINASE 5 participates in flagellin-induced signaling in Arabidopsis. Plant Physiol. 190, 1978–1996.
- van der Luit, A.H., Piatti, T., van Doorn, A., Musgrave, A., Felix, G., Boller, T., and Munnik, T. (2000). Elicitation of suspension-cultured tomato cells triggers the formation of phosphatidic acid and diacylglycerol pyrophosphate. Plant Physiol. 123, 1507–1516.
- de Jong, C.F., Laxalt, A.M., Bargmann, B.O.R., de Wit, P.J.G.M., Joosten, M.H.A.J., and Munnik, T. (2004). Phosphatidic acid accumulation is an early response in the Cf-4/Avr4 interaction. Plant J. 39, 1–12.
- Andersson, M.X., Kourtchenko, O., Dangl, J.L., Mackey, D., and Ellerström, M. (2006). Phospholipase-dependent signalling during the AvrRpm1- and AvrRpt2-induced disease resistance responses in Arabidopsis thaliana. Plant J. 47, 947–959.
- D'Ambrosio, J.M., Couto, D., Fabro, G., Scuffi, D., Lamattina, L., Munnik, T., Andersson, M.X., Álvarez, M.E., Zipfel, C., and Laxalt, A.M. (2017). Phospholipase C2 affects MAMP-triggered immunity by modulating ROS Production. Plant Physiol. 175, 970–981.
- Kiba, A., Nakano, M., Hosokawa, M., Galis, I., Nakatani, H., Shinya, T., Ohnishi, K., and Hikichi, Y. (2020). Phosphatidylinositol-phospholipase C2 regulates pattern-triggered immunity in Nicotiana benthamiana. J. Exp. Bot. 71, 5027–5038.
- 35. Schlöffel, M.A., Salzer, A., Wan, W.L., van Wijk, R., Del Corvo, R., Šemanjski, M., Symeonidi, E., Slaby, P., Kilian, J., Maček, B., et al. (2020). The BIR2/BIR3-associated phospholipase Dγ1 negatively regulates plant immunity. Plant Physiol. 183, 371–384.

- Thor, K., Jiang, S., Michard, E., George, J., Scherzer, S., Huang, S., Dindas, J., Derbyshire, P., Leitão, N., Defalco, T.A., et al. (2020). The calcium-permeable channel OSCA1.3 regulates plant stomatal immunity. Nature 585, 569–573.
- Tian, W., Hou, C., Ren, Z., Wang, C., Zhao, F., Dahlbeck, D., Hu, S., Zhang, L., Niu, Q., Li, L., et al. (2019). A calmodulin-gated calcium channel links pathogen patterns to plant immunity. Nature 572, 131–135.
- Kadota, Y., Sklenar, J., Derbyshire, P., Stransfeld, L., Asai, S., Ntoukakis, V., Jones, J.D., Shirasu, K., Menke, F., Jones, A., and Zipfel, C. (2014). Direct regulation of the NADPH oxidase RBOHD by the PRR-associated kinase BIK1 during plant immunity. Mol. Cell 54, 43–55.
- Li, L., Li, M., Yu, L., Zhou, Z., Liang, X., Liu, Z., Cai, G., Gao, L., Zhang, X., Wang, Y., et al. (2014). The FLS2-associated kinase BIK1 directly phosphorylates the NADPH oxidase RbohD to control plant immunity. Cell Host Microbe 15, 329–338.
- Ma, X., Claus, L.A.N., Leslie, M.E., Tao, K., Wu, Z., Liu, J., Yu, X., Li, B., Zhou, J., Savatin, D.V., et al. (2020). Ligand-induced monoubiquitination of BIK1 regulates plant immunity. Nature 581, 199–203.
- Lu, D., Wu, S., Gao, X., Zhang, Y., Shan, L., and He, P. (2010). A receptor-like cytoplasmic kinase, BIK1, associates with a flagellin receptor complex to initiate plant innate immunity. Proc. Natl. Acad. Sci. USA 107, 496–501.
- Albert, I., Böhm, H., Albert, M., Feiler, C.E., Imkampe, J., Wallmeroth, N., Brancato, C., Raaymakers, T.M., Oome, S., Zhang, H., et al. (2015). An RLP23-SOBIR1-BAK1 complex mediates NLP-triggered immunity. Nat. Plants 1, 15140.
- Zhang, L., Hua, C., Pruitt, R.N., Qin, S., Wang, L., Albert, I., Albert, M., Van Kan, J.A.L., and Nürnberger, T. (2021). Distinct immune sensor systems for fungal endopolygalacturonases in closely related Brassicaceae. Nat. Plants 7, 1254–1263.
- 44. Lal, N.K., Nagalakshmi, U., Hurlburt, N.K., Flores, R., Bak, A., Sone, P., Ma, X., Song, G., Walley, J., Shan, L., et al. (2018). The receptor-like cytoplasmic kinase BIK1 localizes to the nucleus and regulates defense hormone expression during plant innate immunity. Cell Host Microbe 23, 485–497.e5.
- Mirdita, M., Schütze, K., Moriwaki, Y., Heo, L., Ovchinnikov, S., and Steinegger, M. (2022). ColabFold: making protein folding accessible to all. Nat. Methods 19. 679–682.
- Jacobs, D., Glossip, D., Xing, H.M., Muslin, A.J., and Kornfeld, K. (1999).
 Multiple docking sites on substrate proteins form a modular system that mediates recognition by ERK MAP kinase. Genes Dev. 13, 163–175.
- Bi, G., Zhou, Z., Wang, W., Li, L., Rao, S., Wu, Y., Zhang, X., Menke, F.L.H., Chen, S., and Zhou, J.M. (2018). Receptor-like cytoplasmic kinases directly link diverse pattern recognition receptors to the activation of mitogen-activated protein kinase cascades in Arabidopsis. Plant Cell 30, 1543–1561.
- Asai, T., Tena, G., Plotnikova, J., Willmann, M.R., Chiu, W.L., Gomez-Gomez, L., Boller, T., Ausubel, F.M., and Sheen, J. (2002). MAP kinase signal-ling cascade in Arabidopsis innate immunity. Nature 415. 977–983.
- Sun, T., Nitta, Y., Zhang, Q., Wu, D., Tian, H., Lee, J.S., and Zhang, Y. (2018). Antagonistic interactions between two MAP kinase cascades in plant development and immune signaling. EMBO Rep. 19, e45324.
- Yu, X., Li, B., Jang, G.J., Jiang, S., Jiang, D., Jang, J.C., Wu, S.H., Shan, L., and He, P. (2019). Orchestration of processing body dynamics and mRNA decay in Arabidopsis immunity. Cell Rep. 28, 2194–2205.e6.
- Berriri, S., Garcia, A.V., Frei dit Frey, N., Rozhon, W., Pateyron, S., Leonhardt, N., Montillet, J.L., Leung, J., Hirt, H., and Colcombet, J. (2012).
 Constitutively active mitogen-activated protein kinase versions reveal functions of Arabidopsis MPK4 in pathogen defense signaling. Plant Cell 24, 4281–4293.
- Li, W., Song, T., Wallrad, L., Kudla, J., Wang, X., and Zhang, W. (2019). Tissue-specific accumulation of pH-sensing phosphatidic acid determines plant stress tolerance. Nat. Plants 5, 1012–1021.

Cell **Article**



- 53. Castro, B., Citterico, M., Kimura, S., Stevens, D.M., Wrzaczek, M., and Coaker, G. (2021). Stress-induced reactive oxygen species compartmentalization, perception and signalling. Nat. Plants 7, 403-412.
- 54. Zhang, Y., Zhu, H., Zhang, Q., Li, M., Yan, M., Wang, R., Wang, L., Welti, R., Zhang, W., and Wang, X. (2009). Phospholipase dalpha1 and phosphatidic acid regulate NADPH oxidase activity and production of reactive oxygen species in ABA-mediated stomatal closure in Arabidopsis. Plant Cell 21, 2357-2377.
- 55. Lee, D., Lal, N.K., Lin, Z.D., Ma, S., Liu, J., Castro, B., Toruño, T., Dinesh-Kumar, S.P., and Coaker, G. (2020). Regulation of reactive oxygen species during plant immunity through phosphorylation and ubiquitination of RBOHD. Nat. Commun. 11, 1838.
- 56. Wei, H.L., Chakravarthy, S., Mathieu, J., Helmann, T.C., Stodghill, P., Swingle, B., Martin, G.B., and Collmer, A. (2015). Pseudomonas syringae pv. tomato DC3000 type III secretion effector polymutants reveal an interplay between HopAD1 and AvrPtoB. Cell Host Microbe 17, 752-762.
- 57. Hatsugai, N., Igarashi, D., Mase, K., Lu, Y., Tsuda, Y., Chakravarthy, S., Wei, H.L., Foley, J.W., Collmer, A., Glazebrook, J., and Katagiri, F. (2017). A plant effector-triggered immunity signaling sector is inhibited by pattern-triggered immunity. EMBO J. 36, 2758-2769.
- 58. Sun, X., Lapin, D., Feehan, J.M., Stolze, S.C., Kramer, K., Dongus, J.A., Rzemieniewski, J., Blanvillain-Baufumé, S., Harzen, A., Bautor, J., et al. (2021). Pathogen effector recognition-dependent association of NRG1 with EDS1 and SAG101 in TNL receptor immunity. Nat. Commun. 12, 3335.
- 59. Gao, X., Chen, X., Lin, W., Chen, S., Lu, D., Niu, Y., Li, L., Cheng, C., Mc-Cormack, M., Sheen, J., et al. (2013). Bifurcation of Arabidopsis NLR immune signaling via Ca²⁺-dependent protein kinases. PLoS Pathog. 9, e1003127.
- 60. den Hartog, M., Verhoef, N., and Munnik, T. (2003). Nod factor and elicitors activate different phospholipid signaling pathways in suspension-cultured alfalfa cells. Plant Physiol. 132, 311-317.
- 61. Kumar Sah, R., Garg, S., Dangi, P., Ponnusamy, K., and Singh, S. (2019). Phosphatidic acid homeostasis regulated by a type-2 phosphatidic acid phosphatase represents a novel druggable target in malaria intervention. Cell Death Discov. 5, 107.
- 62. Rodrigues, O., and Shan, L. (2022). Stomata in a state of emergency: H₂O₂ is the target locked. Trends Plant Sci. 27, 274-286.
- 63. Hou, S., Rodrigues, O., Liu, Z., Shan, L., and He, P. (2023). Small holes, big impact: stomata in plant-pathogen-climate epic trifecta. Published online December 1, 2023. Mol. Plant.
- 64. Ubersax, J.A., and Ferrell, J.E., Jr. (2007). Mechanisms of specificity in protein phosphorylation. Nat. Rev. Mol. Cell Biol. 8, 530-541.
- 65. Gong, L., Liu, X., Jiao, L., Yang, X., Lemoff, A., and Liu, X. (2022). CK2mediated phosphorylation of SUZ12 promotes PRC2 function by stabilizing enzyme active site. Nat. Commun. 13, 6781.
- 66. Kong, L., Feng, B., Yan, Y., Zhang, C., Kim, J.H., Xu, L., Rack, J.G.M., Wang, Y., Jang, J.C., Ahel, I., et al. (2021). Noncanonical mono(ADP-ribo-

- syl)ation of zinc finger SZF proteins counteracts ubiquitination for protein homeostasis in plant immunity. Mol. Cell 81, 4591-4604.e8.
- 67. Kariola, T., Brader, G., Li, J., and Palva, E.T. (2005). Chlorophyllase 1, a damage control enzyme, affects the balance between defense pathways in plants. Plant Cell 17, 282-294.
- 68. Lu, D., Lin, W., Gao, X., Wu, S., Cheng, C., Avila, J., Heese, A., Devarenne, T.P., He, P., and Shan, L. (2011). Direct ubiquitination of pattern recognition receptor FLS2 attenuates plant innate immunity. Science 332, 1439-1442.
- 69. Lin, W., Li, B., Lu, D., Chen, S., Zhu, N., He, P., and Shan, L. (2014). Tyrosine phosphorylation of protein kinase complex BAK1/BIK1 mediates Arabidopsis innate immunity. Proc. Natl. Acad. Sci. USA 111, 3632-3637.
- 70. Li, B., Jiang, S., Yu, X., Cheng, C., Chen, S., Cheng, Y., Yuan, J.S., Jiang, D., He, P., and Shan, L. (2015). Phosphorylation of trihelix transcriptional repressor ASR3 by MAP KINASE4 negatively regulates Arabidopsis immunity. Plant Cell 27, 839-856.
- 71. Hou, S., Liu, D., Huang, S., Luo, D., Liu, Z., Xiang, Q., Wang, P., Mu, R., Han, Z., Chen, S., et al. (2021). The Arabidopsis MIK2 receptor elicits immunity by sensing a conserved signature from phytocytokines and microbes. Nat. Commun. 12, 5494.
- 72. Liu, J., Huang, Y., Kong, L., Yu, X., Feng, B., Liu, D., Zhao, B., Mendes, G.C., Yuan, P., Ge, D., et al. (2020). The malectin-like receptor-like kinase LETUM1 modulates NLR protein SUMM2 activation via MEKK2 scaffolding. Nat. Plants 6, 1106-1115.
- 73. Li, F., Cheng, C., Cui, F., de Oliveira, M.V., Yu, X., Meng, X., Intorne, A.C., Babilonia, K., Li, M., Li, B., et al. (2014). Modulation of RNA polymerase II phosphorylation downstream of pathogen perception orchestrates plant immunity. Cell Host Microbe 16, 748-758.
- 74. Gao, X., Chen, X., Lin, W., Chen, S., Lu, D., Niu, Y., Li, L., Cheng, C., Mc-Cormack, M., Sheen, J., et al. (2013). Bifurcation of Arabidopsis NLR immune signaling via Ca²⁺-dependent protein kinases. PLoS Pathog 9, e1003127.
- 75. He, P., Shan, L., and Sheen, J. (2007). The use of protoplasts to study innate immune responses. Methods Mol. Biol. 354, 1-9.
- 76. Fagard, M., Dellagi, A., Roux, C., Périno, C., Rigault, M., Boucher, V., Shevchik, V.E., and Expert, D. (2007). Arabidopsis thaliana expresses multiple lines of defense to counterattack Erwinia chrysanthemi. Mol. Plant Microbe Interact. 20, 794-805.
- 77. Yao, D., Arguez, M.A., He, P., Bent, A.F., and Song, J. (2021). Coordinated regulation of plant immunity by poly(ADP-ribosyl)ation and K63-linked ubiquitination. Mol. Plant 14, 2088-2103.
- 78. Liu, Z., Hou, S., Rodrigues, O., Wang, P., Luo, D., Munemasa, S., Lei, J., Liu, J., Ortiz-Morea, F.A., Wang, X., et al. (2022). Phytocytokine signalling reopens stomata in plant immunity and water loss. Nature 605, 332-339.
- 79. Gómez-Merino, F.C., Brearley, C.A., Ornatowska, M., Abdel-Haliem, M.E., Zanor, M.I., and Mueller-Roeber, B. (2004). AtDGK2, a novel diacylglycerol kinase from Arabidopsis thaliana, phosphorylates 1-stearoyl-2arachidonoyl-sn-glycerol and 1,2-dioleoyl-sn-glycerol and exhibits coldinducible gene expression. J. Biol. Chem. 279, 8230-8241.





STAR***METHODS**

KEY RESOURCES TABLE

REAGENT or RESOURCE	SOURCE	IDENTIFIER
Antibodies		
Rat anti-HA-Peroxidase	Roche	Cat#12013819001; RRID: AB_390917
Nouse anti-FLAG-Peroxidase	Sigma-Aldrich	Cat#A8592; RRID: AB_439702
Mouse anti-GFP	Roche	Cat#11814460001; RRID: AB_390913
Mouse anti-cMYC-HRP	Biolegend	Cat#626803; RRID: AB_2572009
Nouse anti-HIS-Peroxidase	Roche	Cat#11965085001; RRID: AB_514487
Mouse anti-GST-Peroxidase	Sigma-Aldrich	Cat#16-209; RRID: AB_310805
Rabbit anti-UBQ11	Agrisera	Cat#AS08 307; RRID: AB_2256904
Rabbit anti-MPK4	Sigma-Aldrich	Cat#6979; RRID: AB_476758
Rabbit anti-pERK1/2	Cell Signaling	Cat#9101; RRID: AB_331646
Anti-mouse IgG HRP-linked antibody	Cell Signaling	Cat#7076; RRID: AB_330924
Anti-rabbit IgG HRP-linked antibody	Cell Signaling	Cat#7074; RRID: AB_2099233
Rabbit anti-PR1	Agrisera	Cat#AS10 687; RRID: AB_10751750
Rabbit anti-RBOHD	Agrisera	Cat#AS15 2962; RRID: AB_3065190
Bacterial and virus strains		
Agrobacterium tumefaciens GV3101	Kong et al. ⁶⁶	N/A
Escherichia coli BL21 (DE3)	Kong et al. ⁶⁶	N/A
Pseudomonas syringae pv. tomato DC3000 (Pst)	Kong et al. ⁶⁶	N/A
P. syringae pv. maculicola ES4326 (Psm)	Kong et al. ⁶⁶	N/A
Pst avrRpt2	Kong et al. ⁶⁶	N/A
Pst avrRpm1	Yu et al. ⁵⁰	N/A
carotovora subsp. carotovora SCC1	Kariola et al. ⁶⁷	N/A
Pst D36E	Hatsugai et al. ⁵⁷	N/A
Pst D36E avrRpt2	Hatsugai et al. ⁵⁷	N/A
Chemicals, peptides, and recombinant proteins		
MG132	Sigma-Aldrich	Cat#99533-80-9
TRIzol™ Reagent	Thermo Scientific	Cat#15596018
(252a	Cell Signaling	Cat#12754S
PD184161	MedChemExpress (MCE)	Cat#HY-10174
-phosphatase	New England Biolabs	Cat#P0753S
RNase-free DNase I	New England Biolabs	Cat#M0303L
sopropyl-β-D-thiogalactopyranoside (IPTG)	Sigma-Aldrich	Cat#16758
	Sigma-Aldrich	Cat#4902
Dexamethasone	Sigma-Aldrich Perkin Elmer	
Dexamethasone ² P-ATP	Perkin Elmer	Cat#BLU502A001MC
Dexamethasone		Cat#BLU502A001MC Cat#NEX053001MC
Dexamethasone P-ATP P-Phosphorus, orthophosphoric acid in water Coomassie brilliant blue (CBB) R-250	Perkin Elmer Perkin Elmer Thermo Scientific	Cat#BLU502A001MC Cat#NEX053001MC Cat#20278
Dexamethasone PP-ATP P-Phosphorus, orthophosphoric acid in water Coomassie brilliant blue (CBB) R-250 Soy Phosphatidic acid (PA)	Perkin Elmer Perkin Elmer Thermo Scientific Avanti Polar Lipids	Cat#BLU502A001MC Cat#NEX053001MC Cat#20278 Cat#840074
Dexamethasone P-ATP P-Phosphorus, orthophosphoric acid in water Coomassie brilliant blue (CBB) R-250 Soy Phosphatidic acid (PA) ,2-dioctadecanoyl-sn-glycerol (DOG)	Perkin Elmer Perkin Elmer Thermo Scientific Avanti Polar Lipids Avanti Polar Lipids	Cat#BLU502A001MC Cat#NEX053001MC Cat#20278 Cat#840074 Cat#800820
Dexamethasone 2P-ATP 2P-Phosphorus, orthophosphoric acid in water Coomassie brilliant blue (CBB) R-250 Soy Phosphatidic acid (PA) ,2-dioctadecanoyl-sn-glycerol (DOG) -stearoyl-2-arachidonoyl-sn-glycerol (SAG)	Perkin Elmer Perkin Elmer Thermo Scientific Avanti Polar Lipids Avanti Polar Lipids Cayman Chemical	Cat#BLU502A001MC Cat#NEX053001MC Cat#20278 Cat#840074 Cat#800820 Cat#10008650
Dexamethasone 2P-ATP 2P-ATP 2P-Phosphorus, orthophosphoric acid in water Coomassie brilliant blue (CBB) R-250 Soy Phosphatidic acid (PA) ,2-dioctadecanoyl-sn-glycerol (DOG) -stearoyl-2-arachidonoyl-sn-glycerol (SAG) 859022	Perkin Elmer Perkin Elmer Thermo Scientific Avanti Polar Lipids Avanti Polar Lipids Cayman Chemical Sigma-Aldrich	Cat#BLU502A001MC Cat#NEX053001MC Cat#20278 Cat#840074 Cat#800820 Cat#10008650 Cat#D5919
Dexamethasone PP-ATP P-Phosphorus, orthophosphoric acid in water Coomassie brilliant blue (CBB) R-250 Soy Phosphatidic acid (PA) ,2-dioctadecanoyl-sn-glycerol (DOG) -stearoyl-2-arachidonoyl-sn-glycerol (SAG) R59022 SelCode Blue Stain Reagent	Perkin Elmer Perkin Elmer Thermo Scientific Avanti Polar Lipids Avanti Polar Lipids Cayman Chemical Sigma-Aldrich Thermo Scientific	Cat#BLU502A001MC Cat#NEX053001MC Cat#20278 Cat#840074 Cat#800820 Cat#10008650 Cat#D5919 Cat#24590
Dexamethasone 2P-ATP 2P-ATP 2P-Phosphorus, orthophosphoric acid in water Coomassie brilliant blue (CBB) R-250 Soy Phosphatidic acid (PA) ,2-dioctadecanoyl-sn-glycerol (DOG) -stearoyl-2-arachidonoyl-sn-glycerol (SAG) 859022	Perkin Elmer Perkin Elmer Thermo Scientific Avanti Polar Lipids Avanti Polar Lipids Cayman Chemical Sigma-Aldrich	Cat#BLU502A001MC Cat#NEX053001MC Cat#20278 Cat#840074 Cat#800820 Cat#10008650 Cat#D5919

(Continued on next page)





Continued			
REAGENT or RESOURCE	SOURCE	IDENTIFIER	
Anti-HA magnetic beads	Thermo Scientific	Cat#88837	
GFP-Trap agarose beads	Chromotek	Cat#gta-20	
ierce glutathione agarose	Thermo Scientific	Cat#16101	
mylose resin	New England Biolabs	Cat#E8021L	
łisPur™ Ni-NTA Resin	Thermo Scientific	Cat#88222	
RNase-free DNase I	New England Biolabs	Cat#M0303L	
uminol	Sigma-Aldrich	Cat#A8511	
Peroxidase from horseradish	Sigma-Aldrich	Cat#P6782	
2',7'-dichlorofluorescein diacetate (H ₂ DCFDA)	Sigma-Aldrich	Cat#D6883	
g22	Lu et al. ⁶⁸	N/A	
9 lf18	Kadota et al. ³⁸	N/A	
ep1	Ma et al. ⁴⁰	N/A	
g23	Zhang et al. ⁴³	N/A	
lp20	Albert et al. ⁴²	N/A	
/yelin basic protein (MBP)	Sigma-Aldrich	Cat#13-104	
-	oigina-Aldiloii	Gath 10 104	
Critical commercial assays	Now England Distant	Cot#M0052I	
M-MuLV Reverse Transcriptase	New England Biolabs	Cat#M0253L	
Taq SYBR green Supermix	Bio-Rad	Cat#1725124	
ClonExpress II one Step Cloning Kit	Vazyme	Cat#C112-02	
experimental models: Organisms/strains			
Arabidopsis thaliana Col-0 wild-type	Lu et al.41	N/A	
rabidopsis thaliana Ler-0 ecotype	Yu et al. ⁵⁰	N/A	
Arabidopsis: dgk5-1	ABRC	SAIL_1212_E10	
Arabidopsis: dgk5-2	ABRC	SAIL_127_B03	
Arabidopsis: bik1	Lu et al. ⁴¹	N/A	
Arabidopsis: fls2	Lu et al. ⁴¹	SALK_141277	
Arabidopsis: mpk4 in Ler-0 background	Yu et al. ⁵⁰	CS5205	
Arabidopsis: mpk6/Dex-amiR-MPK3	Yu et al. ⁵⁰	N/A	
Arabidopsis: pDGK5::DGK5-HA/dgk5-1	This paper	N/A	
rabidopsis: p35S::DGK5-HA/dgk5-1	This paper	N/A	
rabidopsis: pDGK5::DGK5-HA/p35S::BIK1-GFP	This paper	N/A	
Arabidopsis: pDGK5::DGK5 ^{S506A} -HA/dgk5-1	This paper	N/A	
Arabidopsis: pDGK5::DGK5 ^{S506D} -HA/dgk5-1	This paper	N/A	
Arabidopsis: pDGK5::DGK5 ^{T446A} -HA/dgk5-1	This paper	N/A	
Arabidopsis: pDGK5::DGK5 ^{T446D} -HA/dgk5-1	This paper	N/A	
Arabidopsis: pRBOHD::RBOHD-3×HA/rbohd	This paper	N/A	
Arabidopsis: pRBOHD::RBOHD ^{4A} -3×HA/rbohd	This paper	N/A	
rabidopsis: p35S::RBOHD-3×HA/rbohd	This paper	N/A	
rabidopsis: p35S::RBOHD ^{4A} -3×HA/rbohd	This paper	N/A	
rabidopsis: pRBOHD::RBOHD ^N -3×HA/rbohd	This paper	N/A	
rabidopsis: pRBOHD::RBOHD ^{N-4A} -3×HA/rbohd	This paper	N/A	
rabidopsis: p35S::RBOHD ^N -3×HA/rbohd	This paper	N/A	
rabidopsis: p35S::RBOHD ^{N-4A} -3×HA/rbohd	This paper	N/A	
rabidopsis: Dex::avrRpt2/WT	This paper	N/A	
rabidopsis: Dex::avrRpt2/dgk5-1	This paper	N/A	
rabidopsis: PAleon/WT	Li et al. ⁵²	N/A	
Arabidopsis: PAleon/dgk5-1	This paper	N/A	
Saccharomyces cerevisiae strain AH109	Kong et al. ⁶⁶	N/A	

(Continued on next page)





Continued				
REAGENT or RESOURCE	SOURCE	IDENTIFIER		
Nicotiana benthamiana	Kong et al. ⁶⁶	N/A		
Digonucleotides				
Primers for cloning and point mutation, see Table S1	This paper	N/A		
Primers for genotyping, see Table S1	This paper	N/A		
Primers for RT-qPCR and VIGS, see Table S1	This paper	N/A		
Recombinant DNA	- Pode			
HBT	Lu et al. ⁴¹	N/A		
hHBT-GFP-FLAG	Kong et al. ⁶⁶	N/A		
HBT-BIK1-FLAG	Ma et al. ⁴⁰	N/A		
HBT-BIK1 ^{KM} -FLAG	Lu et al. ⁴¹	N/A		
HBT-DGK5-FLAG	This paper	N/A		
HBT-DGK5-HA	This paper	N/A		
HBT-DGK5 ^{S506A} -HA	This paper	N/A		
HBT-DGK5 ^{T446A} -HA	This paper	N/A		
HBT-DGK5 ^{S463A} -HA	This paper	N/A		
HBT-DGK5 ^{T478A} -HA	This paper	N/A		
HBT-DGK5 ^{S488A} -HA	This paper	N/A		
HBT-RBOHD-HA	This paper	N/A		
	Kong et al. ⁶⁶	N/A		
HBT-FLAG-UBQ HBT-Dex::avrRpt2-HA	This paper	N/A		
•		N/A		
HBT-Dex::avrRpm1-HA	This paper Lin et al. ⁶⁹			
HBT-nYFP		N/A		
HBT-DGK5-nYFP	This paper	N/A		
HBT-BAK1-nYFP	Lin et al. ⁶⁹	N/A		
HBT-cYFP	Lin et al. ⁶⁹	N/A		
HBT-BIK1-cYFP	Lin et al. ⁶⁹	N/A		
HBT-BAK1-cYFP	Lin et al. ⁶⁹	N/A		
HBT-DGK5-GFP	This paper	N/A		
HBT-BIK1-GFP	Ma et al. ⁴⁰	N/A		
HBT-BAK1-GFP	Kong et al. ⁶⁶	N/A		
HBT-DGK5-mCherry	This paper	N/A		
HBT-BIR2-mCherry	Kong et al. ⁶⁶	N/A		
HBT-MPK4-mCherry	This paper	N/A		
HBT-FLS2-FLAG	Lu et al.41	N/A		
HBT-BAK1-FLAG	Lu et al.41	N/A		
HBT-MPK4-FLAG	Yu et al. ⁵⁰	N/A		
HBT-MPK4-HA	Yu et al. ⁵⁰	N/A		
HBT-MPK6-FLAG	Yu et al. ⁵⁰	N/A		
HBT-MPK3-FLAG	Yu et al. ⁵⁰	N/A		
HBT-MKP-MYC	Yu et al. ⁵⁰	N/A		
GADT7-DGK5-HA	This paper	N/A		
GADT7-DGK5 ₃₁₇₋₅₀₉ -HA	This paper	N/A		
GADT7-DGK5 ₃₁₇₋₄₈₄ -HA	This paper	N/A		
GADT7-DGK5 ₂₃₄₋₅₀₉ -HA	This paper	N/A		
GBKT7-BIK1 ^{G2A} -MYC	Ma et al.40	N/A		
GST	This paper	N/A		
GST-DGK5	This paper	N/A		
GST-DGK5 ^{S495A}	This paper	N/A		
GST-DGK5 ^{S500A}	This paper	N/A		

(Continued on next page)





Continued		
REAGENT or RESOURCE	SOURCE	IDENTIFIER
pGST-DGK5 ^{S506A}	This paper	N/A
oMAL	Lin et al. ⁶⁹	N/A
oMAL-BIK1-HA	Lin et al. ⁶⁹	N/A
pGST-BIK1	Lin et al. ⁶⁹	N/A
oGST-BIK1 ^{KM}	Lin et al. ⁶⁹	N/A
oGST-BAK1 ^{KD}	Lin et al. ⁶⁹	N/A
pMAL-BAK1 ^{CD}	Lin et al. ⁶⁹	N/A
DET28a-MBP	This paper	N/A
ET28a-DGK5	This paper	N/A
DET28a-DGK5 ^{S506A}	This paper	N/A
DET28a-DGK5 ^{T446A}	This paper	N/A
DET28a-DGK5 ^{S506D}	This paper	N/A
DET28a-DGK5 ^{T446D}	This paper	N/A
DET28a-DGK5 ^{T446D/S506D}	This paper	N/A
DET28a-BIK1	Lin et al. ⁶⁹	N/A
pGST-MPK4 ^{ac}	Berriri et al. ⁵¹	N/A
DET28a-PBL30	This paper	N/A
ET28a-PBL31	This paper	N/A
PAleon	Li et al. ⁵²	N/A
CB302-p35S::DGK5-HA	This paper	N/A
CB302-pDGK5::DGK5-HA	This paper	N/A
CB302-p35S::BIK1-GFP	Ma et al. ⁴⁰	N/A
CAMBIA1300-pRBOHD::RBOHD-3×HA		N/A
CAMBIA1300-pRBOHD::RBOHD ^{4A} -3×HA	This paper	N/A
	This paper	N/A
CAMBIA1300-p35S::RBOHD-3×HA CAMBIA1300-p35S::RBOHD ^{4A} -3×HA	This paper	N/A
•	This paper	
CAMBIA1300-pRBOHD::RBOHD ^N -3×HA	This paper	N/A
CAMBIA1300-pRBOHD::RBOHD ^{N-4A} -3×HA	This paper	N/A
CAMBIA1300-p35S::RBOHD ^N -3×HA	This paper	N/A
CAMBIA1300-p35S::RBOHD ^{N-4A} -3×HA	This paper	N/A
9YL156-DGK5-F1	This paper	N/A
bYL156-DGK5-F2	This paper	N/A
Software and algorithms		
mageJ	NIH	https://imagej.nih.gov/ij/; RRID:SCR_003070
Proteome discoverer 3.1	Thermo Scientific	https://www.thermofisher.com/order/ catalog/product/B51001472?SID= srch-hj-B51001472; RRID:SCR_014477
Biorender	Biorender	https://www.biorender.com/; RRID:SCR_018361
eica Application Suite X (LAS X) software	Leica	https://www.leica-microsystems.com/ products/microscope-software/p/ leica-las-x-ls/; RRID:SCR_013673
GraphPad Prism 9	GraphPad software	https://www.graphpad.com/; RRID: SCR_002798
Photoshop CS	Adobe	https://www.adobe.com/products/ photoshop.html; RRID:SCR_014199
ChimeraX 1.6.1	UCSF	https://www.cgl.ucsf.edu/chimerax/; RRID:SCR_015872





RESOURCE AVAILABILITY

Lead contact

Further information and requests for resources and reagents should be directed to and will be fulfilled by the Lead Contact, Libo Shan (liboshan@umich.edu).

Materials availability

Plasmids and transgenic plants generated in this study will be made available on request to the scientific community, but we may require a payment and/or a completed Materials Transfer Agreement.

Data and code availability

- The published article includes all datasets generated or analyzed during this study. All data are publicly available as of the date
 of publication.
- This paper does not report original code.
- Any additional information required to reanalyze the data reported in this paper is available from the lead contact upon request.

EXPERIMENTAL MODEL AND STUDY PARTICIPANT DETAILS

Arabidopsis thaliana and growth conditions

All *Arabidopsis* plants were grown in soil (Metro Mix 366, Sunshine LP5 or Sunshine LC1, Jolly Gardener C/20 or C/Gs, USA) in a growth chamber at 20-23°C, 50% relative humidity, and 75-100 µE m⁻² s⁻¹ light with a 12-h light/12-h dark photoperiod for four or five weeks before pathogen infection assay, protoplast isolation, and ROS assay. For confocal microscopy imaging, seeds were sterilized, stratified for 2 days at 4°C in the dark, and germinated on vertical half-strength Murashige and Skoog (½MS) medium plates containing 1% (w/v) sucrose, 0.5% agar and 2.5 mM MES at pH 5.8, and grown under the same condition as above for another 5 days. For MAPK activation, Co-IP, protein stability, and RT-qPCR assays, seedlings grown on ½MS plates for 3-5 days were transferred to ½MS liquid medium for another 5 days before treatment with different chemicals or MAMPs.

Nicotiana benthamiana and growth conditions

Nicotiana benthamiana was grown in a growth room in soil under a 12-h light/12-h dark photoperiod at 23°C.

Bacterial and yeast strains

The yeast and bacterial strains used in this study were described in the key resources table. The Saccharomyces cerevisiae AH109 strain was grown on the Yeast extract Peptone Dextrose Adenine (YPDA) medium (10 g yeast extract, 20 g peptone, 20 g glucose, 40 mg adenine hemisulfate for 1 L) plate. Pseudomonas syringae pv. tomato (Pst) DC3000 was grown on the King's B (KB) medium (10 g protease peptone, $0.75 \, \mathrm{g} \, \mathrm{K}_2 \mathrm{HPO}_4 \cdot 3 \mathrm{H}_2 \mathrm{O}$, $7.5 \, \mathrm{g} \, \mathrm{agar}$, $10 \, \mathrm{ml} \, 50\%$ glycerol for $500 \, \mathrm{ml}$) plate with $50 \, \mu \mathrm{g/ml}$ rifampicin. Pst DC3000 carrying avrRpt2 or avrRpm1 was grown on the KB medium plates with $50 \, \mu \mathrm{g/ml}$ kanamycin and $50 \, \mu \mathrm{g/ml}$ rifampicin. Pst D36E and Pst D36E avrRpt2 were grown on the KB medium plates with $50 \, \mu \mathrm{g/ml}$ rifampicin, $50 \, \mu \mathrm{g/ml}$ of spectinomycin, and $30 \, \mu \mathrm{g/ml}$ of kanamycin. P. syringae pv. maculicola ES4326 (Psm) was grown on the KB medium plate with $50 \, \mu \mathrm{g/ml}$ streptomycin. Erwinia carotovora subsp carotovora (now called Pectobacterium carotovorum) strain SCC1 was grown on Luria-Bertani (LB) medium (10 g tryptone, $5 \, \mathrm{g}$ yeast extract, $10 \, \mathrm{g} \, \mathrm{NaCl}$, $15 \, \mathrm{g} \, \mathrm{gagr}$ for $1 \, \mathrm{L}$) plate with $50 \, \mu \mathrm{g/ml}$ ampicillin. All the Pseudomonas strains were grown on plates at $28 \, ^{\circ} \mathrm{C}$ for $2 \, \mathrm{days}$, and further cultured overnight at $28 \, ^{\circ} \mathrm{C}$ in KB liquid medium supplemented with $2 \, \mathrm{mM} \, \mathrm{MgSO_4}$ and appropriate antibiotics as described above. E. carotovora subsp carotovora strain SCC1 was grown on plates at $28 \, ^{\circ} \mathrm{C}$ for $2 \, \mathrm{days}$, and then cultured overnight at $28 \, ^{\circ} \mathrm{C}$ in LB medium.

METHOD DETAILS

Plasmid construction and transgenic plant generation

FLS2, BAK1, BIK1, BIK1, MPK3, MPK4, MPK6, MKP, or BIR2 tagged with HA, FLAG, GFP, mCherry, nYFP, or cYFP in a plant gene expression vector *pHBT* under the CaMV 35S promoter for protoplast assays, and BAK1^{CD}, BIK1, or BIK1, or BIK1 with GST or MBP





for fusion protein isolation from Escherichia coli have been described previously. 40,41,50,69,70,72,73 The cDNA of DGK5 was amplified from Col-0 cDNA library with primers containing BamHI at the 5'-terminus and Stul at the 3'-terminus, followed by digestion with BamHI and Stul and ligated into the pHBT vector with the HA, FLAG, mCherry, or GFP epitope tag at the C-terminus. The cDNA of RBOHD was amplified from Col-0 cDNA library and ligated into the pHBT vector with the 3×HA tag using the ClonExpress II One-Step Cloning Kit (Vazyme, China) according to the manufactural protocols. The RBOHD^{4A}, RBOHD^N, and RBOHD^{N-4A} mutants were cloned using the full-length RBOHD as the template with primers listed in Table S1. The DGK5 mutant variants, including $DGK5^{S495A}$, $DGK5^{S500A}$, $DGK5^{S506A}$, $DGK5^{T446A}$, $DGK5^{S463A}$, $DGK5^{S488A}$, $DGK5^{S488A}$, and $DGK5^{S506D}$ in a pHBT vector were generated by site-directed mutagenesis with primers listed in Table S1 using DGK5 as the template. PBL30, PBL31, DGK5, DGK5^{S495A}, DGK5^{S500A}, DGK5^{S506A}, DGK5^{T446A}, DGK5^{T446A}, or DGK5^{S506D} were sub-cloned into a modified GST or HIS fusion protein expression vector pGEX4T-1 (Pharmacia, USA) or pET28a-SUMO⁷² using BamHI and Stul digestion. The BIK1^{G2A}, DGK5, and its truncation variants, including DGK5₃₁₇₋₅₀₉, DGK5₃₁₇₋₄₈₄, and DGK5₂₃₄₋₅₀₉ in a pHBT vector, were sub-cloned into pGADT7 (AD) and pGBKT7 (Clontech, USA) for yeast two-hybrid (Y2H) assays using BamHI and Stul digestion. The MPK4 fragment released from pHBT-p35S::MPK4-HA by BamHI and Stul digestion was ligated into the pHBT vector with a mCherry tag at the C-terminus to obtain the pHBT-p35S::MPK4-mCherry vector. MPK4ac was generated based on the previous publication,51 and sub-cloned into pGEX4T-1 for GST fusion protein isolation. The fragments of avrRpt2 and avrRpm1 were amplified and ligated into the pHBT vector under Dexamethasone (Dex)-inducible promoter with a 2×HA epitope tag using Spel and Stul digestion.⁷⁴

To make binary constructs, DGK5 was sub-cloned into the binary vector pCB302 with BamHI and Stul digestion to generate pCB302-p35S::DGK5-HA. The promoter of DGK5 (~2,000 bp upstream of the start codon) was PCR-amplified from Col-0 genomic DNA with primers containing SacI and BamHI, and ligated into a pHBT vector. The fragment of pDGK5::DGK5-HA was digested by Sacl and EcoRI, and ligated into pCAMBIA1300 to generate pCAMBIA1300-pDGK5::DGK5-HA. DGK5^{S506A/D} and DGK5^{T446A/D} were sub-cloned into pCAMBIA1300 vector with BamHI and Stul digestion to generate pCAMBIA1300-pDGK5::DGK5^{S506A/D}-HA and pCAMBIA1300-pDGK5::DGK5^{T446A/D}-HA, respectively. RBOHD, RBOHD^{AA}, RBOHD^N, and RBOHD^{N-4A} in a pHBT vector were sub-cloned into pCAMBIA1300 with the 3×HA tag to obtain pCAMBIA1300-p35S::RBOHD/RBOHD^{AA}/RBOHD^N/RBOHD^{N-4A}-3HA using the ClonExpress II One-Step Cloning Kit (Vazyme, China) with primers listed in Table S1. The RBOHD promoter (~2 kb upstream of the start codon) was amplified from Col-0 genomic DNA using primers containing KpnI and BamHI to replace the 35S promoter in pCAMBIA1300 to obtain pCAMBIA1300-pRBOHD::RBOHD/RBOHD^{4A}/RBOHD^N/RBOHD^{N-4A}-3HA.

To construct the pYL156 vectors for virus-induced gene silencing (VIGS) assays, two \sim 500 bp fragments of DGK5 coding region without predicted off-targets were designed using the Solanaceae Genomics Network (https://solgenomics.net), amplified using DGK5 as the template with primers containing EcoRl and Kpnl, and individually ligated into pYL156 to generate pYL156-DGK5-F1 and pYL156-DGK5-F2, respectively.

Primer sequences were listed in Table S1, and all insertions in different vectors were verified by Sanger sequencing.

Transgenic plants were generated using Agrobacterium tumefaciens-mediated floral dipping. Transgenic plants were screened by glufosinate-ammonium (Basta, 50 µg/ml) for the pCB302 vector or hygromycin (50 µg/ml) for pCAMBIA1300, and confirmed by immunoblotting for protein expression.

Yeast two-hybrid (Y2H) assay

To identify BIK1-interacting proteins, a Y2H screen was performed as reported using pGBKT7-BIK1^{G2A} as the bait towards the Arabidopsis cDNA library constructed in a modified pGADT7 vector (Clontech, USA). 40,66 Briefly, among 196 strong interacting colonies screened from \sim 120,000 transformants, DGK5 was identified from 14 individual colonies. DGK5 and truncation variants DGK5₃₁₇₋₅₀₉, DGK5₃₁₇₋₄₈₄, and DGK5₂₃₄₋₅₀₉ in the pHBT vector were sub-cloned into a modified pGADT7 (Clontech, USA) vector with BamHI and Stul digestion. pGADT7-DGK5, pGADT7-DGK5317-509, pGADT7-DGK5317-484, or pGADT7-DGK5234-509 was introduced into the yeast strain AH109 expressing pGBKT7-BIK1^{G2A} using the polyethylene glycol/LiAc-mediated yeast transformation. The yeast colonies containing both indicated genes were selected on the synthetic defined (SD) medium without leucine and tryptophan (SD-LT), and interaction was tested on the SD medium without leucine, tryptophan, and histidine (SD-LTH) supplemented with 1 mM 3-amino-1, 2, 4-triazole (3-AT).

Protoplast isolation and co-immunoprecipitation (Co-IP) assays

Protoplast isolation and gene expression assays have been described previously. For protoplast-based Co-IP assays, protoplasts were transfected with a pair of constructs (the empty vector as a control, 100 μg DNA for 500 μl protoplasts at a density of 2×10⁵/mL for each sample) and incubated at 25°C for 6-12 h. After treatment with flg22 at the indicated concentration and time points, protoplasts were collected by centrifugation and lysed in 300 µl IP buffer (50 mM Tris-HCl, pH 7.5, 150 mM NaCl, 5 mM EDTA, 0.5-1% Triton X-100, 1 × protease inhibitor EDTA-free cocktail, 2 mM DTT, 2 mM NaF, and 2 mM Na₃VO₃) by vortexing. After centrifugation at 10,000 g for 5-10 min at 4°C, 30 μl of supernatant was collected for input control, and 7 μl α-FLAG agarose or magnetic beads were added into the remaining supernatant and incubated at 4°C for 1-3 h. Beads were collected and washed three times with washing buffer (50 mM Tris-HCl, pH 7.5, 150 mM NaCl, 5 mM EDTA, 0.5% Triton X-100) and once with 50 mM Tris-HCl, pH 7.5. Immunoprecipitates were analyzed by immunoblotting with indicated antibodies. For transgenic plant-based Co-IP assays, two-week-old seedlings grown on ½MS plates were transferred to water overnight and treated with flg22 at the indicated concentration and time points described in the figure legends. One gram of transgenic seedlings (fresh weight) was ground into powders with liquid nitrogen before





adding 3 ml of IP buffer and vortexing. After centrifugation at 10,000 g for 10 min at 4°C, 50 μl of supernatant was collected for input control, and 10 µl GFP-trap agarose beads (Chromotek, Germany) were added into the remaining supernatant and incubated at 4°C for 1-3 h. The remaining procedures are similar to protoplast-based Co-IP assays.

Recombinant protein isolation and in vitro kinase assays

Fusion proteins in E. coli BL21 (DE3) strain were induced in LB medium (1% tryptone, 0.5% yeast extracts, 1% NaCl) supplemented with 0.25 mM Isopropyl β -D-1-thiogalactopyranoside (IPTG) at 18°C for 12-18 h. Maltose binding protein (MBP) fusion proteins were purified using amylose resin (New England Biolabs, USA), Glutathione S-transferase (GST) fusion proteins were purified with Pierce glutathione agarose (Thermo Scientific, USA), and HIS fusion proteins were purified with Pierce Ni-NTA agarose beads (Thermo Scientific, USA) according to the manufacture protocols.

The in vitro kinase assays were carried out with 0.5 μg of indicated kinase proteins and 5 μg of substrate proteins in 30 μl kinase reaction buffer (10 mM Tris-HCl, pH 7.5, 5 mM MgCl₂, 2.5 mM EDTA, 50 mM NaCl, 0.5 mM DTT, 50 μ M ATP, and 1 μ Ci [γ -³²P]-ATP). After shaking at the speed of 60 g for 2 h at 24°C, the reactions were stopped by adding 4 × SDS loading buffer, and proteins were separated by 10% SDS-PAGE. Phosphorylated proteins were analyzed by autoradiography.

Immunocomplex kinase assay

Protoplasts were transfected with MPK3-FLAG, MPK4-FLAG, or MPK6-FLAG for 6-12 h before treatment with 100 nM flg22 for 10 min. MPK proteins were immunoprecipitated with 10 μl of α-FLAG agarose beads, washed twice with IP buffer and once with a kinase reaction buffer (10 mM Tris-HCl, pH 7.5, 5 mM MgCl₂, 2.5 mM EDTA, 50 mM NaCl, 0.5 mM DTT). The immobilized MPK protein beads were then incubated with 5 µg of myelin basic proteins (MBP, Upstate, USA) or GST-DGK5 proteins in 30 µl kinase reaction buffer containing 50 μ M ATP and 1 μ Ci [γ - 32 P]-ATP for 2 h at 24 $^{\circ}$ C on a rocker. Protein samples were denatured with 4 × SDS loading buffer and separated by 10% SDS-PAGE. Phosphorylation was analyzed by autoradiography.

Pull-down assay

Recombinant GST or GST-DGK5 proteins were incubated with 10 µl pre-washed glutathione agarose beads in 300 µl incubation buffer (20 mM Tris-HCl, pH 7.5, 100 mM NaCl, 0.1 mM EDTA, and 0.2% Triton X-100) at 4°C for 30 min on a rotator. Immobilized protein beads were washed twice with washing buffer (20 mM Tris-HCl, pH7.5, 300 mM NaCl, 0.1mM EDTA, and 0.1% Triton X-100), followed by incubation with 20 μg bovine serum albumin (BSA, Sigma-Aldrich, USA) in 300 μl incubation buffer at 4°C for 30 min. Protein beads were washed twice with washing buffer and then incubated with 2 µg MBP, MBP-BIK1-HA, or HIS-MPK4 proteins in 300 µl incubation buffer at 4°C for another 1 h in a mini shaker at a speed of 60 rpm. Protein beads were collected and washed three to four times with the washing buffer. Proteins were analyzed by immunoblotting with indicated antibodies.

Bimolecular fluorescence complementation (BiFC) and FRET-FLIM assays

For BiFC assays, protoplasts were transfected with different pairs of BiFC constructs, as shown in the figures. Fluorescence signals in protoplasts were examined 12 h after transfection using Leica TCS SP8 laser scanning confocal microscope (Germany). The excitation wavelengths of YFP and autofluorescence of chlorophyll are 514 nm and 630 nm, respectively. The emission wavelengths for YFP and chlorophyll are 490-530 and 640-700 nm, respectively. The pinhole was set at 1 Airy unit. Imaging analyses were performed using Leica Application Suite X (LAS X) software.

The FRET-FLIM assay was performed as described previously.⁶⁶ Briefly, protoplasts were transfected with different pairs of GFP and mCherry constructs, as indicated in the figures. Fluorescence signals were examined 12 h after transfection under the confocal microscope. The FRET-FLIM was analyzed using LAS X software. The excitation wavelengths of GFP and mCherry are 488 nm and 588 nm, respectively. The emission wavelengths for GFP and mCherry are 495-540 and 590-620 nm, respectively. The GFP fluorescence lifetime (τ) in a specific region of interest (ROI) was measured by Leica LAS X software. The GFP fluorescence lifetime (τ) shown in the figures was calculated as an average of 14 randomly measured protoplasts for each pair of proteins. The FRET efficiency (E) was calculated by the formula $[E = 1 - (\tau_{DA}/\tau_D)]$ (where τ_{DA} represents the GFP lifetime of the donor in the presence of the acceptor; τ_D represents the GFP lifetime of the donor alone). The statistical analysis was performed using one-way ANOVA followed by Tukey's test for multiple comparisons.

Pathogen infection and hypersensitive response assays

Pseudomonas syringae and Erwinia carotovora were collected by centrifugation at 1200 g, washed twice, and re-suspended to the desired concentration with 10 mM MgCl₂ or 0.9% NaCl. Leaves from four-week-old plants were hand-inoculated with the Pseudomonas bacterial suspension using a needleless syringe. The Erwinia carotovora SCC1 infection assay was performed as reported previously. 67,76 Briefly, small cavities were made in four-week-old plant leaves using a needle, into which 5 μl of a bacterial suspension in 0.9% NaCl (2×10' CFU/ml) was inoculated, and disease symptom was recorded at 36 h after inoculation. For flg22-primed protection assays, leaves were pre-inoculated with 100 nM flg22 or ddH₂O as control at 24 h before bacterial pathogen infiltration. To measure in planta bacterial growth, two leaf discs were punched and ground in 100 μl ddH₂O. Serial dilutions were plated on TSA medium (1% tryptone, 1% sucrose, 0.1% glutamic acid, and 1.5% agar) containing 25 μg/ml rifamycin or streptomycin. Plates were incubated at 28°C, and bacterial colony-forming units (cfu) were counted at 0, 2, and 4 days post-incubation.





For hypersensitive response (HR) assays, Pst DC3000 avrRpt2 and D36E avrRpt2 suspensions were prepared as described above, and bacterial suspension at OD₆₀₀ = 0.2 was syringe-infiltrated into leaves. Infiltrated plants were covered by a plastic dome for 30 min, and then kept under 40-50% humidity for about 9 h before tissue collapse was recorded. Fully expanded leaves at a similar developmental stage were chosen (about 3 leaves per plant) for the bacterial inoculation. Wounded leaves caused by infiltration were discarded in the final counting.

Detection of ROS burst

ROS measurement was performed using a luminol-based approach as previously described with minor modifications.⁶⁸ In brief, the third or fourth pair of true leaves from four-week-old soil-grown Arabidopsis plants were punched into leaf discs using a cork borer (5 mm in diameter). Leaf discs were incubated in 150 µl ddH₂O in a 96-well plate overnight with gentle shaking on a rocker with a 12-h light/12-h dark photoperiod. Water was replaced with 100 μl reaction solution containing 50 μM luminol and 10 μg/ml horseradish peroxidase (Sigma-Aldrich, USA) supplemented with or without 100 nM flg22, in combination with or without 25 μM PA liposomes produced from soy PA (Avanti Polar Lipids Inc., USA). The PA liposomes were prepared as previously described with some modifications.⁵⁴ Briefly, 1 mM soy PA dissolved in chloroform was dried under a stream of nitrogen vapor. Lipid films were rehydrated in icecold buffer (25 mM HEPES, pH 7.5, 50 mM KCl, 1 mM MgCl₂), and then sonicated for 5 min (5 cycles of 10 sec-on and 10 sec-off) using the Branson SFX 250 Sonifier (Emerson, USA) at 4°C. The equal volume of chloroform was processed in the same manner and used as mock control. Luminescence was measured by a luminometer (GloMax-Multi Detection System, Promega, USA) for a period of 50 min or 6-7 h with an integration time of 1 or 2 sec. For ROS detection by 2',7'-dichlorofluorescein diacetate (H₂DCFDA) under the confocal microscope, three-week-old soil-grown Arabidopsis plants were infiltrated with 0.1 µM flg22, Pst DC3000 avrRpt2, D36E, or D36E avrRpt2 at OD₆₀₀ of 0.02, and plants were kept in growth rooms after infiltrated leaves dried in the air. After 4 to 5 h, 10 µM H₂DCFDA solution was infiltrated into leaves, and the fluorescent signal was detected 10 min later. Images were captured using a Leica SP8 confocal microscope with a 488 nm excitation and 500-550 nm emission, and chlorophyll auto-fluorescence was detected with a 630 nm excitation and 640-700 nm emission.

Detection of PR1 proteins

Total and secreted PR1 proteins were extracted as previously described. The brief, four-week-old WT and dgk5-1 plants were infiltrated with Pst DC3000, Pst DC3000 avrRpt2, or D36E avrRpt2 at OD₆₀₀ = 0.001. Inoculated leaves were collected at the indicated time points, and two leaves were lysed in 100 μ l IP buffer to detect total PR1 protein. For detecting secreted PR1 proteins, detached inoculated leaves were vacuumed in a solution buffer (100 mM Tris-HCl, pH 7.8, 500 mM sucrose, 10 mM MgCl₂, 10 mM CaCl₂, 1 mM β -mercaptoethanol, and 1×protein inhibitor cocktail) using a 20 ml needleless-syringe, followed by removing the solution completely. The 20 ml needleless syringe containing the leaves was placed in a 50 ml tube for centrifugation at 1500 g (5 min, 4°C) to obtain the secreted PR1 proteins. Total and secreted proteins were separated on 12.5% SDS-PAGE for immunoblotting with α -PR1 antibodies (Agrisera, Sweden).

MAPK activation and in vivo DGK5 mobility shift assays

Three 10-day-old *Arabidopsis* seedlings grown on vertical ½MS plates were transferred into water overnight before 100 nM flg22 treatment for the indicated time. Seedlings were collected, ground, and lysed in 100 μ l IP buffer. Protein samples were denatured with 4 × SDS loading buffer and separated by 12.5% SDS-PAGE to detect phosphorylated MPK3, MPK6, and MPK4 by immunoblotting with α -pERK1/2 antibodies (Cell Signaling, USA). Goat α -rabbit IgG-HRP (Cell Signaling, USA) was used as the secondary antibodies.

For *in vivo* DGK5 mobility shift assay, total proteins were separated in the 8% SDS-PAGE containing 15 or 30.5 μ M Phos-tagTM (FUJIFILM Wako Chemicals, Japan) and 100 μ M MnCl₂, and immunoblotted with α -HA-HRP (1:2000, Roche, USA) or α -FLAG-HRP antibodies (1:2000, Sigma-Aldrich, USA). For Phos-tag SDS-PAGE, the molecular weight cannot be exactly indicated. For relative phosphorylation of DGK5 (pDGK5), upper and lower band intensities of phosphorylated DGK5 (pDGK5-U and pDGK5-L) and unphosphorylated DGK5 were quantified by ImageJ or Image Lab software. The relative pDGK5-U and pDGK5-L represent the ratio of phosphorylated to unphosphorylated DGK5, respectively.

Total RNA isolation and RT-qPCR analysis

Total RNA was isolated from two-week-old seedlings grown on ½MS plate with or without 100 nM flg22 treatment using TRIzol reagent (Invitrogen, USA). One microgram of total RNA was treated with RNase-free DNase I (NEB, USA), and then was reverse transcribed to synthesize the first-strand cDNA with M-MuLV reverse transcriptase (NEB, USA) and oligo (dT)18 primer. The quantitative RT-PCR (RT-qPCR) was performed using iTaq SYBR green Supermix (Bio-Rad, USA) with primers listed in Table S1 in a Bio-Rad CFX384 Real-Time PCR System (Bio-Rad, USA). The expression of indicated genes was normalized to *UBQ10*. The data analysis was performed using unpaired two-tailed Student's *t*-test.

Measurement of stomatal aperture

Stomatal apertures were measured as previously described with minor modifications.⁷⁸ In brief, epidermal peels excised from the abaxial side of leaves of three-week-old soil-grown plants were used for stomatal aperture measurement. To detect flg22-induced





stomatal closure, epidermal peels from WT and dgk5-1 plants were incubated in a bathing solution (30 mM KCI, 10 µM CaCl₂, 10 mM MES, pH 6.0) under light for 2-3 h to induce maximal stomatal opening, and then followed by treatment with 1 µM flg22, 25 µM PA liposomes produced from soy PA (Avanti Polar Lipids Inc., USA), or a combination of flg22 and PA liposomes for another 2 h. Stomatal apertures were monitored after the indicated treatments. The width and the length of the stomatal aperture were measured using Leica SP8 LAS X software, and the stomatal aperture index was calculated by dividing the aperture width by the length as described.⁷⁸

Mass spectrometry analysis of phosphorylation sites

To identify DGK5 phosphorylation sites, DGK5-FLAG was expressed in *Arabidopsis* protoplasts (∼10 ml at a concentration of 2 x 10⁵/ml) for 12 h and treated with 0.1 μM flg22 for 10 min. Protoplasts were then lysed with lysis buffer (20 mM Tris-HCl, pH 7.5, 100 mM NaCl, 10% glycerol, 0.5-1% Triton X-100, 1mM EDTA, 2 mM DTT, 2 mM NaF, and 2 mM Na₃VO₃, and 1×protease inhibitor cocktail) and immunoprecipitated with α -FLAG agarose (Sigma-Aldrich, USA). The immunoprecipitants were separated by 10% SDS-PAGE and stained with GelCode Blue Stain Reagent (Thermo Fisher, USA). A small aliquot of immunoprecipitated DGK5 was subjected to immunoblotting using α-FLAG antibodies (Sigma-Aldrich, USA). The DGK5 bands were sliced, trypsin-digested, and phospho-peptides were enriched for LC-MS/MS analysis using an Orbitrap QE LC-MS/MS system (Thermo Scientific, USA). The MS/MS spectra were analyzed with Mascot software, and the identified phosphopeptides were manually inspected to ensure confidence in the phosphorylation site assignment.

In vitro diacylglycerol kinase activity assay

The *in vitro* DGK5 activity assay was performed as described previously with some modifications.⁷⁹ In brief, 2 µg of purified GST-DGK5, HIS-DGK5, or its different variant proteins were incubated with 500 µM DAG (1, 2-dioleoyl-sn-glycerol or 1-stearoyl-2arachidonoyl-sn-glycerol; Avanti Polar Lipids Inc., USA) in a 250 µl reaction buffer [40 mM Tris-HCl, pH 7.5, 5 mM MgCl₂, 0.1 mM EGTA, 0.5 mM DTT, 1 mM sodium deoxycholate, 1 mM 3-[(3-cholamidopropyl) dimethylammonio]-1-propanesulfonate (CHAPS), 0.02% Triton X-100] containing 1 μ Ci [γ - 32 P]-ATP and 5 μ M ATP for 30 min at 30°C. The lipids DOG and SAG, dissolved in chloroform, were placed in 7 ml SCHOTT glass disposable reaction tubes with screw caps (SCHOTT, Germany), dried under a stream of nitrogen vapor, resuspended in a solution of 1.47 mM sodium deoxycholate dissolved in water, and followed by sonication for 5 min (5 cycles of 10 sec sonication and 10 sec stop) using the Branson SFX 250 Sonifier (Emerson, USA) at 4°C. The reaction was stopped by adding 750 µl chloroform/methanol (1:2, v/v) containing 1% HCl. Phospholipids were extracted by adding 1 ml chloroform/methanol (1:1), 500 μl solution containing 1 M KCl and 0.2 M H₃PO₄, mixing thoroughly by vortexing, and centrifuging at 2,000 rpm for 5 min. The lower organic phase (lipids) was transferred to a new glass tube, dried under a stream of nitrogen vapor, and resuspended in 50 μl chloroform/methanol (2:1). The lipids were separated by thin layer chromatography (TLC) silica plates (Merck, USA) that had been activated by heating for 15 min at 110°C. The plates were run in an acidic solvent system (CHCl3:MeOH:CH3COCH3:HAc:H2O, 50:10:20:10:5 by volume), and then put on paper towels to dry for 5-10 min. For the detection of organic compounds, the dried TLC plate was stained in a glass container with saturated iodine (I₂) vapor for 20-30 min and photographed for input control. After being photographed, the same TLC plate was placed in the hood for 20-30 min until the iodine staining disappeared for the subsequent radioactive analysis. The radioactive lipid products were visualized by autoradiography using GE Typhoon FLA 9500 (GE Healthcare, USA).

In vivo and in vitro PA detection

In vivo PA formation was performed as described previously with minor modifications. 31 Briefly, 1 ml protoplasts from four-week-old WT, dgk5-1, or bik1 mutant plants were transferred to SCHOTT glass disposable reaction tubes with a screw cap (SCHOTT, Germany), and pre-incubated with 1 μCi ³²P-orthophosphate (³²PO₄ ³⁻, Perkin Elmer, USA) for 2 h, followed by treatment with or without 0.1 μM flg22 for the indicated time in the figure. Incubation was stopped, and lipids were extracted by adding 2.4 ml ice-cold CHCl₃: MeOH: HCI (50:100:1.5 by volume) and mixing well for 10 sec. Then, 2.4 ml CHCl₃ and 2.4 ml 9% NaCl were added. The tubes were vigorously shaken, and two phases formed on ice for about 30 min. The organic lower phase was transferred to a new SCHOTT glass tube and dried under a stream of nitrogen vapor. Lipids were resuspended in 100 µl chloroform and PA was separated from the rest of the phospholipids by thin layer chromatography (TLC) using an acidic solvent (CHCl₃:MeOH:CH₃COCH₃:HAc:H₂O, 50:10:20:10:5 by volume). Radioactivity was visualized by autoradiography using GE Typhoon FLA 9500 (GE Healthcare, USA) and quantified by ImageJ software. Relative intensities of PA bands were normalized to the sum of phosphatidylethanolamine (PE), phosphatidylglycerol (PG), and phosphatidylcholine (PC),³¹ and PA fold-change was calculated as the ratio of the value from treated samples divided by the value from untreated samples, which was set as 1.

To detect in vitro plant lysate-mediated PA production, plant lysates were isolated from 0.1 g of 10- to 14-day-old WT, dgk5-1, or bik1 mutant seedlings grown on ½MS plate (treated with 100 nM flg22) in 200 μl lysis buffer (40 mM Tris-HCl, pH 7.5, 5 mM MgCl₂, 0.1 mM EGTA, 0.5 mM DTT, 0.2% Triton X-100). $50~\mu g$ of indicated lysates were used to incubate with DOG substrate in a $250~\mu l$ reaction buffer (as described above) containing 1 μ Ci [γ - 32 P]-ATP and 5 μ M ATP for 0.5 to 1 h at room temperature. The extraction and separation of phospholipids were the same as for the in vivo activity described above. The radioactive lipid products were analyzed by autoradiography using GE Typhoon FLA 9500 (GE Healthcare, USA).





For PA detection using the PAleon biosensor, experiments were performed as previously described. In brief, five-day-old transgenic seedlings of WT and dgk5-1 plants expressing PAleon sensor were placed in a Nunc® Lab-Tek™ Chambered Coverglasses (Thermo Fisher, USA) and overlaid with wet cotton to continuously perfuse the root with the buffer (5 mM KCl, 10 mM CaCl₂, 10 mM MES, pH 5.8), followed by overlaying with a water agar block. The PA dynamics were recorded by a Leica SP8 confocal microscope in the root. The CFP fluorescence lifetime (excitation at 440 nm and emission at 450-500 nm) was recorded by LAS X software and calculated as an average of six randomly measured images in the transgenic plant roots. The calculation of FRET efficiency (E) was analyzed as described for the FRET-FLIM assay.

Protein accession number

Sequence data in this study can be found in The Arabidopsis Information Resource (TAIR) database under the following accession numbers: BIK1 (AT2G39660), DGK5 (AT2G20900), WRKY29 (AT4G23550), PR1 (AT2G14610), PR5 (AT1G75040), FRK1 (AT2G19190), MPK3 (AT3G45640), MPK4 (AT4G01370), MPK6 (AT2G43790), UBQ10 (AT4G05320), BAK1 (AT4G33430), FLS2 (AT5G46330), BIR2 (AT3G28450), PBL30 (AT4G35600), PBL31 (AT1G76360), and RBOHD (AT5G47910).

QUANTIFICATION AND STATISTICAL ANALYSIS

Data for quantification analyses are presented as mean \pm SEM or SD as indicated in the figure legends. The statistical analyses were performed by one-way analysis of variance (ANOVA) followed by Tukey's test or unpaired two-tailed Student's t-test. The number of biologically independent replicates is shown in the figure legends or figures. The p-values are provided in the graphs.



Supplemental figures

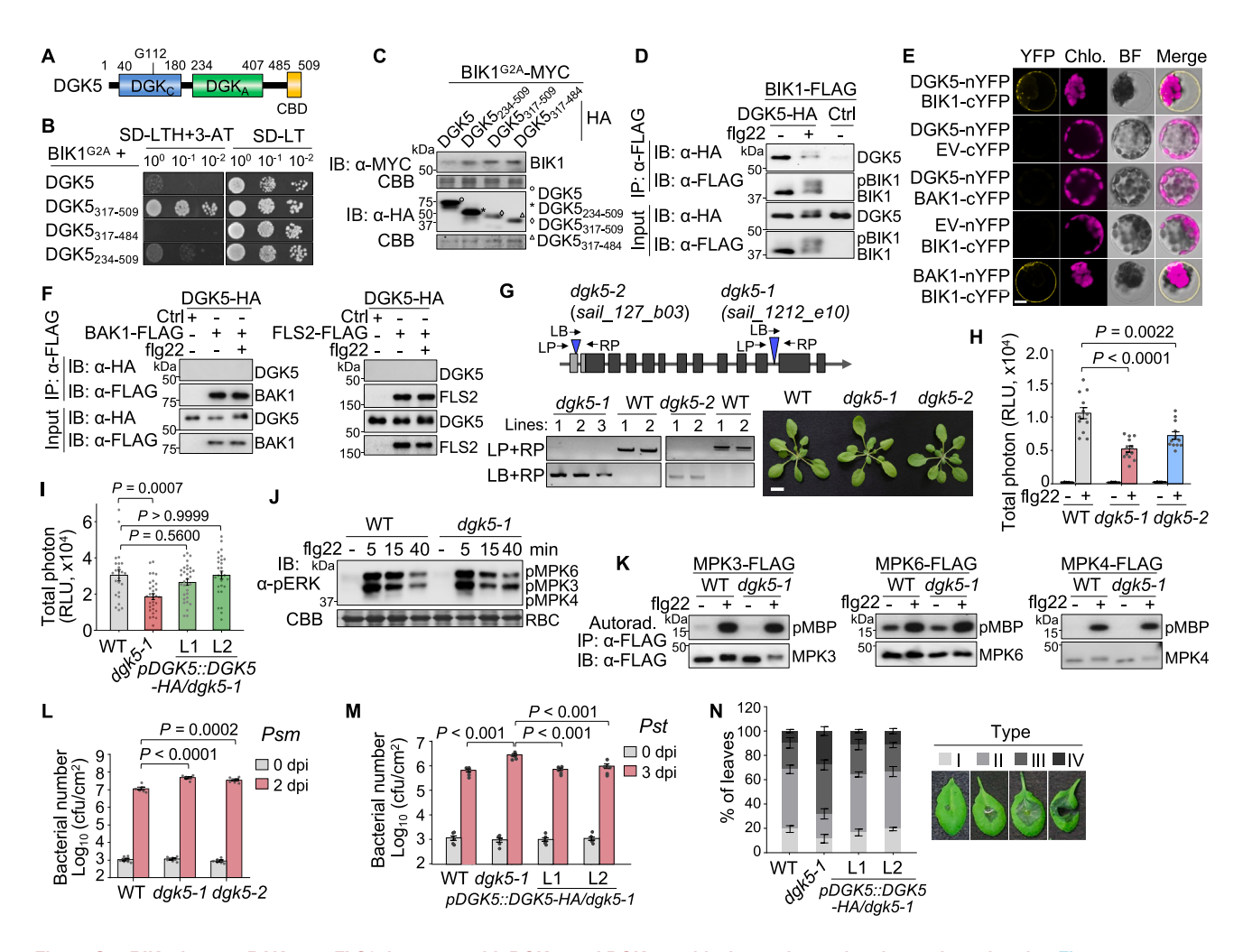


Figure S1. BIK1, but not BAK1 nor FLS2, interacts with DGK5, and DGK5 positively regulates plant immunity, related to Figure 1

(A) Diagram of DGK5 domains. The catalytic domain (DGK5_C), accessory domain (DGK5_A), catalytic site (G112), and calmodulin-binding domain (DGK5_{CBD}) are shown with the corresponding amino acid positions labeled.

(B) BIK1 interacts with DGK5 in a yeast two-hybrid assay. Yeast transformants co-expressing DGK5 or truncation variants in the pGADT7 (pAD) vector and BIK1^{G2A} in the pGBKT7 (pBK) vector were spotted as 10-fold serial dilutions on synthetic drop-out (SD) medium without leucine and tryptophan (SD-LT), or without leucine, tryptophan, and histidine (SD-LTH) supplemented with 1 mM 3-amino-1, 2, 4-triazole (3-AT). Yeast colonies were photographed 3-4 days later. (C) The protein expression of BIK1^{G2A} and DGK5 variants in yeast. The indicated plasmids were co-transformed into AH109 yeast cells and cultured in the SD-LT medium. Proteins were isolated for immunoblotting with α -MYC or α -HA antibodies. BIK1^{G2A} was tagged with an MYC-epitope in the pBK vector, and DGK5 variants were tagged with an HA epitope in the pAD vector. Protein loading is shown by CBB staining.

(D) BIK1 associates with DGK5 in protoplasts. Protoplasts from WT Arabidopsis plants were transfected with BIK1-FLAG and DGK5-HA or a control vector (Ctrl) for 12 h, followed by treatment with or without 0.1 μ M flg22 for 10 min. Co-immunoprecipitation (coIP) assay was carried out with α -FLAG agarose beads and followed by immunoblotting (IB) with α -HA or α -FLAG antibodies (top two panels). Input proteins are shown in the bottom two panels.

(E) BIK1 interacts with DGK5 in a bimolecular fluorescence complementation (BiFC) assay. Indicated proteins fused with either C-terminal YFP (cYFP) or N-terminal YFP (nYFP) were expressed in protoplasts for 16 h before imaging with a laser-scanning confocal microscope. Chlo., chloroplasts; BF, bright field. The pair of BAK1-nYFP and BIK1-cYFP serves as the positive control. Scale bars, 10 μm.

(F) DGK5 does not associate with BAK1 or FLS2. Indicated proteins were expressed in protoplasts for 12 h, followed by treatment with or without 0.1 μ M flg22 for 10 min. CoIP assays were performed as in (D).

(G) Genomic structure and transfer DNA (T-DNA) insertion mutants of *DGK5*. Gray and black rectangles represent the 5' untranslated region (5' UTR) and exon, respectively. Blue triangles represent T-DNA insertion positions. Arrows indicate primer positions. Genotyping PCR using genomic DNA was performed with the following primers: LP for the left genomic DNA primer, RP for the right genomic DNA primer, and LB for the left border primer of the T-DNA insertion. Growth phenotype of two *dgk5* mutants is shown 4 weeks after germination in soil. Scale bars, 1 cm.





(H) Compromised flg22-induced ROS production in dgk5 mutants (dgk5-1 and dgk5-2). Data of total ROS from Figure 1E are shown as mean \pm SEM (n = 12) analyzed by one-way ANOVA followed by the Tukey's test.

⁽I) DGK5-HA restores flg22-induced ROS production in dgk5-1. Leaf discs from 4-week-old soil-grown WT, dgk5-1, and two complementation lines (L1, L2) of pDGK5::DGK5-HA in the dgk5-1 background were treated with 0.1 μ M flg22. Total ROS production is calculated from Figure 1F, and data are shown as mean \pm SEM (n = 24 for WT; n = 32 for dgk5-1 and L1; n = 28 for L2) analyzed by one-way ANOVA followed by the Tukey's test.

⁽J) DGK5 is not required for flg22-triggered MAPK activation. 10-day-old seedlings of WT or dgk5-1 were treated with or without 0.1 μ M flg22 for the indicated time. MAPK activation was analyzed with α -pERK1/2 antibodies (top), and protein loading is shown by CBB staining for RBC (bottom).

⁽K) DGK5 is not required for flg22-triggered MAPK phosphorylation. FLAG-tagged MPK3, MPK4, or MPK6 were expressed in protoplasts from WT or dgk5-1 for 12 h, followed by treatment with 0.1 μ M flg22 for 10 min. FLAG-tagged MPKs were immunoprecipitated using α -FLAG agarose beads and incubated with myelin basic protein (MBP) for in vitro kinase assays using [γ - 32 P]-ATP. Phosphorylation was detected by autoradiography (top). Immunoprecipitated MPK proteins are shown by immunoblotting with α -FLAG antibodies (bottom).

⁽L) Increased susceptibility of dgk5 mutants (dgk5-1 and dgk5-2) to Psm infection. 4-week-old soil-grown plants were syringe-inoculated with bacterial suspension at 5×10^5 CFU/mL. Bacterial growth was measured at 0 and 2 days post-inoculation (dpi). Data are shown as mean \pm SEM (n = 6) analyzed by one-way ANOVA followed by the Tukey's test.

⁽M) DGK5-HA complements dgk5-1 disease resistance against Pst DC3000 infection. The experiment was performed as in (L), and data were analyzed by unpaired two-tailed Student's t test.

⁽N) Increased susceptibility of dgk5-1 to the necrotrophic bacterium Erwinia infection. Leaves of 4-week-old plants were inoculated with E. carotovora subsp. carotovora strain SCC1 at an $OD_{600} = 0.02$, and the percentage of leaves in different categories (1–4) of disease symptom severity was recorded at 36 hpi. 1, maceration at the site of inoculation; 2, maceration covering about half of the leaf; 3, maceration covering approximately two-thirds of the leaf; 4, maceration in the entire leaf. Data are shown as mean \pm SD (n = 3). 72 leaves were inoculated for each genotype in each repeat. Experiments were repeated three times in (B–K) and four times in (L–N) with similar results.



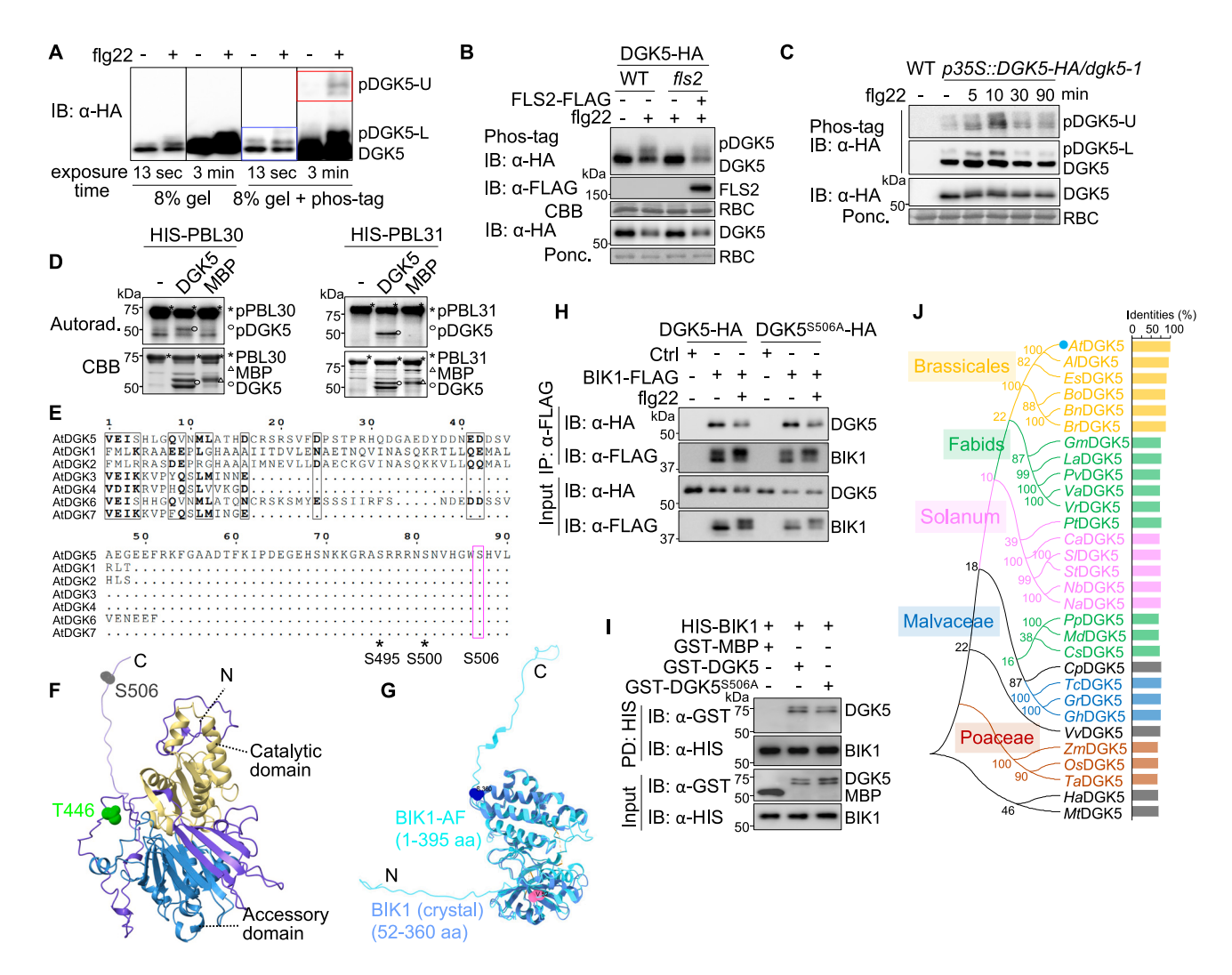


Figure S2. Ser-506 is required for DGK5 phosphorylation by BIK1, related to Figure 2

(A) Flg22 induces DGK5 phosphorylation in a regular or Mn^{2+} -Phos-tag SDS-PAGE. Protoplasts expressing DGK5-HA were treated with or without 0.1 μ M flg22 for 10 min. Total proteins were separated with 8% SDS-PAGE with or without Mn^{2+} -Phos-tag, followed by immunoblotting with α -HA antibodies at different exposure times. Blue and red boxes mark the lower (pDGK5-L) and upper mobility shifted bands (pDGK5-U) of phosphorylated DGK5, respectively.

(B) Flg22-induced DGK5 phosphorylation is blocked in the *fls2* mutant. Protoplasts from WT or *fls2* were transfected with *DGK5-HA* together with or without *FLS2-FLAG* for 12 h, followed by 0.1 μ M flg22 treatment for 10 min. DGK5 and FLS2 proteins were detected by immunoblotting with α -HA or α -FLAG antibodies. Protein loading is shown by CBB or Ponceau S staining for RBC.

(C) Flg22 induces DGK5 phosphorylation in transgenic plants. 11-day-old WT or p35S::DGK5-HA/dgk5-1 seedlings were treated with 0.2 μ M flg22 for the indicated time. Total proteins were separated with 8% Mn²⁺-Phos-tag or regular SDS-PAGE, followed by immunoblotting with α -HA antibodies.

- (D) PBL30 (left) and PBL31 (right) phosphorylate DGK5 *in vitro*. Purified proteins of HIS-PBL30 and HIS-PBL31 were incubated with MBP (control) or DGK5 proteins in a kinase reaction buffer containing [γ -³²P]-ATP for 2 h at room temperature. Phosphorylation was analyzed by autoradiography (top), and the protein loading is shown by CBB staining (bottom).
- (E) DGK5^{S506} is not present in other *Arabidopsis* DGK family members. C-terminal amino acid sequences of DGK1 to DGK7 from *Arabidopsis* were aligned by Esprit 3.0, and the Ser⁵⁰⁶ residue in DGK5 was boxed in pink.
- (F) Predicted structure of DGK5. The structure was predicted using AlphaFold Protein Structure Database (https://www.alphafold.ebi.ac.uk/). The DGK5 catalytic and accessory domains are marked with yellow and steel blue, respectively, and the remaining sequences of DGK5 are marked with purple. Thr⁴⁴⁶ and Ser⁵⁰⁶ residues are marked with green and gray, respectively. N and C represent the N and C termini of DGK5.
- (G) Overlay of truncated BIK1 crystal structure (PDB: 5TOS) with its AlphaFold-predicted structure using ChimeraX software. The BIK1 crystal structure (52–360 aa) and its predicted structure (1–395 aa) are shown with blue and cyan, respectively. The BIK1 crystal structure was determined from Val⁵² (labeled with pink) to Ser³⁶⁰ (labeled with dark blue).
- (H) DGK5^{S506A} does not affect its association with BIK1 *in vivo*. Protoplasts were co-expressed with BIK1-FLAG and DGK5-HA or DGK5^{S506A}-HA, followed by treatment with or without 0.1 μ M flg22 for 10 min. Control (Ctrl) is an empty vector. CoIP assay was carried out with α -FLAG agarose and analyzed by immunoblotting with α -HA or α -FLAG antibodies (top two panels). Input proteins are shown in bottom two panels.
- (I) DGK5^{S506A} does not affect its interaction with BIK1 *in vitro*. HIS-BIK1 proteins immobilized on Ni-NTA agarose were incubated with GST-MBP, GST-DGK5, or GST-DGK5^{S506A} proteins. Eluted and input proteins were subjected to immunoblotting with α -GST or α -HIS antibodies.





(J) DGK5 is conserved in different plant species. Protein sequences were blast-searched in NCBI using Arabidopsis DGK5 (AtDGK5, marked with a blue dot) as a query, and the phylogenetic analysis was generated by MEGA11 using the neighbor-joining method with 1,000 bootstrap replicates. Identities (%) indicate the percentage of homology of DGK5 in different plant species to AtDGK5. At, Arabidopsis thaliana; Al, Arabidopsis lyrate; Es, Eutrema salsugineum; Bo, Brassica oleracea; Bn, Brassica napus; Br, Brassica rapa; Gm, Glycine max; La, Lupinus angustifolius; Pv, Phaseolus vulgaris; Va, Vigna radiata; Vr, Vigna radiata; Pt, Populus trichocarpa; Ca, Capsicum annuum; Sl, Solanum lycopersicum; St, Solanum tuberosum; Nb, Nicotiana benthamiana; Na, Nicotiana attenuate; Pp, Prunus persica; Md, Malus domestica; Cs, Cucumis sativus; Cp, Carica papaya; Tc, Theobroma cacao; Gr, Gossypium raimondii; Gh, Gossypium hirsutum; Vv, Vitis vinifera; Zm, Zea mays; Os, Oryza sativa; Ta, Triticum aestivum; Ha, Helianthus annuus; Mt, Medicago truncatula.

Experiments were repeated three times in (A, B, D, H, and I) and twice in (C) with similar results.



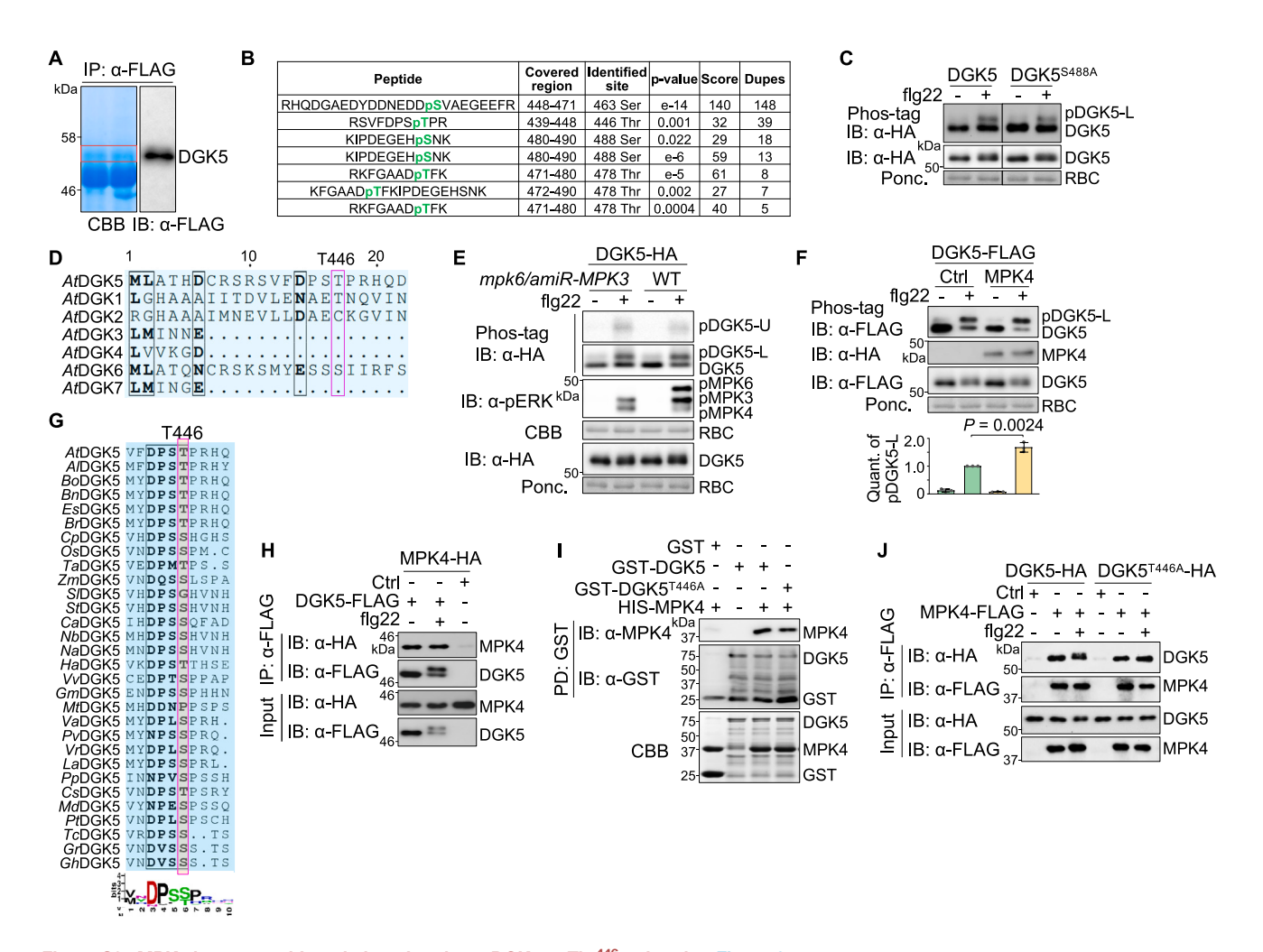


Figure S3. MPK4 interacts with and phosphorylates DGK5 at Thr⁴⁴⁶, related to Figure 3

(A) Sample preparation for the identification of fig22-induced DGK5 phosphorylation sites by LC-MS/MS. Protoplasts expressing DGK5-FLAG were treated with 0.2 μ M fig22 for 10 min. DGK5-FLAG was immunoprecipitated with α -FLAG agarose and separated by SDS-PAGE, followed by CBB staining (left) and immunoblotting with α -FLAG antibodies (right). Gels boxed in red containing the unphosphorylated and phosphorylated DGK5 were cut for trypsin digestion to identify DGK5 phosphorylation sites using LC-MS/MS analysis.

- (B) Flg22-induced DGK5 phosphorylation peptides identified by LC-MS/MS analysis. The score indicates the confidence of the identified serine (S) and threonine (T) phosphorylation residues; dupes indicate the repeat times of the identified peptides.
- (C) DGK5^{S488A} does not affect flg22-induced DGK5 phosphorylation in protoplasts. DGK5-HA or DGK5^{S488A}-HA was expressed in protoplasts, followed by treatment with 0.1 μ M flg22 for 10 min. Protein extracts were separated with Mn²⁺-Phos-tag or regular SDS-PAGE, followed by immunoblotting with α -HA antibodies. Protein loading is shown by Ponceau S staining for RBC.
- (D) Protein sequence alignment of *Arabidopsis* DGK family members. Partial amino acid sequences of DGK1-DGK7 were aligned by Esprit 3.0, and the Thr⁴⁴⁶ residue in DGK5 and the corresponding residue in other DGK members were boxed with pink. The conserved sites are boxed in black.
- (E) Flg22 induces a similar DGK5 phosphorylation pattern in WT and mpk6/amiR-MPK3. Protoplasts from WT and mpk6/amiR-MPK3 plants were transfected with DGK5-HA and treated with $0.1~\mu$ M flg22 for 10 min. Dex of 30 μ M containing 0.01% silwet L-77 was sprayed on the leaves 3 days before protoplast isolation. Total proteins were separated with Mn^{2+} -Phos-tag or regular SDS-PAGE, followed by immunoblotting with α -HA or α -pERK1/2 antibodies. The protein loading is shown by the CBB or Ponceau S staining for RBC.
- (F) MPK4 enhances flg22-induced DGK5^{T446} phosphorylation (pDGK5-L) *in vivo*. DGK5-FLAG was co-expressed with MPK4-HA or an empty vector (Ctrl) in protoplasts, followed by treatment with 0.1 μ M flg22 for 10 min. The experiment was performed as in (E). Quantification of pDGK5^{T446}-L was calculated as relative band intensities of pDGK5^{T446}-L divided by the unphosphorylated DGK5 band intensities. Data are shown as mean \pm SD (n = 3) analyzed by unpaired two-tailed Student's treat
- (G) DGK5^{T446} is conserved in different plant species. Multiple sequence alignment and WebLogo analyses of DGK5^{T446} from different plant species are shown with Thr⁴⁴⁶ boxed in pink. The names of different plants are listed in the figure legend of Figure S2J. The conserved sites are boxed in black.
- (H) MPK4 associates with DGK5. Protoplasts were co-expressed with DGK5-FLAG and MPK4-HA, followed by treatment with 0.2 μ M flg22 for 10 min. Control (Ctrl) is an empty vector. CoIP assay was carried out with α -FLAG agarose followed by immunoblotting with α -HA or α -FLAG antibodies (top two panels). Input proteins of DGK5-FLAG and MPK4-HA are shown on bottom two panels.
- (I) DGK5^{T446A} interacts with MPK4 *in vitro*. Glutathione sepharose beads immobilized with GST, GST-DGK5, or GST-DGK5^{T446A} were incubated with HIS-MPK4 proteins followed by immunoblotting with α-MPK4 or α-GST antibodies (top two panels). Input proteins are shown by CBB staining on the bottom panel.







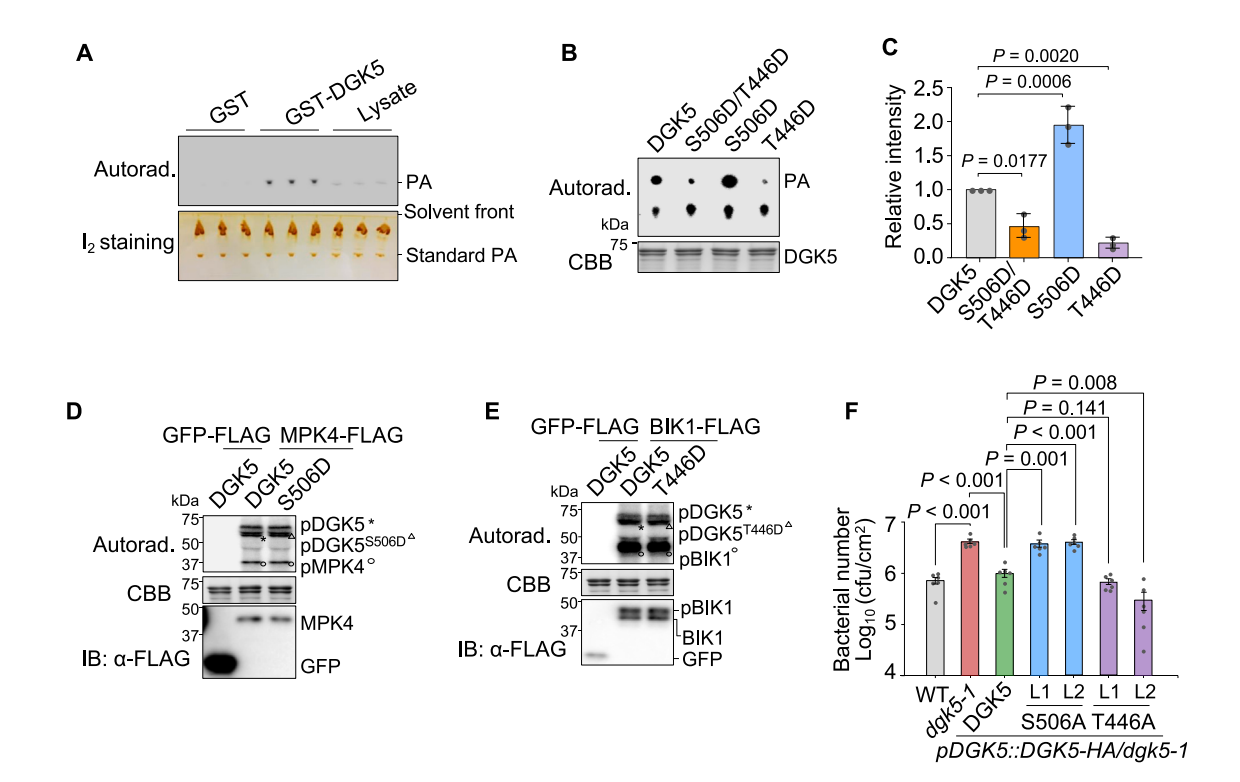


Figure S4. DGK5 mediates PA production and is required in plant immunity, related to Figure 4

(A) DGK5 phosphorylates DOG for PA production. Recombinant GST, GST-DGK5 proteins, or WT plant lysates were incubated with DOG in a reaction buffer containing $[\gamma^{-32}P]$ -ATP for 30 min. Plant lysates were obtained from 10-day-old seedlings grown on ½MS plates. Chloroform-soluble products were separated by the thin-layer chromatography (TLC) plate, and PA was detected by autoradiography (top). Standard PA (16:0-18:1, Avanti Polar Lipids Inc., USA) (2 μ g) was added to each sample before lipid extraction. The iodine (I_2) staining of the standard PA on the TLC plate is shown at the bottom. The solvent front indicates the side of the TLC plate immersed in the acidic solvent liquid.

(B and C) Phosphomimetic mutant of DGK5^{SS06D/T446D} has reduced PA production. Purified proteins of DGK5 and its variants were incubated with DOG substrate in a reaction buffer containing [γ -³²P]-ATP for 30 min. Chloroform-soluble products were separated by the TLC plate, and PA was detected by autoradiography (top). Input proteins are shown by CBB staining (bottom). Quantification of relative intensities of PA produced by DGK5 and its variants are shown in (C). The value of the DGK5 sample was set as 1.0. Data are shown as mean \pm SD (n = 3) analyzed by one-way ANOVA followed by the Tukey's test.

(D) MPK4 phosphorylates DGK5 SS06D . Protoplasts expressing MPK4-FLAG were treated with 0.1 μ M flg22 for 10 min. The activated MPK4-FLAG and GFP-FLAG (control) were immunoprecipitated with α -FLAG magnetic beads and incubated with HIS-DGK5 or HIS-DGK5 proteins for the *in vitro* kinase assay using [γ - 32 P]-ATP. Phosphorylation was detected by autoradiography (top). Immunoprecipitated MPK4 and GFP proteins are shown by immunoblotting with α -FLAG antibodies (bottom). HIS-DGK5 and HIS-DGK5 input proteins are shown by CBB staining (middle).

(E) BIK1 phosphorylates DGK5^{T446D}. The experiment was performed as in (D).

(F) DGK5^{S506A}, but not DGK5^{T446A}, fails to restore *dgk5-1* disease resistance against *Psm* infection. 4-week-old soil-grown plants were hand-inoculated with bacterial suspension at 5 × 10⁵ CFU/mL. Bacterial growth at 2 dpi is shown as mean ± SEM (n = 6) analyzed by unpaired two-tailed Student's t test. Experiments were repeated three times with similar results.



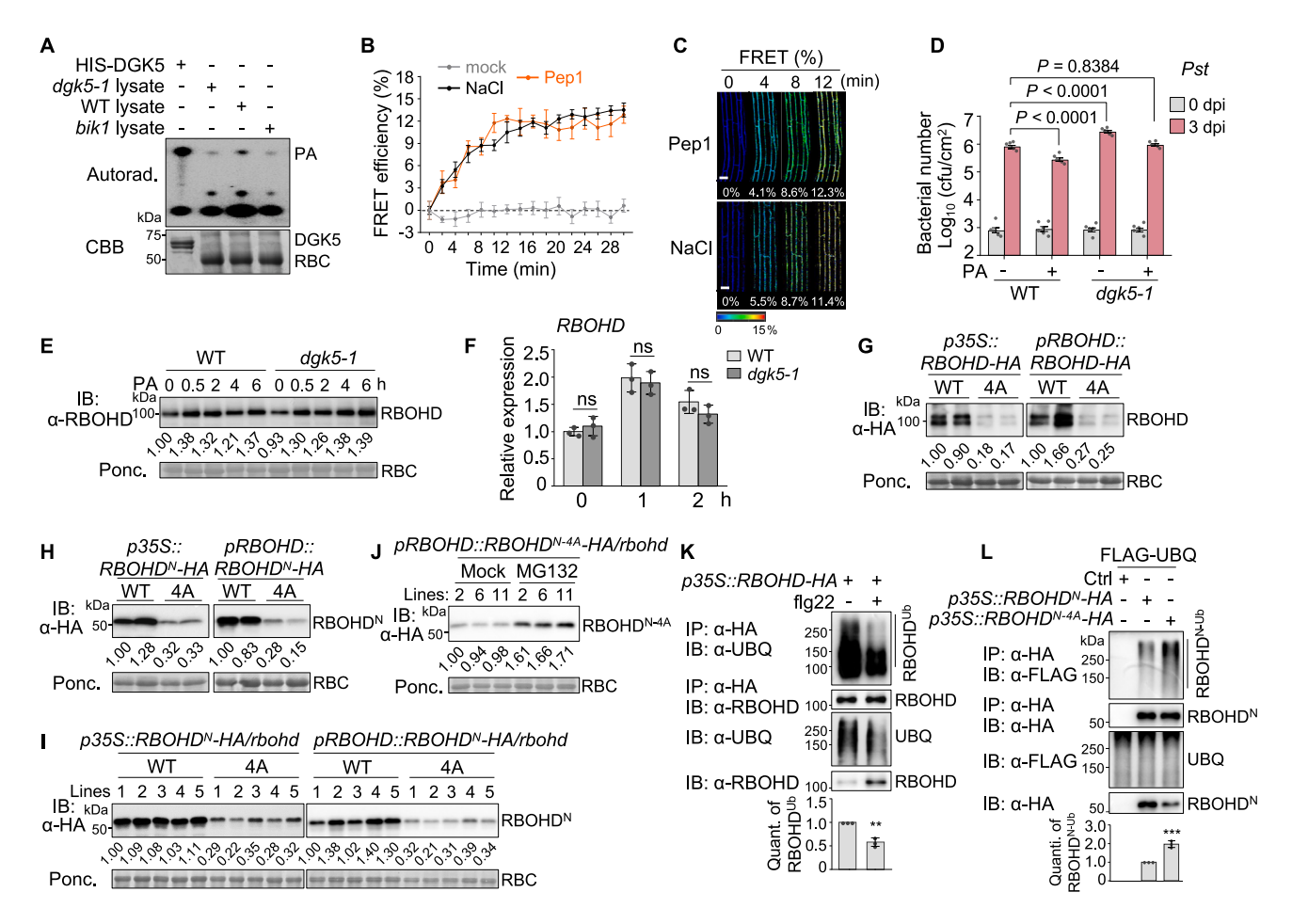


Figure S5. DGK5-mediated PA production regulates plant immunity and RBOHD protein accumulation, related to Figures 5 and 6

(A) PA production is reduced in dgk5-1 and bik1 mutants after flg22 treatment. Recombinant GST-DGK5 proteins or plant lysates from WT, dgk5-1, or bik1 were incubated with DOG in a reaction buffer containing [γ - 32 P]-ATP for 30 min. Plant lysates were obtained from 10-day-old seedlings grown on ½MS plates after the treatment with 0.1 μ M flg22 for 5 min. Chloroform-soluble products were separated by the TLC plate placed in an acidic solvent system, and PA was detected by autoradiography (top). The protein loading is shown by CBB staining on the bottom.

(B and C) Salt- and Pep1-induced PA production is monitored by a PA biosensor PAleon-based FRET-FLIM assay. PA production was monitored in the root maturation zone of WT seedlings expressing PAleon. 5-day-old seedlings were treated with or without $0.5 \,\mu$ M Pep1 or $100 \, \text{mM}$ NaCl for the indicated time, and FRET efficiency (%) was captured by the Leica laser-scanning confocal microscope at different time points. Data are shown as mean \pm SEM (n = 6). Representative confocal images with FRET efficiencies (%) from (B) at 0.4, 8, and $12 \, \text{min}$ are shown in (C).

- (D) Exogenous PA treatment restores the disease resistance of dgk5-1 to Pst DC3000 infection. Leaves of 4-week-old soil-grown plants were pre-infiltrated with 10 μ M PA liposomes for 24 h followed by hand-inoculation with bacterial suspension at 5 \times 10⁵ CFU/mL. Bacterial growth was measured at 0 and 3 dpi. Data are shown as mean \pm SEM (n = 6) analyzed by one-way ANOVA followed by the Tukey's test.
- (E) Exogenous PA treatment induces RBOHD protein accumulation in WT and dgk5-1. 10-day-old seedlings were treated with 25 μ M PA liposomes for the indicated time. RBOHD proteins were detected by immunoblotting using α -RBOHD antibodies (top). The protein loading is shown by Ponceau S staining for RBC. (F) Transcripts of RBOHD in WT and dgk5-1 plants after flg22 treatment. 10-day-old seedlings were treated without or with 0.1 μ M flg22 for 1 or 2 h and subjected to RT-qPCR analysis. Expression levels of RBOHD were normalized to UBQ10 and presented as fold change relative to WT 0 h treatment (no treatment). Data are shown as mean \pm SD (n = 3) analyzed by one-way ANOVA followed by the Tukey's test. n.s., not significant.
- (G) Mutations of RBOHD PA-binding sites (RBOHD^{4A}) reduce RBOHD protein accumulation. RBOHD-3×HA (WT) and RBOHD^{4A}-3×HA (4A) driven by the 35S promoter or RBOHD native promoter (p35S::RBOHD-HA and pRBOHD::RBOHD-HA, WT, and 4A) were expressed in *N. benthamiana* for 2 days. Proteins were detected by immunoblotting using α -HA antibodies. The protein loading is shown by Ponceau S staining for RBC (bottom).
- (H) Mutations of PA-binding sites reduce RBOHD^N protein accumulation. The experiment was performed as in (G) with *p35S::RBOHD^N-HA* and *pRBOHD::R-BOHD^N-HA* (WT and 4A). RBOHD^N: N terminus of RBOHD.
- (I) Mutations of PA-binding sites reduce RBOHD^N protein accumulation in *Arabidopsis* transgenic plants. The N-terminal RBOHD (RBOHD^N, WT) or its PA-binding site mutant RBOHD^{N-4A} (4A) tagged with $3 \times \text{HA}$ under the 35S or native promoter (p35S:: $RBOHD^N$ -HA and pRBOHD:: $RBOHD^N$ -HA, WT and 4A) was transformed into rbohd, and multiple transgenic lines were subjected to immunoblotting using α -HA antibodies (top). The protein loading is shown by Ponceau S staining for RBC.





(J) MG132 stabilizes RBOHD^{N-4A} proteins in *Arabidopsis* transgenic plants. 10-day-old seedlings of three independent transgenic lines of $pRBOHD^{N-4A}$ -HA/rbohd were treated without or with 100 μ M MG132 for 4 h, and the samples were collected for immunoblotting using α -HA antibodies.

Relative band intensities of RBOHD normalized to input proteins were labeled underneath the immunoblotting images (E, G, and H–J). Experiments were repeated three times with similar results.

⁽K) flg22 treatment reduces RBOHD ubiquitination in p35S::RBOHD-HA/rbohd transgenic plants. 10-day-old seedlings were treated with 0.1 μM flg22 for 2 h. Total proteins were extracted and subjected to immunoprecipitation using α -HA magnetic beads followed by immunoblotting using α -UBQ or α -RBOHD antibodies (top two panels). The input proteins are shown with immunoblotting by α -UBQ and α -RBOHD antibodies (3rd and 4th panels). Intensities of the ubiquitinated RBOHD (RBOHD^{Ub}, top panel) and immunoprecipitated RBOHD (2nd panel) were quantified by ImageJ software. The quantification of RBOHD^{Ub} was normalized to RBOHD. The value of RBOHD^{Ub} without treatment was set as 1.0. Data are shown as mean \pm SD (n = 3). Asterisks denote statistically significant differences according to unpaired two-tailed Student's t test (p < 0.01).

⁽L) RBOHD^{N-4A} exhibits increased ubiquitination. Protoplasts from p35S:: $RBOHD^N$ -HA and p35S:: $RBOHD^{N-4A}$ -HA transgenic plants were expressed with FLAG-UBQ and subjected to immunoprecipitation using α -HA magnetic beads, followed by immunoblotting using α -FLAG or α -HA antibodies (top two panels). The input proteins are shown with immunoblotting by α -FLAG or α -HA antibodies (3rd and 4th panels). The quantification and data analysis were performed as in (K) (p < 0.001).





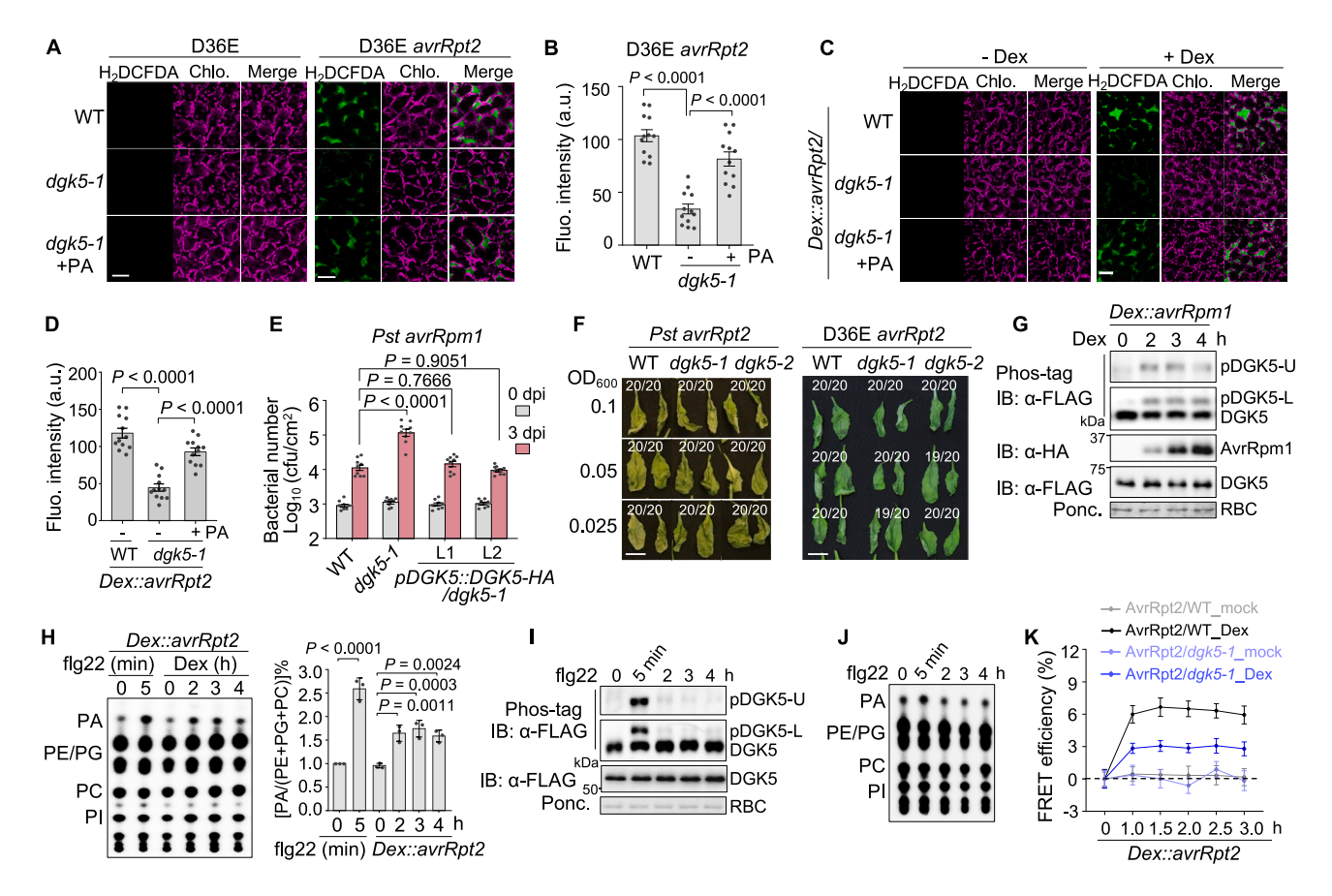


Figure S6. DGK5-mediated PA production is involved in ETI signaling, related to Figure 7

(A and B) D36E avrRpt2, not D36E, induces apoplastic ROS production. ROS production was detected with the fluorescent dye H₂DCFDA in WT and dgk5-1 leaves 5 h after infiltration of D36E or D36E avrRpt2 at 2 × 10⁷ CFU/mL or in combination with 12.5 μ M PA liposomes for dgk5-1. Confocal images show the fluorescence intensity stained by H₂DCFDA (A). Chlo, chlorophyll. Scale bars, 50 μ m. Fluorescence intensities were quantified by ImageJ software. Data are shown as mean \pm SEM (n = 12) analyzed by one-way ANOVA followed by the Tukey's test (B).

(C and D) Dex::avrRpt2-induced ROS production is reduced in dgk5-1. The Dex::avrRpt2/WT and Dex:avrRpt2/dgk5-1 leaves were infiltrated with 2 µM Dex for 5 h or in combination with 12.5 µM PA liposomes for dgk5-1. The experiment and data analysis were performed as in (A and B).

(E) Increased susceptibility to Pst DC3000 avrRpm1 infection in dgk5-1. Leaves of 4-week-old soil-grown plants were hand-inoculated with bacterial suspension at 5 × 10⁵ CFU/mL. Bacterial growth was measured at 0 and 3 dpi. Data are shown as mean ± SEM (n = 9) analyzed by one-way ANOVA followed by the Tukev's test

(F) AvrRpt2-triggered hypersensitive response (HR) is not affected in *dgk5-1*. WT and *dgk5-1* leaves were infiltrated with *Pst avrRpt2* or D36E *avrRpt2* at different OD₆₀₀. Pictures were taken at 9–12 hpi. The numbers of infiltrated leaves (20 for each genotype and treatment) and those with HR are indicated in the image. Scale bars. 1.0 cm.

(G) AvrRpm1 induces two DGK5 phosphorylation patterns. Protoplasts co-expressing Dex::avrRpm1-HA and DGK5-FLAG were treated with 2 μ M Dex for the indicated time. Total proteins were separated with Mn²⁺-Phos-tag (top two panels) or regular SDS-PAGE (bottom three panels), followed by immunoblotting with α -FLAG or α -HA antibodies. Protein loading is shown by Ponceau S staining for RBC.

(H) AvrRpt2 induces PA production. Protoplasts from Dex::avrRpt2/WT plants were pre-incubated with ^{32}P -orthophosphate for 2 h, followed by treatment with 2 μ M Dex or 0.1 μ M flg22 for the indicated time. Total lipids were extracted and separated by the TLC plate placed in an acidic solvent system, and PA was detected by autoradiography. Relative intensities of PA production were normalized to the sum of phosphatidylethanolamine (PE), phosphatidylglycerol (PG), and phosphatidylcholine (PC) (right panel). The value of the sample without treatment is set as 1.0. Data are shown as mean \pm SD (n = 3) analyzed by one-way ANOVA followed by the Tukey's test.

(I) FIg22 does not induce DGK5 phosphorylation at the late time points. Protoplasts expressing DGK5-FLAG were treated with 0.1 µM flg22 for the indicated time. The experiment was performed as in (G).

(J) Fig22 does not induce PA production at the late time points. Protoplasts from WT plants were treated with 0.1 μM fig22 for the indicated time. The experiment was performed as in (H).

(K) AvrRpt2-induced PA production is reduced in dgk5-1 with a PA biosensor PAleon-based FRET assay. Protoplasts isolated from Dex::avrRpt2/WT or Dex::avrRpt2/dgk5-1 were expressed with PAleon for 6 h. The PA production is monitored at the indicated time after 2 μ M Dex treatment, and FRET efficiency (%) was recorded by the Leica laser-scanning confocal microscope. Data are shown as mean \pm SEM (n = 6). Experiments were repeated three times with similar results.

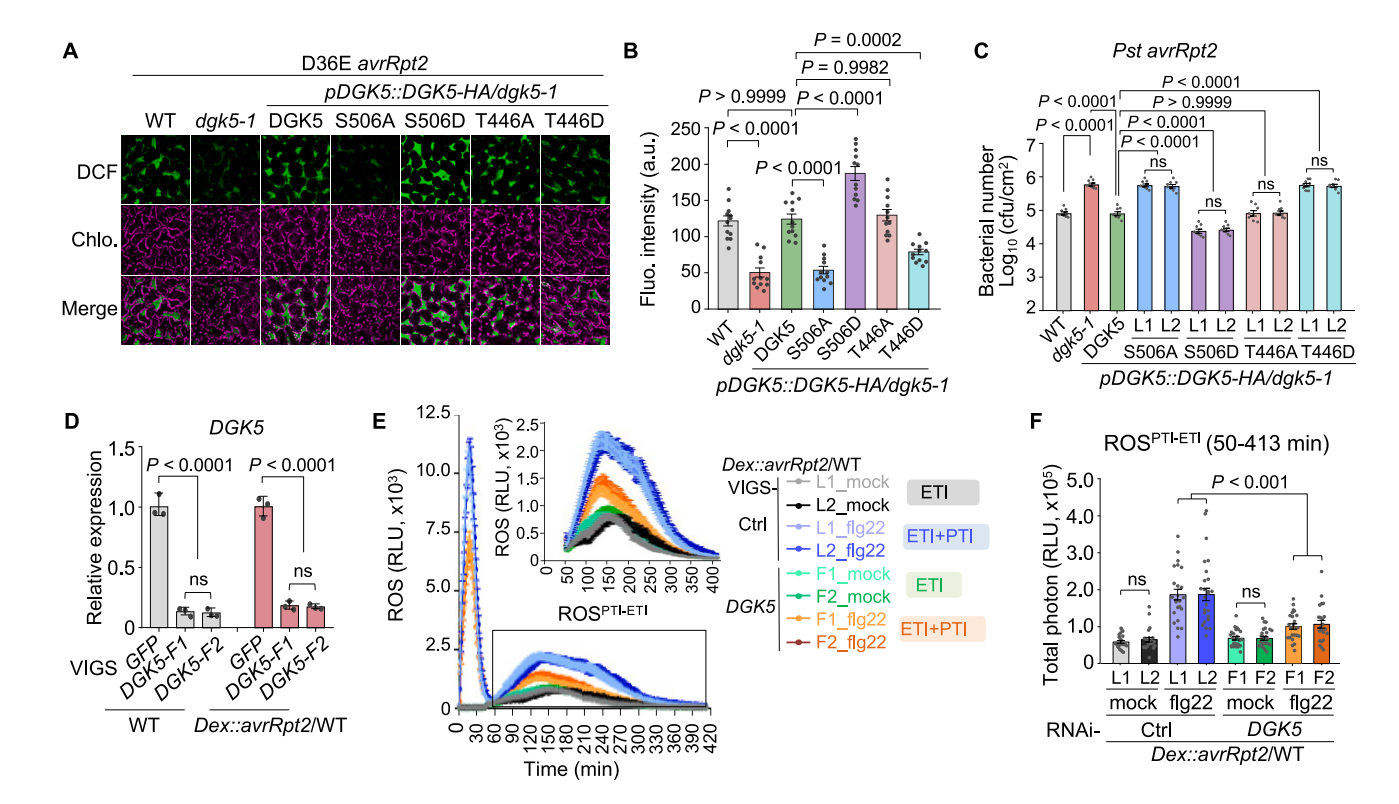


Figure S7. DGK5 phosphorylation is involved in ETI, related to Figure 7

(A and B) D36E avrRpt2-induced ROS production in different DGK5 phosphorylation mutant complementation lines. The experiment was performed as Figure S6A (A). Data are shown as mean ± SEM (n = 12) analyzed by one-way ANOVA followed by the Tukey's test (B).

(C) Pst avrRpt2-induced disease resistance in different DGK5 phosphorylation mutant complementation lines. Leaves of 4-week-old soil-grown plants were hand-inoculated with bacterial suspension at 5×10^5 CFU/mL. Bacterial growth was measured at 3 dpi. Data are shown as with mean \pm SEM (n = 8) analyzed by one-way ANOVA followed by the Tukey's test.

(D) Silencing *DGK5* in WT or *Dex::avrRpt2* transgenic plants by VIGS. Total RNA was extracted from VIGS-*DGK5* (F1 and F2 are two fragments targeting different *DGK5* regions) or VIGS-GFP control plants in WT or *Dex::avrRpt2* transgenic plants for RT-qPCR analysis. The *DGK5* gene expression was normalized to *UBQ10* and presented as a fold change to VIGS-GFP. Data are shown as mean ± SD (n = 3) analyzed by one-way ANOVA followed by the Tukey's test.

(E and F) The flg22-potentiated AvrRpt2-induced ROS burst (ROS^{PTI-ETI}) is reduced in DGK5 silencing plants. Leaf discs from Dex::avrRpt2/WT silenced with Ctrl (GFP) or DGK5 were treated with 25 μ M dexamethasone (Dex) and without (mock) or with 0.1 μ M flg22. ROS production was measured as relative light units (RLUs) by a luminometer. F1 and F2 indicate DGK5 silencing plants generated by two targeting fragments of DGK5. The ROS burst during 50–400 min (ROS^{PTI-ETI}) was highlighted on the top right (E), and the total ROS production during 50–400 min (ROS^{PTI-ETI}) is shown in (F). Data are shown as mean \pm SEM (n = 24) analyzed by one-way ANOVA followed by the Tukey's test.

Experiments were repeated three times with similar results.